2.8 Special Form

This section is not applicable to the Universal Transport Cask because the fuel to be transported in the cask does not satisfy the definition in 10 CFR 71.4 for special form radioactive material.

THIS PAGE INTENTIONALLY LEFT BLANK

2.9 Fuel Rods

Regulatory Guide 7.9 [41] requires that analysis or test data be provided showing that the structural integrity of the fuel rod cladding justifies the amount of integrity claimed. An assessment of fuel rod buckling is performed. The bounding load condition for the assessment of fuel rod buckling is the end drop condition. The end drop orientation maximizes not only the axial force component that would buckle the fuel rod, but it is also the orientation that has the maximum axial acceleration. Both PWR and BWR fuel rod configurations are evaluated. The evaluations show that buckling of PWR or BWR fuel rods does not occur in the UMS® Transport Cask.

2.9.1 PWR Fuel Rod Buckling Assessment

Of the PWR assemblies to be transported in the cask, the following four are identified as representative assemblies:

- Westinghouse 15 x 15 Std (Class 1)
- Westinghouse 17 x 17 Std (Class 1)
- Babcock & Wilcox 15 x 15 Mark B (Class 2)
- Combustion Engineering 16 x 16 System 80 (Class 3)

Characteristics of the PWR fuel rods are shown in Table 1.2-4 and Table 5.2-2.

2.9.1.1 Overview of Analysis Methodology

During the end drop, the fuel rod is expected to impact the fuel assembly base. The fuel rod itself will respond as an elastic bar under a sudden compression load at its bottom end. The duration of this impact is bounded by the first extensional mode shape of the fuel rod. Contribution of higher frequency extensional modes of the rod would tend to shorten the duration of impact of the fuel rod with the fuel assembly base. The fuel rod, upon initiation of the impact, corresponds to an undeformed state. In the process of the impact, the compression of the fuel rod will increase to a maximum and then return to a near uncompressed state. At this point, the time of impact is completed. This actually represents half of a cycle of the lowest

frequency of an extensional mode shape of the fuel rod. The frequency of this mode shape is evaluated using ANSYS Revision 5.2. The shape of the time dependence of the deformation is sinusoidal. The single extensional mode shape can also be considered to be a single degree of freedom (SDOF) with a corresponding mass and stiffness. In viewing such an event as a spring mass system, the time variation of the deformation during the impact is expected to be sinusoidal.

The buckling mode for the fuel rod is governed by the boundary conditions. Lateral support is provided at the intermediate fuel bundle supports (grids). The only vertical restraint is considered to be at the point of contact of the fuel rod and the base of the assembly. The weight of the fuel rod pellets and cladding is assumed to be uniformly distributed along the length of the fuel rod. In the end drop, this results in the maximum compressive load occurring at the base of the fuel rod. The first buckling mode shape corresponding to these conditions is computed using ANSYS Revision 5.2.

Typically, eigenvalue buckling is applied for static environments. For dynamic loading, it is assumed that the duration of the loading is sufficiently long to allow the system to experience the complete load, even as the deformation associated with buckling is commenced. For dynamic loading, the lateral motion, which would correspond to the buckled shape, will correspond to the lowest mode shape. The similarity of the two shapes (the lateral dynamic mode shape and the buckling mode shape) is expected since both have the same displacement boundary conditions, the same stiffness matrix, and the same governing finite element equations, i.e.:

$$[K]\{\phi_i\} = \lambda_i[A]\{\phi_i\}$$

where:

K = structure stiffness matrix
ϕ_i = eigenvector
λ_i = eigenvalue
A = mass matrix for the mode shape calculation or stress stiffening matrix for the buckling evaluation.

Based on the time duration of the impact and the inherent inability of the fuel rod to rapidly displace in the lateral direction, the effect of the actual lateral motion of buckling can be computed with a dynamic load factor, DLF [47]. The expression for the DLF for a half-sine loading for an SDOF is given by:

$$DLF = \frac{-2\beta}{1-\beta^2}\cos\left(\frac{\pi}{2\beta}\right)$$

where:

β = ratio of first extensional model frequency to the first lateral mode frequency

The maximum dynamic acceleration (g-load), which may potentially result in the buckling of the fuel rod, is determined by applying the DLF to the design acceleration of 60g for the 30 foot end drop condition (See Section 2.7.1).

The critical buckling load for the fuel rod is calculated using the same ANSYS model employed for the dynamic mode shape calculation. The maximum dynamic g-load is compared to the g-load first buckling mode shape. If the maximum dynamic g-load is less than the first buckling mode shape g-load, the fuel rod will not buckle under a 30-foot end drop.

2.9.1.2 Fuel Rod Mode Shapes and Buckling Evaluation

Evaluation is performed for the four representative PWR fuel assemblies as shown in Section 2.9.1. The fuel pellet weight is combined with the cladding weight in the evaluation. To be consistent with this approach, an effective cross sectional property is used in the evaluation, which incorporates the properties of the fuel pellet and the fuel cladding. The model used in this evaluation is comprised of ANSYS two-dimensional beam elements (BEAM3). In the model, the beam elements considered the weight of the fuel pellet, as well as the cladding. The modulus of elasticity (E_x) for the fuel pellet has a nominal value of 27.5×10^6 psi [48]. To be conservative, the E_x for the fuel pellet used in the model is taken as 13.0×10^6 psi (less than 50% of the nominal value). The E_x used for the Zircaloy cladding is 11.5×10^6 psi [48]. Densities for cladding and fuel are 0.237 lb/in^3 and 0.396 lb/in^3, respectively [48]. Figure 2.9-1 shows a

typical fuel rod model used for the buckling analysis. Location of constraints for the four PWR fuel types considered in the analysis can be found in Table 2.9-1. Only one vertical constraint is specified in the model, which is located at the bottom end of the fuel rod.

The results for the PWR fuel rod buckling evaluation are shown in Table 2.9-2. A typical dynamic mode shape plot and the buckling mode shape plot are shown in Figures 2.9-2 and 2.9-3, respectively. For the four PWR fuel classes evaluated, the maximum dynamic g-load is less than the first buckling mode g-load; therefore, the PWR fuel rods do not buckle during the 30-foot end drop condition.

2.9.2 BWR Fuel Rod Buckling Assessment

Of the BWR assemblies to be transported in the cask, the following are identified as representative assemblies:

- GE 7 x 7 BWR/2-3 version GE-2b (Class 4)
- GE 8 x 8-2 BWR/2-3 version GE-5 (Class 4)
- GE 8 x 8-4 BWR/2-3 version GE-8 (Class 4)
- GE 7 x 7 BWR/4-6 version GE-2 (Class 5)
- GE 8 x 8-2 BWR/4-6 version GE-5 (Class 5)
- GE 8 x 8-4 BWR/4-6 version GE-10 (Class 5)
- GE 9 x 9-2 BWR/4-6 version GE-11 (Class 5)

Characteristics of the BWR fuel rods are shown in Table 1.2-5 and Table 5.2-6.

The representative BWR fuel assemblies are further bounded by three BWR configurations (based on rod diameter and length), the GE 7x7 BWR/4-6, GE 8x8-2 BWR/4-6, and GE 9x9-2 BWR/4-6. Using the similar method for the PWR fuel rod evaluation as described in Section 2.9.1, ANSYS models are used to determine the critical buckling g-loads. Location of lateral constraints for the BWR fuel rods are shown in Table 2.9-3.

The buckling g-loads for BWR fuel rods are shown in Table 2.9-4. The buckling mode shapes are similar to those of the PWR fuel rods. For the three BWR fuel classes evaluated, the critical buckling g-load is greater than the design acceleration of 60g for the 30-foot end drop (the DLF is conservatively ignored); therefore, the BWR fuel rods do not buckle during a 30-foot end drop.

Figure 2.9-1 Typical Fuel Rod Finite Element Model and Boundary Conditions

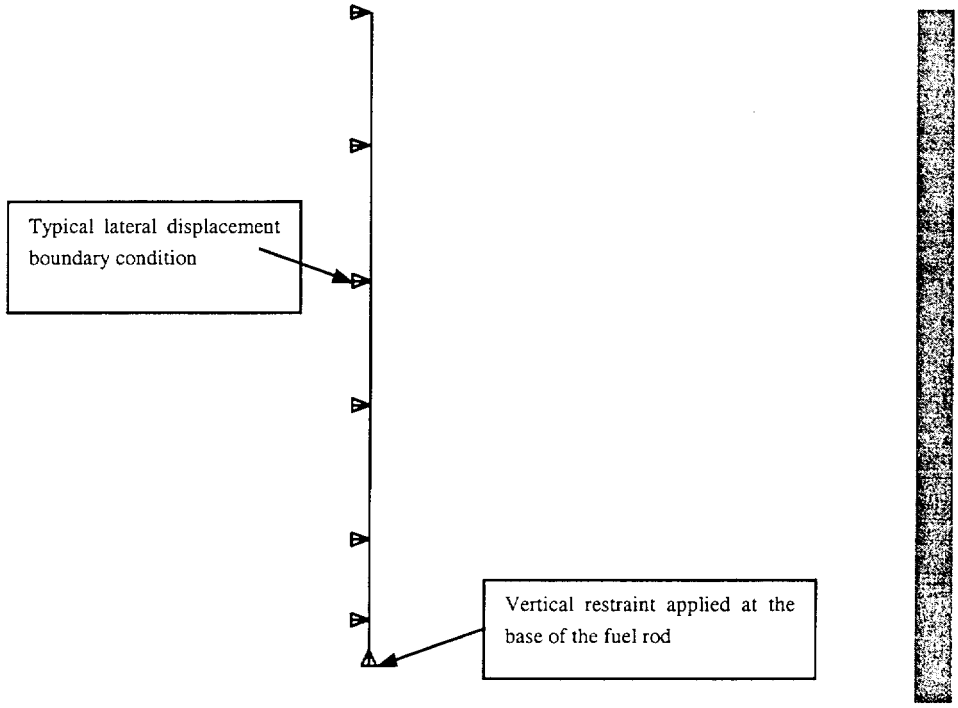

Figure 2.9-2 Typical First Lateral Mode Shape Plot for Fuel Rod

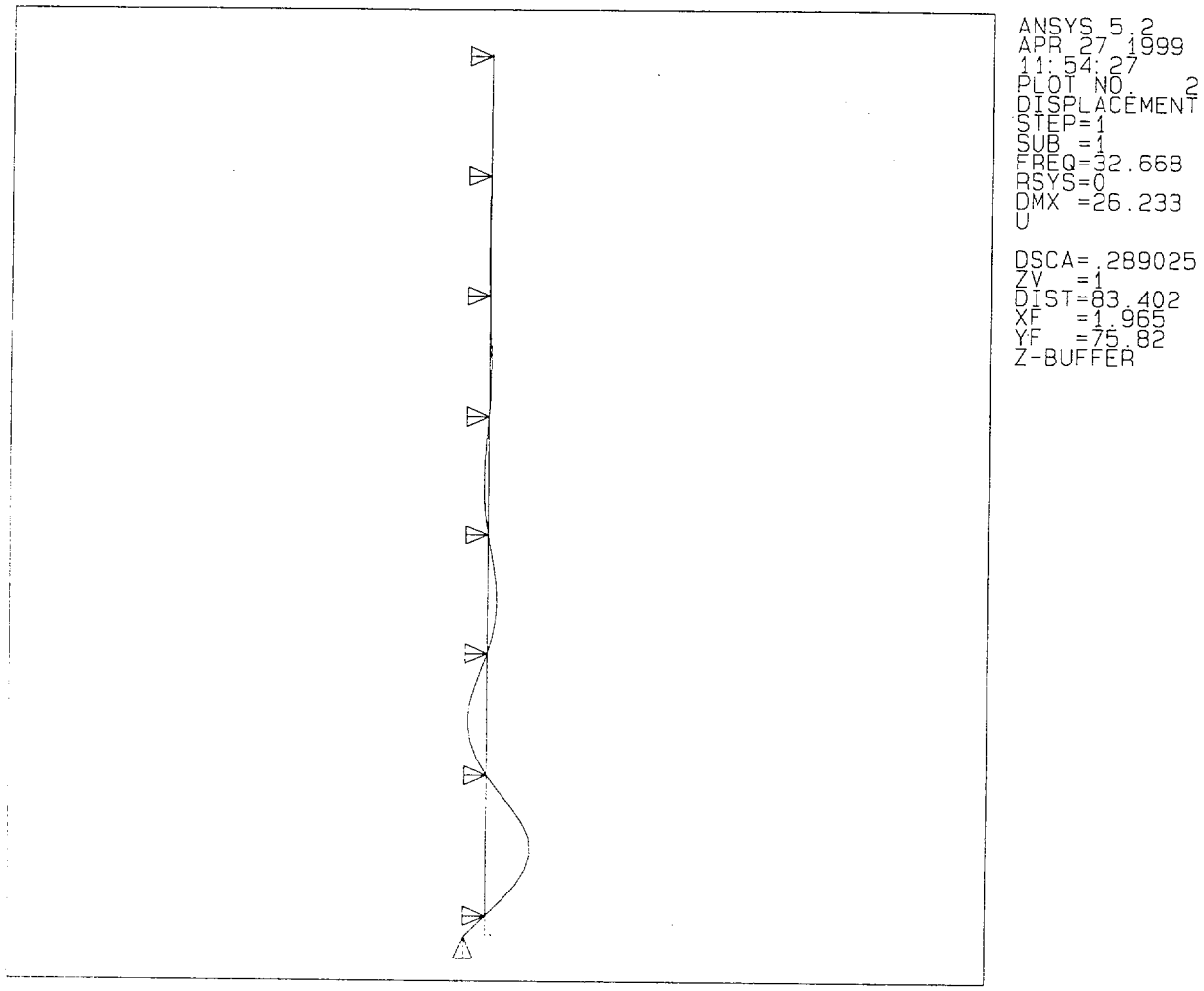

Figure 2.9-3 Typical First Buckling Mode Shape for Fuel Rod

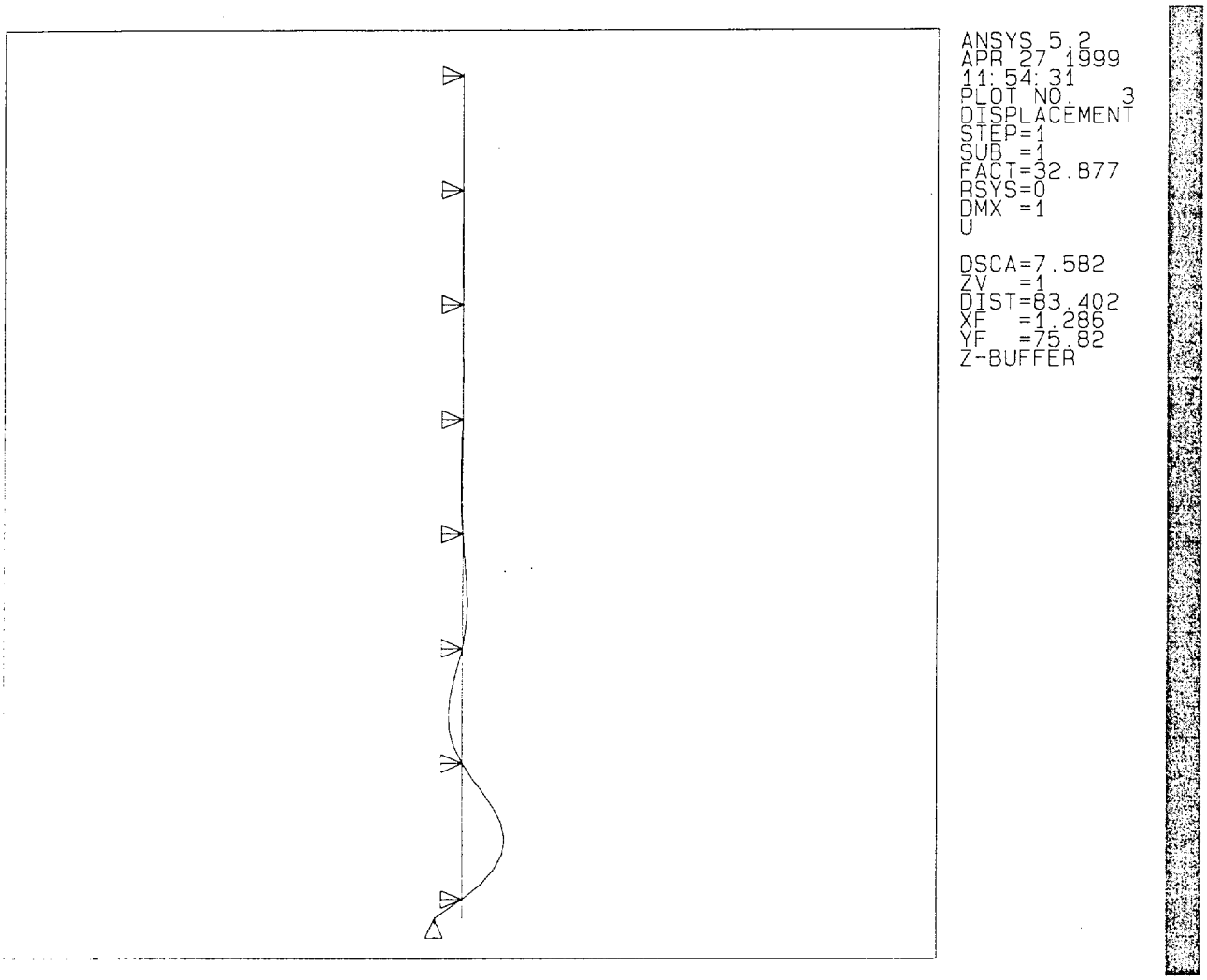

Table 2.9-1 Location of Lateral Constraints – PWR Fuel Rods

Fuel Assembly Type	Location of Lateral Constraints (inch)*										
Westinghouse 15x15 Std (Class 1) L_{rod}=151.88 in.	2.9	27.1	53.3	79.5	105.7	131.9	150.6				
Westinghouse 17x17 Std (Class 1) L_{rod}=151.64 in.	3.45	27.9	48.4	68.9	89.5	110.1	130.6	151.2			
Babcock & Wilcox 15x15 Mark B (Class 2) L_{rod}=153.68 in.	4.9	27.2	48.4	69.5	90.6	111.7	132.7	153.7			
Combustion Engineering 16x16 System 80 (Class 3) L_{rod}=161.00 in.	4.1	19.8	35.5	51.2	66.9	82.6	98.2	113.9	129.6	145.3	161.0

* Measured from the bottom end of the fuel rod.

Table 2.9-2 PWR Fuel Rod Analysis Summary

Fuel Assembly Class	First Extensional Frequency (Hz)	First Lateral Frequency (Hz)	Frequency Ratio, β	Dynamic Load Factor, DLF	Maximum Dynamic g-Load*	First Buckling Mode g-Load
Westinghouse 15 x 15	211.5	29.1	7.268	0.280	16.8	40.9
Westinghouse 17 x 17	212.2	32.7	6.490	0.316	18.9	32.9
Babcock &Wilcox 15 x 15	209.5	41.0	5.110	0.407	24.4	40.3
Combustion Engineering 16 x 16	200.4	68.9	2.909	0.780	46.8	53.7

* Maximum dynamic g- load = DLF x 60g.

Table 2.9-3 Location of Lateral Constraint for BWR Fuel Rods

Fuel Assembly Class	Location of Lateral Constraints (inch)*								
GE 7 x 7 BWR/4-6 L_{rod}=163.42 in.	0.00	22.88	43.03	63.18	83.33	103.48	123.63	143.78	163.42
GE 8 x 8-2 BWR/4-6 L_{rod}=163.42 in.	0.00	22.88	43.03	63.18	83.33	103.48	123.63	143.78	163.42
GE 9 x 9-2 BWR/4-6 L_{rod}=163.42 in.	0.00	22.88	43.03	63.18	83.33	103.48	123.63	143.78	163.42

* Measured from the bottom end of fuel rod.

Table 2.9-4 BWR Fuel Rod Analysis Summary

Fuel Assembly Class	Buckling g-Load
GE 7 x 7 BWR/4-6	104.3
GE 8 x 8-2 BWR/4-6	77.8
GE 9 x 9-2 BWR/4-6	64.6

THIS PAGE INTENTIONALLY LEFT BLANK

2.10 Appendices

THIS PAGE INTENTIONALLY LEFT BLANK

2.10.1 Computer Program Descriptions

The structural evaluation of the Universal Transport Cask body, closure lid, canister, baskets, and impact limiters is accomplished using two computer codes, ANSYS and RBCUBED. Each program is described in the following sections.

2.10.1.1 ANSYS

The structural analysis of the main body, the closure lid, the canister, and the baskets of the Universal Transport Cask is performed by the finite element analysis method using the ANSYS structural analysis computer program [32]. The ANSYS computer program is a large-scale, general purpose computer program for the solution of several classes of engineering analyses that include: static and dynamic; elastic, plastic, creep and swelling; buckling; and small and large deflections. The matrix displacement method of analysis based on finite element idealization is employed throughout the program. The large variety of element types available gives ANSYS the capability of analyzing two-dimensional and three-dimensional frame structures, piping systems, two-dimensional plane and axisymmetric solids, three-dimensional solids, flat plates, axisymmetric and three-dimensional shells, and nonlinear problems, including gap element interfaces.

A three-dimensional model is used in the analysis of the cask for the 3 free-drop cases. Two-dimensional axisymmetric models are used to evaluate the cask lid for puncture. The interface gap elements provide the capability of realistic modeling and evaluation of the interactions between the lead layer and the surrounding stainless steel shells; between the top forging, and the lid; and between the neutron shield material and the steel in the bottom of the cask.

The ANSYS preprocessing routine (PREP7) is used to construct the finite element mesh, describe each cask component material (temperature-dependent) property, assign unique identifiers for cask components, model displacement boundary conditions and prescribe temperature, point loads, or surface tractions of appropriate element faces or nodes. The PREP7 graphics option is a valuable tool that permits the user to check the model for completeness. The

ANSYS analysis option uses the PREP7 file to generate a solution file and to provide a user-oriented printout of the solution phase.

A variety of ANSYS post-processors (for example, Post1) utilizes the solution file to sort, print, or plot selected results from the ANSYS analysis. The post-processors can provide many useful features including a maximum set of variables (such as stress components or displacements) or sectional stresses along a designated path. Additionally, the structural behavior can be viewed by model displacement and stress contour plots.

2.10.1.2 RBCUBED

RBCUBED [33] is an impact limiter analysis computer program developed by NAC and used in the Universal Transport Cask impact limiter analyses. RBCUBED utilizes quasi-static methodology; that is, each iteration freezes an instant in time during which all calculations are performed, and then, proceeds to the next time increment. The methodology employed in the program sizes the impact limiter and calculates the deceleration forces used to calculate the stresses imposed on the cask structure, but does not implement any load factor. There are several assumptions that are attendant to this methodology:

1. Gravity is the only force that acts on the cask during free fall. While falling, the cask is translating vertically and continues to do so until the initial (first) impacting end has been brought to rest. In oblique and side-drop cases, after the first end has been stopped, the cask rotates until the second limiter strikes the unyielding surface and absorbs the remaining kinetic energy.

2. There is no sliding or lateral motion of the cask at any time during the impact(s).

3. The cask weight includes the impact limiters, but the length of the cask does not.

4. The deceleration force generated during crushing of the isotropic energy absorption material acts at the centroid of the area engaged in crushing for that increment in time.

5. Crushing of the energy absorption material occurs from the outside toward the cask body.

6. The component of the cask weight acting downward and the crush force acting upward are assumed to act colinearly. The magnitude of the weight component is very small compared to the crush force.

7. The impact limiter material that is not between the cask and the unyielding surface does not absorb any kinetic energy. The extraneous limiter material is ineffective for the purposes of this impact limiter analysis.

RBCUBED is capable of analyzing any cask impact orientation from vertical (0°) to horizontal (90°).

The input data for RBCUBED includes the following: (1) height of drop; (2) weight of cask system; (3) cask length; (4) impact orientation angle; (5) deflection increment; (6) material crush properties (stress-strain curve or force deflection curve); and (7) impact limiter geometry. Geometric modeling of the impact limiter is performed using combinatorial geometry based on the MORSE-CG computer program.

The output data from RBCUBED includes the following: (1) a verbatim input return; (2) a processed input of general problem parameters and material properties; (3) the results of the RBCUBED execution—deflection; (4) resultant force; (5) remaining kinetic energy; (6) velocity; (7) elapsed time since the beginning of impact; (8) area currently involved in crushing; and (9) a series of crush "footprints" at crush intervals of one inch.

The computer program, RBCUBED—A Program to Calculate Impact Limiter Dynamics, is benchmarked for validity by comparison of analysis results to manual calculations using crush areas determined by drafting methods.

THIS PAGE INTENTIONALLY LEFT BLANK

2.10.2 Finite Element Model - Universal Transport Cask

Finite element analysis methods are used to perform the stress evaluation of the Universal Transport Cask for normal and accident free drop conditions. Each drop condition is analyzed using a three-dimensional model. All primary structural components are modeled using ANSYS. Figure 2.10.2-1 shows the major components of the cask represented in the model.

As shown in Figure 2.10.2-2, the model corresponds to half (180°) of the entire cask. The cask body is represented using solid elements, beam elements, contact elements, mass elements and spring/damper elements. The cask components identified in Figure 2.10.2-1 are modeled using SOLID45 three-dimensional eight node brick elements. Associated with these elements are the material properties defined in Section 2.3. Specifically, they are employed for the steel cask components and the NS-4-FR in the neutron shield in the cask bottom. The lead comprising the radial gamma shield is modeled with a reduced modulus of elasticity. Using the stress strain curve from [44] for the largest strain rate (.0231 in/in/sec), a secant modulus of 40,000 psi is computed based on a 5% strain, and Poisson's ratio is set to .4999. This approach is used to simulate the low yield strength of the lead.

The lower neutron shield, gamma shield, ligaments, and bottom ring (in Figure 2.10.2-1) require the use of CONTACT52 line elements which only allow compression to be transmitted between the nodes. The neutron shield, gamma shield, and bottom ring are connected to the model only through the CONTACT52 elements. No friction is assumed to exist between these components and the adjacent cask body elements, which introduces a slight conservatism in the model. The size of the gap associated with the CONTACT52 is taken to be zero in order to maximize the compressive load from the lead onto adjacent shells. In the drops, it is expected that the lead fills any gap between the lead and the shells.

The two ligaments form the bottom boundary of the lead cavity and separate the bottom ring from the bottom of the lead. Additionally, the ligaments support the bottom of the inner shell. Connection of the ligaments to the shells is provided by a full penetration weld at their inner radius to the inner shell and at the outer radius of the ligament to the outer shell. While the two ligaments are adjacent, they are assumed to act independently of the other ligament. This is accomplished by connecting the adjacent nodes between the ligaments with CONTACT52 elements.

CONTACT52 elements are also employed to model the compressive force of the lid onto the upper forging.

The bolts and preload are modeled using BEAM4 elements. They are used to simulate the bolt head, the bolt shank and the bolt threads. The bolt circle annulus region is a reduced stiffness volume used to model the hole pattern for the bolts.

Mass elements (MASS21) distributed over nodes on the exterior surface of the assembly are used to adjust the mass of the model to account for components such as the radial neutron shield and impact limiters. Minor adjustments in loading to the shells and the overall mass of the cask is made possible with the use of mass elements. This flexibility allows for the inclusion of component masses not initially model (i.e., spacers).

Figure 2.10.2-1 Primary Components of the Universal Transport Cask

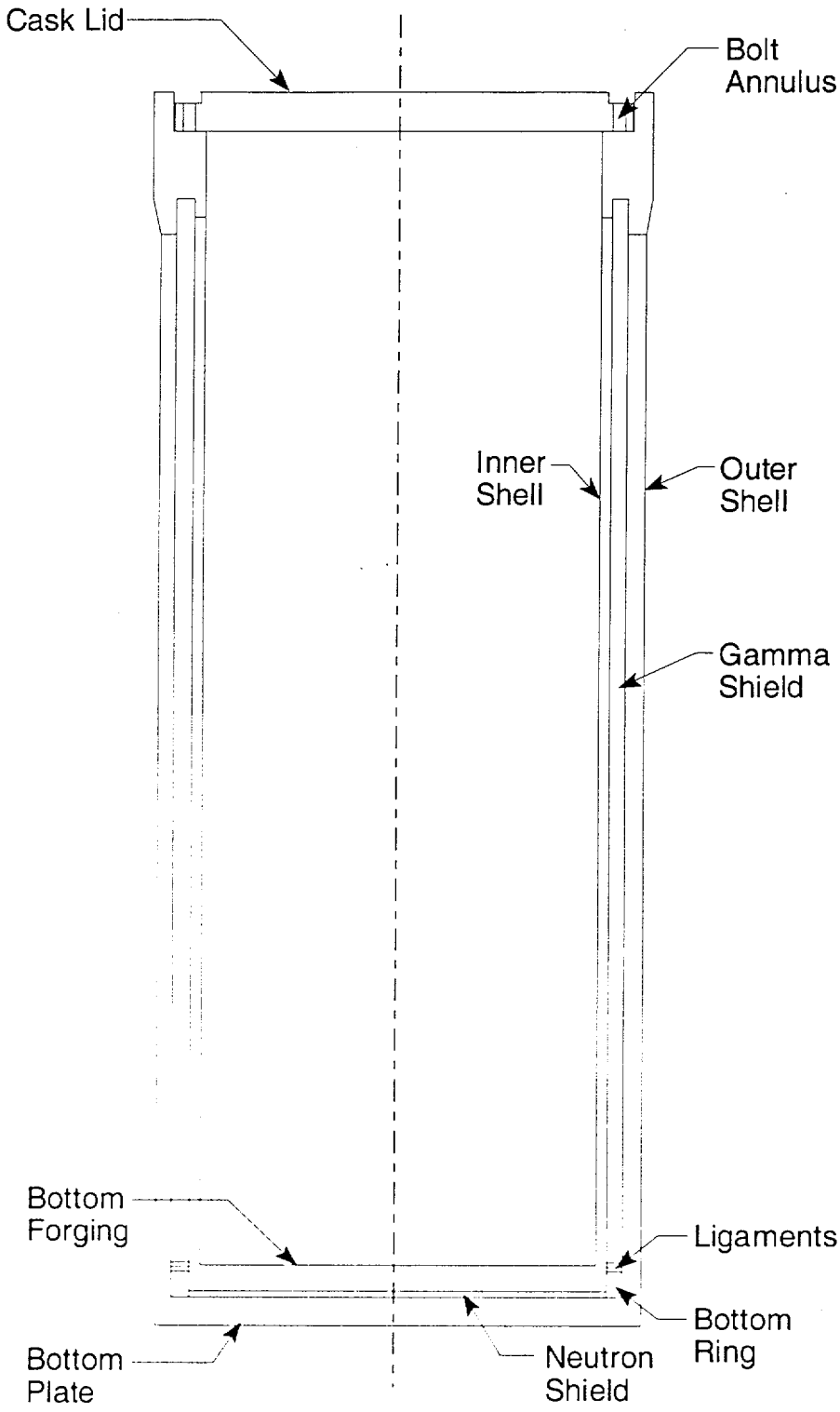

Figure 2.10.2-2 Universal Transport Cask 3-D Model

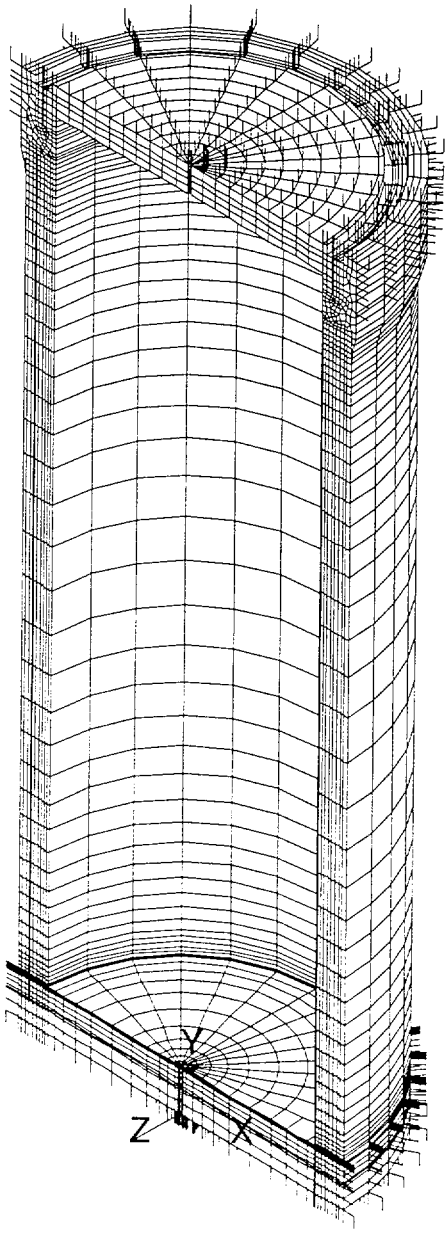

2.10.2.1 Load Application and Boundary Conditions

The four categories of cask loading considered in the free drop event are closure lid bolt preload, internal pressure load, thermal load, and inertial body load.

1. Closure Lid Bolt Preload. The required total bolt preload on the cask lid bolts is 5.4×10^6 lb, as calculated in Section 2.6.7.6. Bolt preload conservatively applied to the model by imposing initial strains to the bolt shafts is 5.9×10^6 lb. The bolts are modeled as beam (ANSYS BEAM4) elements.

The standard technique for applying bolt preload to a finite element model is employed. The bolts are modeled using beam elements, ANSYS STIF4 elements. Each bolt is modeled by four beam elements, two that represent the bolt head and two that represent the bolt shaft. The two bolt head elements are defined by three nodes that are an integral part of the non-threaded plate. The bolt head elements are assigned a stiffness of 10 times the actual bolt stiffness. The first bolt shaft element connects the center node of the bolt head with a node located at the top of the threaded hole. This element represents the portion of the bolt that is not engaged in the threaded hole. This portion of the bolt will be in tension due to the bolt preload. The second bolt shaft element connects the node at the top of the threaded hole with a node at the bottom of the threaded hole. This element represents the portion of the bolt that is engaged in the threaded hole. The two bolt shaft elements are assigned material property values (area and stiffness) equal to the actual bolt properties.

The effect of bolt preload is imposed on the model by applying an initial strain to the bolt shaft. The initial strain is applied only to the beam element representing the portion of the bolt shaft not engaged in threads. The initial strain values, which result in the required preload values, are determined by first running ANSYS analyses on the three-dimensional models with a "trial" initial strain, applied to the bolt shaft element, as the only loading condition. The resulting beam element force (from the element representing the portion of the bolt shaft not engaged in threads), is then used to ratio the trial initial strain to a value that will result in a beam element force closer to the actual bolt preload. This procedure is performed iteratively until the beam element force is effectively equal to the actual bolt preload.

The trial initial strain values are first determined by performing hand calculations of the value of $P/(n \times A \times E)$ for both the inner and the outer lid bolts. For the cask lid bolts, the calculation considers a required total bolt preload (P) of 5.9×10^6 lb pounds for 48 bolts, a quantity (n) of 48 bolts, a bolt cross-sectional area (A) of 2.77 $in.^2$ per bolt, and a Young's modulus (E) of 28.3×10^6 psi.

2. Pressure Loading. A pressure of 150 psig is used to conservatively envelope the normal conditions design pressure of 25 psig for all impact loadings considered.

Inertial loads resulting from the weight of the cask contents are imposed by applying an appropriate deceleration factor to the cask contents. The applied decelerations are determined by considering the crush strength and the geometry of the impact limiter. The inertial load resulting from the contents design weight is represented as an equivalent static pressure load uniformly applied on the interior surface of the cask.

The pressure load for the canister with fuel is applied to the cask body using a cosine-shaped pressure distribution. To account for the total load of the contents and overall package weight, the mass elements were modified until the total force sum for a 1 *g* load equaled the total weight of the package. Using this method, the overall deviation from the actual package weight is less than 4%.

Gap elements are defined at both ends of the cask to simulate the pressure applied by the impact limiters during drop conditions.

Pressure loading—cask end drop

For the end drop analyses, the contents weight is assumed to be uniformly distributed on the cask end, over an area determined by the inside diameter of the cask. Therefore, one-half the contents weight of 74,203 lb and the cask cavity inside radius of 33.8 in. are used to calculate a contact pressure of:

$$p = \frac{37{,}101.5}{(\pi)(33.8)^2} = 10.34 \text{ psi}$$

Mass elements located in the shells to account for the spacers bring the total mass of the contents to 75,903 lb. Note that the calculated stresses are ratioed up to account for the actual contents weight of 77, 432 pounds.

This pressure applies to a 1 *g* loading condition. Pressure values for the 1-foot and 30-foot end drop analyses are determined by ratioing this pressure by the g-load values applicable to the specific case, which are documented in Sections 2.6.7 and 2.7.1.

Pressure loading—side drop

The inertial load produced by the 74,203 lb contents weight is represented as an equivalent static pressure applied on the interior surface of the cask. The pressure is uniformly distributed along the cavity length over a section equal to the length of a 173.75 in. canister, and is varied in the circumferential direction as a cosine distribution. The maximum pressure occurs at the impact centerline; the pressure decreases to zero at locations that are 57° either side of the impact centerline, as illustrated in Figures 2.10.2.1-1 and 2.10.2.1-2. The method used to determine the varying pressures on the elements within the 57° arc is presented in the following paragraphs.

The following formula is used to determine the contents pressures for the side drop analyses, which vary around the circumference. This method uses a summation scheme to approximate the integration of the cosine-shaped pressure distribution:

$$F_{total} = \sum_{i=1}^{6} P_{max} A_i \cos(\theta_i) \cos(\theta_i')$$

where F_{total} = 37,101.5 lb (cask contents weight is 74,203 lb)

P_{max} = maximum pressure (at impact centerline)

θ_i = average angle of subtended arc of i^{th} element measured from centerline at point of impact, to obtain vertical component of pressure

i = i^{th} circumferential sector

θ'_i = normalized angle to peak at 0° and to be zero at 57°

$$= \theta_i \left(\frac{90}{57}\right) = 1.5789(\theta_i)$$

A_i = i^{th} circumferential area over which the pressure is applied

$$= R\,(\Delta\theta_i)(\pi/180)\,L$$

$\Delta\theta_i$ = increment of the angle corresponding to arc length of i^{th} element

R = inner radius of cask = 33.8 in.

L = canister length = 173.5 in. (shortest canister length)

As previously noted, the calculated stresses are ratioed up to account for the actual contents weight of 77, 432 pounds.

Corner and oblique drops (accident conditions only)

For the corner and oblique drop analyses, the contents pressure loading is a combination of the end drop pressure load and the side drop pressure load. The corner and oblique drop pressure loads are determined by breaking up the contents pressure load into longitudinal and lateral components, based on the drop angle. The longitudinal component is applied to the cask end, and the lateral component is applied to the cask inner shell as described previously for the side drop case.

Effect of increased mass on side and oblique drop analyses

An additional mass applied to the cask shells accounts for the mass of the spacers. Therefore, the effective content weight is 75,903 lb and the total weight of the cask model with contents is 252,444 lb. To offset design changes made after the cask analyses were complete, the side and oblique drop stresses were increased by 2.7% (affects only the 1-ft side drop, Tables 2.6.7.2-1 through 2.6.7.2-8; the 30-ft side drop, Tables 2.7.1.2-1 through 2.7.1.2-4; and the 30-ft oblique drop, Tables 2.7.1.4-1 through 2.7.1.4-8). Therefore, the final effective canister and cask weights are 77,952 lb and 259,260 lb, respectively. These values bound the maximum canister and cask weights reported in Table 2.2-2 (77,432 lb for the canister and 255,022 lb for the cask).

3. Thermal. According to Regulatory Guide 7.8, three credible thermal conditions must be considered.

Condition 1: 100°F ambient temperature with maximum decay heat load and maximum solar insolation.

Condition 2: -20°F ambient temperature with maximum decay heat load and no solar insolation.

Condition 3: -40°F ambient temperature with no decay heat load, and no solar insolation.

Conditions 3 is not evaluated because it results in a uniform temperature within the cask body and only thermal stresses, associated with differential thermal expansion between dissimilar materials, are generated. These thermal conditions are bounded by Condition 1. The heat transfer analyses performed in Section 3.4 determine the cask temperature distributions for the following combinations of ambient temperature, heat load, and solar insolation:

Thermal Hot: maximum decay heat generation, ambient temperature = 100°F, with full solar insolance

Thermal Cold: maximum decay heat generation, ambient temperature = -40°F, no solar insolance

The -40°F ambient temperature is conservatively used to bound the -20°F ambient temperature requirement.

The cask temperature distributions calculated for Conditions 1 and 2 are used as inputs to the ANSYS analyses. The ANSYS analyses determines the stresses arising from the thermal expansion of the cask from its initial 70°F condition, including the effects of the differential thermal growth within the components, which are a result of the temperature difference across the cask walls. The cask temperature distributions are also used in the ANSYS structural analyses to determine the values of the temperature-dependent material properties.

To apply the appropriate temperature distribution for thermal stress calculations, a thermal analysis run is made using data taken from the cask thermal analysis (as described in Section 3.4). The temperatures for the structural analyses are obtained from the thermal results.

4. Inertial body load. The inertial effects, which occur during impact, are represented by equivalent static forces, in accordance with D'Alembert's principle. Inertial body load include the weight of the empty cask and the weight of the cavity contents. The cavity contents is comprised of the weight of the canister and the spacers.

The weight of the spacers is included in the weight of the canister and content. Gap elements are defined at both ends of the cask to simulate the pressure applied by the impact limiters during drop conditions (based on a cosine distribution). The stiffness of the gap elements is varied as a cosine function from a maximum value (1×10^6 lb/in) at the line of impact to a lower value (2.4×10^5 lb/in) at an angle of 57° from the line of impact, and a minimal value (100 lb/in) from 66.5° to 180°). The load distribution that results from the crushing of the impact limiter is shown in Fig. 2.10.2.1-1.

Figure 2.10.2.1-1 Cask Body Loading for Side-Drop Conditions

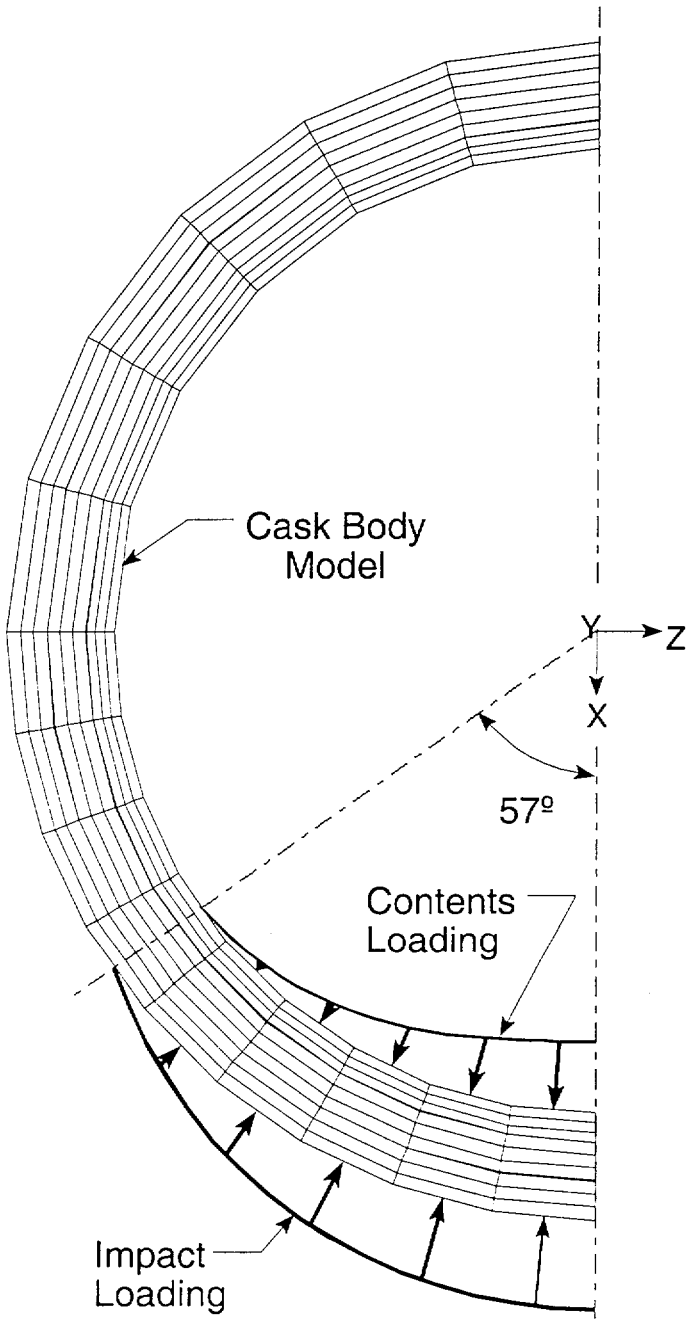

Figure 2.10.2.1-2 View of Cask Model Showing Pressure Distribution for Side-Drop Analysis

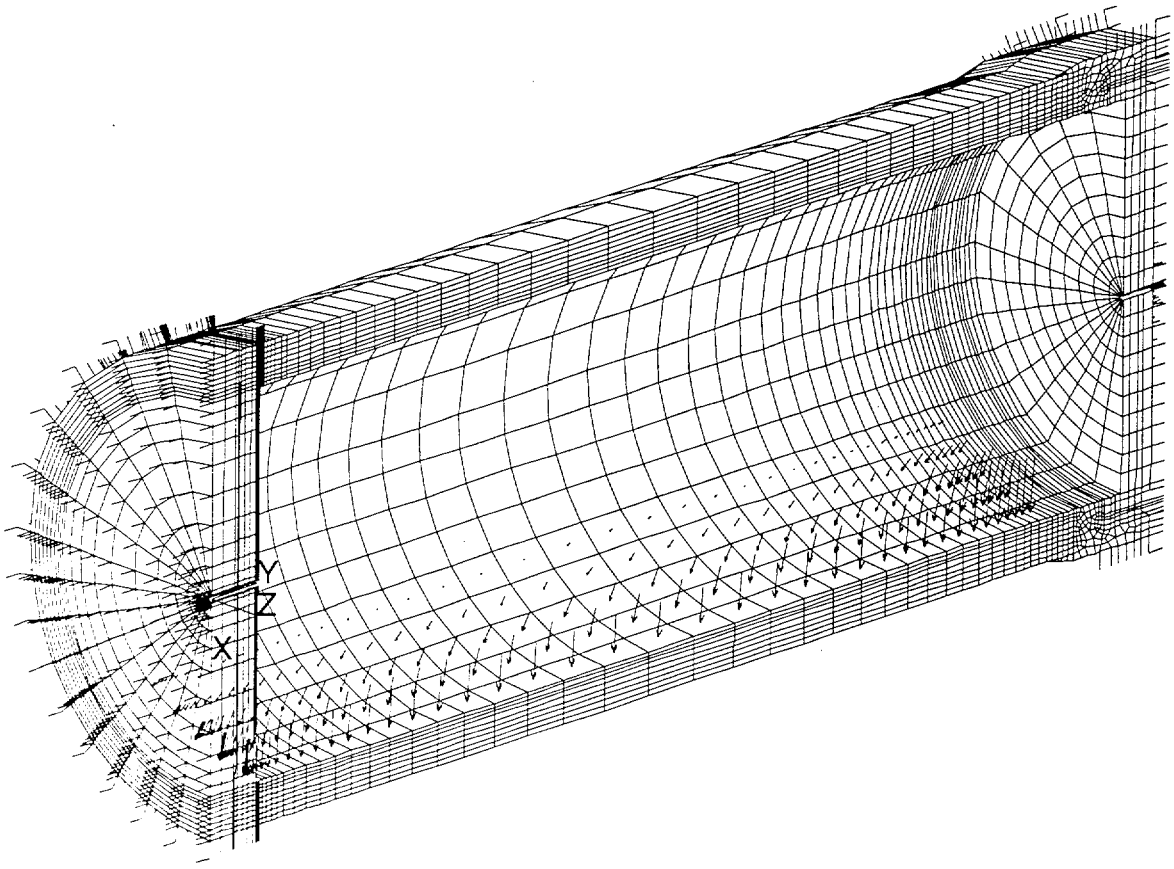

2.10.2.2 Post-Processing of Results

Table 2.10.2.2-1 defines the components and temperatures used in the processing of the cask body results. The post-processing evaluates stress sections at every circumferential node (every 10° from 0 to 90° and every 15° from 90 to 180°) at each axial location (see Figures 2.10.2.2-1 through 2.10.2.2-4 for diagrams of section locations) and determines the section stresses where the maximum stress intensity occurs. In addition, the angle where the maximum stress intensity occurs is noted.

Table 2.10.2.2-2 provides a listing of the locations of the sections used in the stress evaluations. These coordinates correspond to the model coordinate system. Sections are generated at circumferential locations around the cask body (every 10° from 0 to 90° and every 15° from 90 to 180°) based on these coordinates at 0°. Figures 2.10.2.2-1 through 2.10.2.2-4 depict the sections used in the post-processing of the cask body results.

The allowable stress limit criteria for containment and non-containment structures are provided in Section 2.1.2. These criteria are used to determine the allowable stresses for each cask component. The maximum operating temperature within a given component is conservatively used to determine the allowable stress throughout that component. Note that higher temperatures result in lower allowable stresses. The set of cask component allowable stress values is determined for the most conservative temperature conditions that occur in the cask during normal conditions (100°F thermal heat condition evaluated in Section 3.4).

Figure 2.10.2.2-1 Lower Cask Body Section Locations

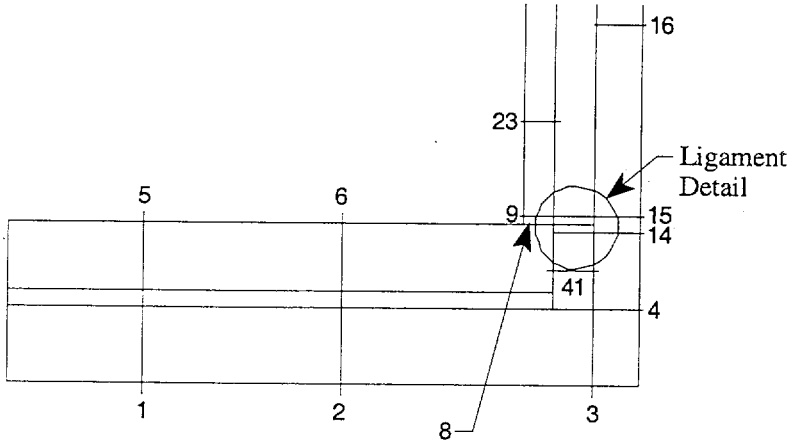

Figure 2.10.2.2-2 Sections Through Cask Body Ligaments

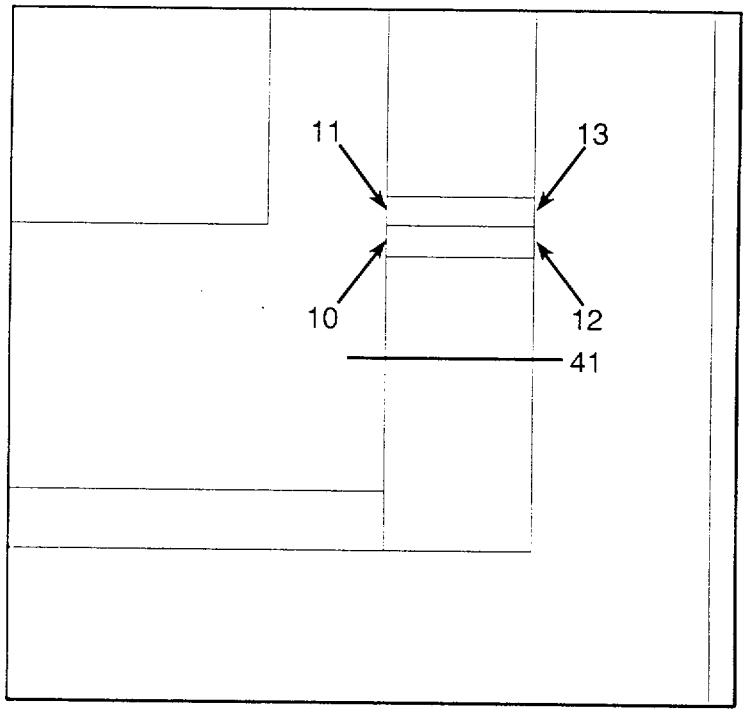

Figure 2.10.2.2-3 Cask Body Sections at Center

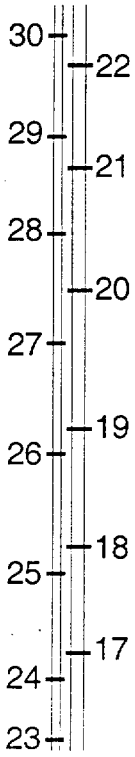

Figure 2.10.2.2-4 Cask Body Sections in Upper Cask

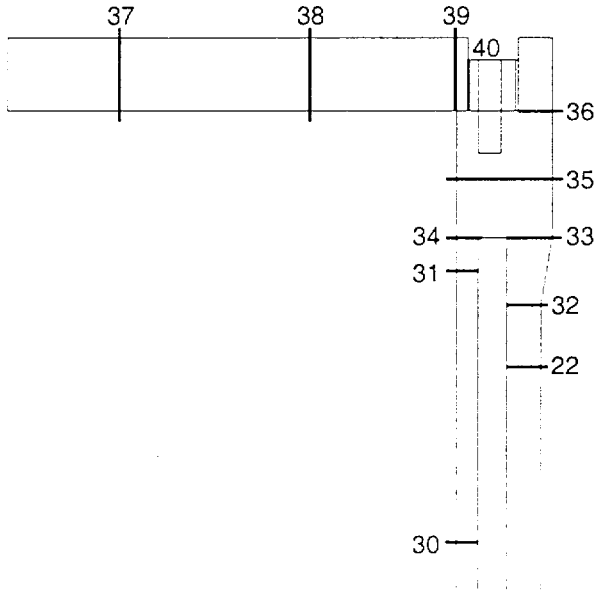

Table 2.10.2.2-1 Component Section and Temperature Definition

Component Number	Component	Section Numbers	Temperature (°F)
1	Bottom Plate	1-4	218.0
2	Bottom Forging	5-9	225.4
3	Ligaments	10-13	367.7
4	Outer Shell (bottom)	14-15	322.6
5	Outer Shell (middle)	16-21	322.6
6	Outer Shell (top)	22	322.6
7	Inner Shell (bottom)	23	367.7
8	Inner Shell (middle)	24-30	367.7
9	Inner Shell (top)	31	367.7
10	Top Forging	32-36	274.7
11	Lid	37-40	267.9
12	Bottom Ring	41	225.4

Table 2.10.2.2-2 Stress Section Locations

	Node 1 Coordinates (in.)			Node 2 Coordinates (in.)		
Section No.	X	Y	Z	X	Y	Z
1	11.268	0	0	11.268	5.0	0
2	22.537	0	0	22.537	5.0	0
3	38.555	0	0	38.555	5.0	0
4	38.555	5.0	0	41.305	5.0	0
5	11.268	6.0	0	11.268	10.25	0
6	22.537	6.0	0	22.537	10.25	0
7	33.805	6.0	0	33.805	10.25	0
8	33.805	10.25	0	35.805	10.25	0
9	33.805	11.0	0	35.805	11.0	0
10	35.805	9.5	0	35.805	10.25	0
11	35.805	10.25	0	35.805	11.0	0
12	38.555	9.5	0	38.555	10.25	0
13	38.555	10.25	0	38.555	11.0	0
14	38.555	9.5	0	41.305	9.5	0
15	38.555	11.0	0	41.305	11.0	0
16	38.555	35.019	0	41.305	35.019	0
17	38.555	59.037	0	41.305	59.037	0
18	38.555	83.056	0	41.305	83.056	0
19	38.555	107.074	0	41.305	107.074	0
20	38.555	131.093	0	41.305	131.093	0
21	38.555	155.111	0	41.305	155.111	0
22	38.555	179.13	0	41.305	179.13	0
23	33.805	16.0	0	35.805	16.0	0
24	33.805	32.016	0	35.805	32.016	0
25	33.805	53.782	0	35.805	53.782	0
26	33.805	75.549	0	35.805	75.549	0
27	33.805	97.315	0	35.805	97.315	0
28	33.805	119.081	0	35.805	119.081	0
29	33.805	140.848	0	35.805	140.848	0
30	33.805	162.614	0	35.805	162.614	0
31	33.805	184.38	0	35.805	184.38	0
32	38.555	185.13	0	41.305	185.13	0
33	38.555	191.0	0	42.63	191.0	0
34	33.805	191.0	0	35.805	191.0	0
35	33.805	196.25	0	42.63	196.25	0
36	39.18	201.5	0	42.63	201.5	0
37	13.028	201.5	0	13.028	208.0	0
38	26.057	201.5	0	26.057	208.0	0
39	33.805	201.5	0	33.805	208.0	0
40	34.93	201.5	0	34.93	206.0	0
41	35.805	8.0	0	38.555	8.0	0

THIS PAGE INTENTIONALLY LEFT BLANK

2.10.3 Confirmatory Testing Program – UMS® Impact Limiters and Attachments

This section provides a description of the scale model test program, which was carried out as confirmatory support of the analysis and licensing effort for the design qualification of the NAC-UMS® Transport Cask impact limiters and attachments. More specifically, the purpose of the UMS® Scale Model Test Program was to confirm (1) the capability of the impact limiters to restrict the deceleration of the cask to the design limits used in the structural evaluation of the transport cask; and (2) the impact limiters remain attached to the cask body.

The test results confirm the impact limiter analysis and provide physical evidence that UMS® impact limiters will function as designed to limit the deceleration applied to the cask and its contents and to remain attached to the transport cask during an accident condition impact.

The scale model test program for the NAC-UMS® impact limiters included: (1) 30-foot drops of a quarter-scale model of the UMS® cask in the top end, side, and top corner impact orientations and (2) a static compression test for the top end drop cask orientation. The total weight of the model and scaled impact limiters corresponded to the full-scale 260,000 pounds design limit of the NAC-UMS® Transport Cask.

This section presents the scale model impact limiter and attachment drawings, the test descriptions, test results, and conclusions that demonstrate the design qualification of the impact limiters and their attachments.

2.10.3.1 Confirmatory Testing Program Results Summary

Three 30-foot drop tests were performed at the drop test facility at the Oak Ridge National Laboratory. The cask orientations for the three drop tests were:

1. Top end drop
2. Side drop
3. Top corner drop (CG over corner)

Since the purpose of the UMS® Drop Test Program was to confirm the design of the UMS® transport cask impact limiters and attachments, the design of the scale model package focused on the limiters and their attachments to the cask body. The scale model body was designed to accurately represent the interface between the cask body and the impact limiters and the weight, CG and mass moment of inertia of the cask body and its contents. The use of a scale model is appropriate to perform these tests and the scale selected for the tests was a quarter-scale model. Using a smaller scale model would present fabrication difficulties, while use of a larger scale model would increase the drop pad requirement (mass and geometric size). The drop pad at ORNL meets the requirement of the IAEA to simulate an unyielding surface for the UMS® quarter-scale model. The test data consisted of measurements of the deformations of the impact limiters, the package accelerations, and inspection of the retaining rods. Impact limiter measurements were performed before and after each test to determine the crush depth of the impact limiters. The measured crush depths are used to demonstrate that the impact limiter design calculations are bounding. The accelerations are recorded by accelerometers attached to the model body. The accelerometers are positioned and oriented so that a single accelerometer would record the vertical acceleration of the model. The acceleration data obtained from the accelerometers contained contributions to the acceleration signal that were extraneous based on the frequencies of the contributions. For this reason, the acceleration data was further processed to extract accelerations, which were compared to the accelerations calculated by NAC's RBCUBED impact limiter analysis program. Additional test documentation included high speed photography that confirmed the orientation of the cask at impact and still photographs of the scale model, impact limiters, and the impact limiter retaining rods. Post-test inspection of the retaining rods and the impact limiters confirmed that the impact limiters have a significant margin of safety for remaining attached to the cask body during and after a 30-foot drop test impact.

The resulting 30-foot drop test accelerations (divided by four to convert them to an equivalent full-scale model) and crush strokes (multiplied by four to convert them to a full-scale model), along with the RBCUBED calculated design-basis values, are presented as follows for the UMS® transport cask impact limiter design. The values for the RBCUBED calculated maximum design basis crush stroke and maximum design basis acceleration are obtained from Table 2.6.7.5-4.

Drop Test	Maximum Scale Model Impact Limiter Crush Stroke x 4 (in)	Maximum Scale Model Package Acceleration/4 (g)	RBCUBED Calculated Design Basis Crush Stroke (in)	RBCUBED Calculated Design Basis Acceleration (g)	Package Design Basis Acceleration (g)
Top end drop	8.0	51.8	14.7	46.3	60
Side drop	11.8	51.1	13.0	52.1	60
Top corner drop	12.8	30	27.7	47.8	60

In reviewing the 30-foot side drop test acceleration results, some positive accelerations were noted.

These results of the UMS® Drop Test Program confirm the design-basis accelerations used for the evaluation of the UMS® transport cask:

1. The scale model body did not impact the pad surface confirming that the UMS® transport cask possesses a sufficient depth of wood to absorb all of the energy of a 30-foot drop in any orientation.
2. The maximum accelerations determined from the scale model tests are less than, or equal to, the design-basis values used to evaluate the UMS® transport cask components for a 30-foot drop accident.
3. The impact limiters remain attached to the transport cask body.

2.10.3.2 Description of the UMS® Cask Scale Model for the 30-Foot Drop Tests

A quarter-scale model was used for the confirmatory testing of the UMS® impact limiters and attachments. The quarter-scale model was only required to represent the materials and physical dimensions of the impact limiters and their attachments to the cask body in conjunction with the appropriate cask body weight, center of gravity, and attachment interface dimensions. For this reason, a 20-inch diameter Schedule 160S stainless steel pipe was used to represent the cask body. To properly represent the weight and the location of the center of gravity of the cask, and the mass moment of inertia, a series of weight disks (circular steel plates) were positioned inside the pipe. Three of the weight disks were 4 inches thick while a fourth was 4.5 inches thick. The actual location of the plates and the corresponding axial location of the center of gravity are shown in the model drawing 790-301, Sheets 1 through 3.

The total weight of the quarter-scale model including the impact limiters was 4,033 pounds which closely approximates $(1/4)^3 = 1/64$ of the full-scale transport cask weight of 260,000 pounds.

The overall length of the model (without the impact limiters) is 52.31 inches, which is comprised of a 41.31-inch length of 20-inch diameter pipe welded to a 6-inch thick plate at the top end and a 5-inch thick plate at the bottom end. Both plates are Type 304 stainless steel. The top end plate was machined to represent the scaled outside diameters and axial dimensions of the upper forging and the neutron shield top plate. A 16.06-inch diameter through hole was machined in the center of the top end plate of the model body. Also, a recess was machined into the top end plate to accommodate the placement of the bolted lid. Two steel bars, scaled to represent the diameter and length of the cask lifting trunnions, were welded in the appropriate locations on the outside diameter of the top end plate.

The model lid outer diameter and lid bolt recess diameter are quarter-scale dimensions, but the lid thickness and the number of bolts were not scaled. Scaling of the lid thickness and the bolts was not necessary because the purpose of the lid and bolts was only to back the upper impact limiter and to retain the dummy weights in the cavity of the model cask.

The 5-inch thick bottom end plate of the model was machined to represent the scaled outside diameters and the axial dimensions of the bottom end of the UMS® cask, including the neutron shield bottom end plate. The bottom plate thickness is not scaled since it is only required to provide backing area for the bottom impact limiter and to contribute to the weight and CG location of the scale model.

The four interior circular weight disks were positioned by spacers (cylinders), but were not attached (welded or bolted) to the spacers or the body of the scale model. The spacers were fabricated from 16-inch diameter Schedule 160 pipe, which provided adequate strength to maintain the position of the weight disks. The lengths of the spacers were designed to properly

position the CG of the scale model package. This ensures that the load distribution to the model impact limiters for the drop tests is representative of the loading that would occur on the full-scale UMS® transport cask.

Since the top end drop and top corner drop tests involve only the top end of the model, there was no need to include a bottom impact limiter on the model for these tests. To ensure that the total scale model package weight and CG are properly represented for the top end and top corner drop tests, a steel plate corresponding to the weight of the bottom impact limiter was designed and fabricated for bolted attachment to the bottom end of the model.

The model impact limiters are quarter-scale representations of the full-scale impact limiters. The redwood and balsa wood used in the model limiters meets the same specifications that are defined for the full-scale UMS® transport cask in this SAR. The wood section shapes, joints, and bonds of the scale model impact limiters duplicate those of the full-scale impact limiters. The grain orientation of the redwood and balsa wood in the scale model impact limiters is identical to that as designed in the full-scale UMS® transport cask impact limiters. The scale model impact limiter shells were fabricated from 16 gauge (0.0625-inch thick) Type 304 stainless steel sheets and the screw tubes which serve as the penetrations for the impact limiter retaining rods were fabricated from 0.035-inch thick, 0.75-inch diameter tubes. Each model impact limiter is attached to the cask by sixteen quarter-scale retaining rods fabricated from SA-193 Grade B8S stainless steel.

The model impact limiter shells - i.e., material thickness, geometry, and welds - are appropriately quarter-scale. The diameter of the screw tubes is quarter-scale, but the tube wall thickness is full-scale due to fabricability and material availability limitations. The use of the thicker tube is considered to be conservative, since it tends to increase the stiffness of the limiter, if it has any effect at all. The axial stiffness of the model screw tube is increased by a factor of four, and the rotational stiffness of the screw tube attached to the impact limiter shell is also significantly increased. The effect of the tube thickness on the drop test results is insignificant, since the tubes are not located in the primary crush regions of the impact limiter.

2.10.3.3 Acceptance Criteria for Model Performance

Acceptance criteria was established only for the scale model impact limiters and their attachment components, since the purpose of the test program was to confirm their performance capabilities. The function of the scale model impact limiters is to limit the deceleration of the scale model package during the 30-foot drop event, while remaining firmly attached to the cask body. The impact limiter acceptance criteria requires that:

1) The crush stroke be limited to prevent an impact of the cask body on the impact surface.

2) The accelerations be limited to be less than or equal to those used in the design analysis.

3) The impact limiters remain attached to the cask body and in position after the impact event.

2.10.3.4 Equipment and Instrumentation

All drop tests were performed at the Oak Ridge National Laboratory in Oak Ridge, Tennessee. The pad which functions as the essentially unyielding impact surface at this facility meets IAEA requirements. The pad consists of concrete and armor plate and the total weight is approximately 60 tons, which is approximately 30 times the test weight of the UMS® quarter-scale model. The 60-ton weight of the pad is considered to be conservative, since the pad rests on a 3-foot diameter column of reinforced concrete that extends vertically down 10 feet to bedrock. The armor plate, which is the impact surface of the pad, is 6-inch thick steel plate.

Lifting and dropping the model was performed with a mobile crane with a single point suspension system, in conjunction with an explosive cable cutting release. This release mechanism allowed the free fall of the package to be initiated in an unimpeded fashion with minimum perturbation to the angular position of the model or its lateral position with respect to the pad surface.

To assess the model performance with respect to the acceptance criteria, a set of basic data was required to be collected throughout each test. This data included:

1) Acceleration data – to determine the maximum impact acceleration of the cask. All of the accelerometers used in the drop tests were the same model and they were calibrated to NIST traceable standards corresponding to frequencies ranging from 2K Hz to 10K Hz. Individual accelerometers were mounted on steel blocks welded to the cask model; the actual locations of the blocks are shown on Drawing 390-301, Items 23, 24, and 25. All of the accelerometers were positioned to record only the vertical acceleration component. Therefore, a combination of time histories was not required to compute the resultant vertical acceleration. The number and locations of the accelerometers were tailored to each individual drop test, as shown below.

Drop Test	Number of Accelerometers	Accelerometer location
Top end drop	3	All three accelerometers were located 11 inches from the top end of the model and were spaced circumferentially at 60°, 150°, and 270° positions.
Side drop	4	A set of accelerometers was located 11 inches from each end of the cask body. Each set was comprised of two accelerometers, located 180° apart circumferentially, in the same horizontal plane as the center of gravity.
Top corner drop	3	Two accelerometers were located 8 inches from the top end of the cask body and 180° apart, circumferentially. A third accelerometer was located 12.5 inches from the top end of the cask body and was at the same circumferential location as one of the other accelerometers.

The acceleration time histories were stored electronically, which permitted them to be filtered after the tests were completed. The unfiltered data consisted of acceleration (in units of gravity "g") points corresponding to time increments of 30.5 microseconds.

2) Impact limiter deformation data – to evaluate the behavior of the impact limiters, the crush stroke for each orientation and the condition of the limiter attachment to the model body after each test. After each test the impact limiters were inspected to determine the amount of deformation that had occurred (the crush stroke) and to determine the condition of the retaining rods. Photographs were taken to record the post-test condition of the impact limiters and retaining rods.

3) High speed photography – to review and assess the actual angle of impact and the behavior of the cask body and impact limiters during the impact.

Two high speed cameras were used to record the behavior of the quarter-scale model as it impacted the target surface. Film speeds were 500 frames/second or greater. One camera was positioned and focused to obtain a close up view of the impact deformation. The other camera was focused to record an overall view of the impact and to verify the orientation of the cask as the impact was initiated.

2.10.3.5 Filter Frequency Identification for the Accelerometer Data

Accelerometers can be sensitive to high frequency vibrations in parts of the structure that could be considered to be remote from the actual location of the accelerometer. The purpose of the accelerometer is to determine the rigid body deceleration of the model body during the impact, not the high frequency vibration dynamic response of other components of the model body. High frequency vibrations typically correspond to mode shapes, which are excited by the impact.

The electronically stored acceleration time histories include the peaks corresponding to the high frequency vibration dynamic response of the spacers and weight disks inside the model body. To reduce the effects of the high frequency responses in the acceleration time histories, the acceleration time histories are filtered, i.e., a filter frequency is determined, such that acceleration time points corresponding to the high frequency vibration dynamic responses are effectively removed from the data. Since these high frequency vibration dynamic responses are a function of the loadings on the model body, separate filter frequencies are determined and applied for each of the different drop orientations. There are two basic orientations of the model body for the drop tests; the end drop orientation and the side drop orientation. The corner drop impact orientation produces an axial loading on the cask components in a manner similar to the end drop and the oblique drop impact orientation is, likewise, similar to the side drop.

2.10.3.5.1 End Drop Orientation Filter Frequency Determination

While the end drop orientation does provide excitation to the weight disks and spacers, the lowest frequency of concern corresponds to the longitudinal mode which combines the mass of the shell weldment (2,107 pounds) and the lid (157 pounds) and the bottom test weight (134 pounds). The total weight (W) of these components is W = 2,398 pounds. The mass (m) is computed as 2,398/386.4 or 6.21 lb-sec^2/inch. The equivalent axial stiffness (K) of the system is;

$$K = A \times E/L$$

Where

A = cross sectional area of the model body = 111.5 in^2

E = modulus of elasticity of Type 304 stainless steel (70°) = 28.3 E6 psi
L = distance from the 5-inch thick bottom plate to the inner surface of the 2-inch thick model lid = 45.3 inches

Substituting:

K = (111.5)(28.3+E6)/45.3 pound/inch
K = 69.7E+6 pound/inch

The corresponding natural frequency is

$f = (1/2\pi)\sqrt{K/m}$ (Hz)
f = 533 Hz

A filter frequency of 550 Hz is used to avoid including the high frequency vibration dynamic response of the shell of the body of the model.

2.10.3.5.2 Side Drop Filter Frequency Determination

In the side drop (horizontal) orientation the load in the model body must be transferred to the impact limiters attached to the ends of the model body. The fundamental mode shape for the side drop corresponds to a beam with free-free end boundary conditions. Since the length to diameter ratio is approximately 2, the flexibility due to shear must be included. This is accomplished by computing the natural frequency due to the shear and the corresponding frequency due to flexure and then combining them.

The natural frequency for the mode shape due to shear for free-free end boundary conditions, (fs), is given by:

$$fs = \frac{\lambda}{2\pi L}\sqrt{\frac{k'G}{\rho}}$$

Blevins[50], Table 8-15, Case #1

Where:

$\lambda = \pi$ (Blevins, Table 8-15)

L = distance between supported ends by the limiters = 41.3 inches

k′ = shear coefficient = 0.54

G = shear modulus of elasticity = (28.3E+6)/((2) (1+v)) = 10.9 E+6 psi

ρ = effective mass density = 2281 /(111.5*41.3)/386.4 = 0.00128 lb-sec^2/in

Note that the 2,281 pounds include the weight of the 20-inch pipe (1,340 pounds) plus the 4-inch and 4.5-inch thick weight disks (941 pounds).

The shear coefficient, k′, is dependent on the cross sectional shape of the model body:

$$k' = \frac{6(1+v)(1+M^2)^2}{(7+6v)(1+M^2)^2+(20+12v)M^2}$$

Blevins, Table 8-14

Where:

M = b/a

v = Poisson's ration = 0.3

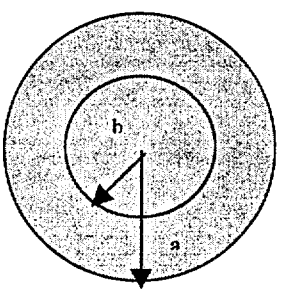

For a 20-inch diameter Schedule 160S pipe

b = 8.032 in

a = 10.0 in

Therefore:

k′ = 0.54

Substituting,

fs = 821 Hz

The natural frequency for the mode shape due to bending for the free-free end boundary conditions, (fb), is given by:

$$fb = \frac{\lambda^2}{2\pi L^2}\sqrt{\frac{EI}{\rho'}}$$ Blevins, Table 8-1

Where:

$\lambda = \pi$

L = 41.3 inches

$$I = \frac{\pi}{64}(D_0^4 - D_i^4) = \frac{\pi}{64}(20^4 - 16.06^4) = 4{,}588 \text{ inch}^4$$

E = 28.3E+06 psi

ρ' = effective mass per unit length of beam

= 2,281/41.3/386.4 = .143 lb-sec^2 / in^2

Substituting,

fb = 877 Hz

In accordance with Blevins, the shear and bending mode frequencies are combined as:

$1/fc = 1/fs + 1/fb$

or

fc = 424 Hz

The filter frequency for the side drop is selected to be 450 Hz.

2.10.3.6 Results/Evaluation for the 30-Foot Top End Drop Test

The 30-foot top end drop was performed first. Prior to lifting the scale model package to the 30-foot drop height, the torque for the retaining rods and nuts was verified to ensure that the torque specifications were met.

Two high speed cameras were used to record the top end drop impact. In reviewing the high speed camera results, it was determined that the high speed camera recording the detailed view of the impact limiter crush had malfunctioned, causing the film to be under-exposed. The high speed camera used to record an overall view of the drop test showed that the scale model's longitudinal axis was essentially vertical and that the model impacted the drop test facility pad as targeted. The scale model remained upright during and after the impact. The high speed camera also showed that the model rebounded an estimated 18 to 24 inches back up into the air after the initial 30-foot drop impact.

2.10.3.6.1 Impact Limiter Deformation and Attachment Data

After the top end drop test the scale model package was lifted off the ground to remove the top end impact limiter. Removal of the top impact limiter from the cask body required that two hydraulic jacks be inserted between the impact limiter and the bottom end plate to force the impact limiter off the cask body. During the impact limiter removal, it was noted that several retaining rods were broken. The retaining rods were removed from the impact limiter and inspected, whereupon it was observed that the rods had undergone plastic buckling, having been confined to the screw tube, which is surrounded by redwood oriented in its strongest direction.

The impact limiters were then sectioned by sawing into approximately four equal quarter-sections to permit observation of the deformations of the impact limiter shells in the crushed region of the impact limiter directly under the cask. The crush depth of the four quarter sections was measured, and the average crush stroke was found to be 2.04 inches. The post-test inspection of the scale model top impact limiter indicated that the "pseudo" top neutron shield plate on the model body had contacted the impact limiter and had left an indentation on the outer top surface of the impact limiter. The pretest nominal gap between the top surface of the impact limiter and the top neutron shield plate is (4.61 - 2.75) inches, or 1.86 inches. The observed

average crush depth of 2.04 inches corroborates the observed indentation, since the associated model movement would have closed the 1.86 inch pretest gap and resulted in the top surface indentation as observed.

2.10.3.6.2 Accelerometer Data

The unfiltered accelerometer traces were electronically stored to permit filtering after the tests. Three accelerometer traces were obtained and a portion of one of those is shown in Figure 2.10.3-1. The trace shown captured the initial impact of the scale model. An initial observation of the trace is the significant "noise" vibrations associated with the accelerations. Additionally, inspection of the traces showed that the initial acceleration change was over 500 g, which occurred over three time points and the time between individual time points in the trace is 30.5 microseconds. Thus, the trace suggests that the acceleration achieves this initial value in approximately 60 microseconds and then begins to subside (from the maximum value). The impact limiter is evaluated to determine whether there is a basis for this large accelerometer response. A cursory review of the immediate load paths in the impact limiter does not support the ability to generate this type of loading. Four considerations are discussed below.

1. If the scale model retaining rods (SA-193 Grade B8S) did not buckle, but instead, initiated metal flow, the load path through the rods would be an immediate load path from the scale model to the impact plane. This immediate load path could arise, since the retaining rods attach directly to the scale model lid.

   The immediate acceleration (A_{flow}) in units of gravity would be the ratio of the product of the total area of the retaining rods multiplied by the dynamic flow stress of the material to the weight of the scale model package.

   $$A_{flow} = N(\pi/4)(d)^2(\sigma_d)/W = 22.2 \text{ (g)}$$

   Where:

   σ_d = (95+50)/2 = 72.5 ksi (the average of the tensile and yield strengths at 70°F for SA-193 Grade B8S)

W= model weight acting on the retaining rods = 3,945 pounds (3,811 pounds for the model body and 134 pounds for the test weight representing the bottom impact limiter)

N= number of retaining rods = 16 rods

d= diameter of the retaining rod = 0.31 inch

2. If the scale model impact limiter shell did not buckle at the 18.7-inch inner recess diameter, but instead, initiated metal flow, this section of the shell would be an immediate load path between the model lid and the impact plane. Before other sections of the model impact limiter shell can deform in the axial direction, the load must be transferred through the inner recess shell first.

The immediate acceleration (A_{flow}) in units of gravity would be the ratio of the product of the total area of this section of the model impact limiter shell and the dynamic flow stress of the material to the weight of the scale model package.

$$A_{flow} = (\pi)(18.7)(.06)(52,500)/3,945 = 46.9 \text{ (g)}$$

Where:

d = Thickness of the scale model impact limiter shell is 0.06 inch

σ_d = (75+30)/2 = 52.5 ksi (the average of the tensile and yield strengths at 70°F for Type 304 stainless steel)

W = model weight = 3,945 pounds (3,811 pounds for the model body and 134 pounds for the test weight representing the bottom impact limiter)

3. If the entire area of the redwood in the scale model impact limiter (outside diameter = 31 inches) would instantly initiate crushing, the force applied to the model for deceleration would be the ratio of the product of the cross-section area of the impact limiter and the intial crush strength of the redwood to the weight of the scale model package.

$$A_{flow} = (\pi/4)(31)^2(640)/4,078 = 118 \text{ (g)}$$

Where:

d = Outer diameter of the model impact limiter shell = 31 inches

σ_d = The initial crush strength of the redwood in the direction perpendicular to the grain = 640 psi

W = model weight acting on the top impact limiter bolts = 4,078 pounds (3,811 pounds for the model body, 133 pounds for the top impact limiter, and 134 pounds for the test weight representing the bottom impact limiter).

4. If the redwood in the backed area of the model impact limiter (area directly under the model cask body) is considered as an elastic component only, the minimum immediate response time can be computed using the fundamental mode of the mass of the model acting on the redwood.

The total weight (W) of these components is W = 3,945 pounds (3,811 pounds for the model body and 134 pounds for the test weight representing the bottom impact limiter). The corresponding mass (m) is computed as 3,945/386.4 or 10.21 lb-sec^2/inch. The equivalent axial stiffness (K) of the system is:

$$K = A \times E/L = 48.1 \text{ E6 pounds/ inch}$$

Where:

A = cross sectional area (back area) of the redwood = $(\pi/4)\ (18.7)^2 = 274.6$ in.^{2}

E = modulus of elasticity of redwood = 1.4 E6 psi

L = 8 inches (10.75-2.75)

The corresponding natural frequency is:

$$f = (1/2\pi)\sqrt{(K/m)}\ (Hz)$$

$$f = 345\ Hz$$

Based on this natural frequency, the accelerometer trace should indicate that for the initial peak the acceleration varies from a positive maximum value to a negative one, corresponding to the signal period/2 or (1/345)/2 = 1,449 micro-seconds. Since the time points on the acceleration trace are 30.5 micro-seconds, there should be approximately 48 (1,449/30.5) acceleration points showing the motion from zero to the initial maximum negative value. The accelerometer traces do not demonstrate this hypothesis. Thus, the use of the elastic properties for the redwood is significantly over-conservative.

It is concluded from the foregoing four considerations that these conservative calculations confirm that the initial acceleration values are a result of high frequency effects in the accelerometer and, therefore, filtering the acceleration data is appropriate. The filtered results do not show the steep rise time nor the associated level of accelerations that are present in the unfiltered trace. The filtered result is superimposed on the unfiltered trace in Figure 2.10.3-2. The filtered data was integrated to obtain the velocity of the model body and was shown to match the 527.4 in/sec initial velocity. The peak acceleration is shown to be 51.8 g for the full-scale UMS® package.

2.10.3.7 Static Crush Test for the End Drop Orientation

To further confirm the design of the UMS® impact limiters, a static crush test in a top end drop orientation was conducted. The purpose of the static test was to: 1) identify any potential initial stiffness in the impact limiter, which would corroborate the large accelerations observed on the accelerometer traces during the early part of the 30-foot top end drop impact; and, 2) indicate any effect of the thick-walled screw tubes on the impact limiter crush force in the end drop orientation.

To provide test data for these objectives, two tests were performed:

1. Static Test 1 used an uncrushed section of the quarter-scale impact limiter design exactly as tested in the 30-foot end drop test.
2. Static Test 2 used an uncrushed section of the quarter-scale impact limiter without the 0.035-inch thick screw tubes, but otherwise identical to the end drop test limiter.

For the UMS® impact limiter design in the end drop orientation, the grain direction of the redwood is perpendicular to the direction of crush. The retaining rods and the screw tubes are equally spaced every (360°/16), or 22.5°. The static crush test used a 45° section of a model impact limiter, which included two retaining rods and two screw tubes. Thus, the lateral circumferential edges of the test section correspond to the circumferential midpoint between two bolts. For a 45° section, the boundary conditions at the edges require that all displacements perpendicular to the side be zero. For the thin impact limiter shell, the additional requirement of constraining certain rotation components (as would be performed in an analytical evaluation) is required. For structures developing their strength from flexure, this is a significant restraint condition, but the strength of the impact limiter shell is due to membrane stiffness not flexural stiffness. Therefore, relaxing the rotation condition at the edge of the section of the model impact limiter for this test has no effect on the results.

Additionally, the model lid must remain horizontal as it moves into the model impact limiter, just as in the case of an end drop. Two new retaining rods and associated nuts were used to connect the 45° section of the impact limiter to a 45° section of the model lid. The section of the model lid used in the static crush test included the recess for the lid bolts. The static test 45° uncrushed

section model used the same design and materials for the retaining rods and lid bolts as used in the 30-foot end drop test.

The test 45° section of the scale model impact limiter was inserted into the static test fixture between the lid, which connected to the upper head of the testing machine, and a bottom plate representing the impact plane. The details of the fixture are shown in NAC Drawing 790-401, "Crush Fixture, End Drop, UMS® Testing," Sheets 1 through 3.

In the static test fixture, the lateral restraints were provided by 1-inch thick steel plates supported by 1-inch thick, triangular gussets. The sides of the fixture and the gussets were welded to the 1-inch thick base plate. All welds were fillet welds and all were located outside the region containing the 45° section of the model impact limiter. To ensure that the 45° section of the impact limiter did not move radially outward in the test fixture during the test, a curved bar (rectangular cross section of 0.18 inch by 1 inch) was fitted around the outer surface of the model impact limiter section and bolted to the lateral plates of the test fixture.

The recorded test data included the force-deflection curve for the 45° section of the model limiter, as well as the displacements at the lateral sides of the test fixture and the radial displacement of the limiter.

The static tests were conducted at Precision Components Corporation in York, Pennsylvania, using a Tinius Olsen testing machine capable of applying 500,000 pounds of compressive load. The use of this equipment established a slow compression speed representative of a static test. Thus, the crush strengths observed in the test correspond to static crush strengths. To account for the dynamic effect in crushing the redwood, the static forces are factored by 1.058 (Section 2.6.7.5.3). Since the static test uses an $1/8^{th}$ section (45°) of the quarter-scale model impact limiter, the total force (F_{total}) generated for a full quarter-scale model is determined as eight (8) times the force value observed in the static test. The corresponding acceleration for the quarter-scale model is (F_{total}/4,033), where 4,033 pounds corresponds to the minimum weight of the quarter-scale model.

The energy absorbed ($E_{limiter}$) by the model impact limiter section during the static test is computed by integrating the area under the force-deflection curve. In the end drop orientation,

the crush depth of the limiter must be included in the total potential energy (E_{total}) calculation for a 30-foot drop.

$$E_{total} = (4,033)(360+\delta),$$

Where:

W = model weight = 4,033 pounds
D = drop height = 360 inches
δ = the crush depth.

The force applied in the static crush test was increased until the energy absorbed by the model impact limiter section ($E_{limiter}$) was equivalent to, or greater than, the total potential energy (E_{total}) of the quarter-scale model for a 30-foot drop.

2.10.3.7.1 Static Test Results

1. The lateral displacements of the sides of the test fixture were measured to be less than 0.001 inch and the outward radial displacement of the test article was less than 0.1 inch. These values indicate that the boundary conditions were satisfied.

2. No malfunctions of the equipment or instrumentation were experienced.

3. The force-deflection curves for the model impact limiter sections used in Static Test 1 and Static Test 2 are shown in Figures 2.10.3-3 and 2.10.3-4, respectively. These curves include the previously discussed geometry and dynamic load factors of 8 and 1.058, respectively.

4. The following crush and accelerations were determined based on Static Test 1 and Static Test 2. These values correspond to the conditions at the end of the test in which the energy absorbed by the model limiter section equals or exceeds the total potential energy of the scale model for a 30-foot drop. The force values include the geometry and dynamic load factors of 8 and 1.058, respectively.

Static Test	Crush (in) (δ)	Force (kips) (F_{total})	Acceleration (g) (F_{total}/W)
1 (base line case)	3.24	701.7	174
2 (without the screw tube)	3.70	680.0	168.6

2.10.3.7.2 Static Test Observations

1. No initial peaks in the loading were observed for either Static Test 1 or Static Test 2. The crush forces developed in a monotonic manner increasing from zero to the maximum force reported above. During the static tests, there were no mechanical shocks observed in the equipment nor in the floor on which the testing machine was supported.

2. While the screw tubes are a source of significant strength, the initial deformation of the impact limiter does not occur in the region of the screw tubes. The calculated final accelerations for the model impact limiter design with the screw tube was only 3 percent larger than the design without the screw tubes.

3. The axial section of the model impact limiter shell at the 18.7-inch diameter next to the model lid buckled in the same general shape in the static test as in the 30-foot top end drop. Since the crush force developed in a monotonic manner and the mode of deformation between the static and dynamic drops are the same, it indicated that this section of the model impact limiter shell does not deform by plastic flow of the metal and does not contribute to large initial accelerations.

4. The crush and the accelerations reported above for the section of a model impact limiter can be converted to correspond to the full-scale impact limiter by factoring the static test force results by four and the accelerations by 1/4. The factored values are compared to the RBCUBED results from Table 2.6.7.5-2 as follows:

Quarter-Scale End-Impact Static Test	Quarter-scale Crush x 4 (in)	Quarter-scale Acceleration Divided by 4 (g)	RBCUBED calculated Full-scale Crush (Table 2.6.7.5-4) (in.)	RBCUBED calculated Full-scale Acceleration (Table 2.6.7.5-4) (g)
Test 1	13.0	43.5	14.7	46.3
Test 2	14.8	42.2		

For the maximum acceleration case, the Static Test results are enveloped by the RBCUBED analyses.

2.10.3.7.3 Summary of the Static Tests

The results of the static tests indicate that the initial high accelerations observed in the drop tests are a result of accelerometer high frequency effects. The filtered acceleration data more accurately reflects the response of the impact limiter in an end drop impact. Additionally, the static tests confirm the validity of the RBCUBED program analyses of the UMS® impact limiters.

2.10.3.8 Results/Evaluation for the 30-Foot Side Drop Test

The 30-foot side drop was the second drop test to be performed using the UMS® quarter-scale model. Prior to lifting the scale model package to the 30-foot drop height, the torques for the retaining rods and two nuts were inspected to ensure that the torque specifications were met.

Two high speed cameras were used to record the side drop impact. One of the cameras recorded a detailed view of the top impact limiter crush in the area of the trunnion nearest the impact plane. The other camera recorded an overall view of the drop test and confirmed the model's longitudinal axis was effectively horizontal at the time of impact on the drop test pad.

2.10.3.8.1 Impact Limiter Deformation and Attachment Data

After the side drop test, the scale model package was lifted off the ground and placed on a temporary support to remove the impact limiters. Upon removing the upper impact limiter, it was observed that the three retaining rods nearest the impact plane were broken. The remaining 13 of the 16 retaining rods were intact and were still threaded into the model body. Upon removing the bottom impact limiter, it was observed that all of the retaining rods were intact and were still threaded into the model body. These results indicate that both impact limiters remained attached to the cask model during and after the side drop test.

Measurements of the deformed model impact limiter dimensions were obtained after the side drop test, which allowed the crush stroke to be determined. These dimensions are tabulated in the following, along with the ratioed full-scale crush strokes and the crush strokes calculated by the RBCUBED impact limiter program. In order to ratio the quarter-scale model test results to the full-scale design values, the scale model crush stroke test results were factored by 4. The high speed camera, which recorded an overall view of the model impact indicated that during the impact, the limiters rotated (tilted) slightly upward on the ends of the model body. As a result of this rotation, the portion of the impact limiter opposite the impact plane actually was pressed against the end of the model body. This resulted in some nonuniform crushing of the redwood (the redwood positioned between the side of the model and the impact plane). The crush stroke reported below is the maximum crush stroke for the redwood outside the trunnion cutout region.

Quarter-Scale Model Side Impact	Quarter-scale model impact limiter crush (in)	Quarter-scale impact limiter crush x 4 (in)	RBCUBED calculated redwood crush (Table 2.6.7.5-4) (in)
Upper limiter	2.94	11.8	13.0
Bottom limiter	2.86	11.4	13.7

The ratioed crush strokes from the side drop test for the quarter-scale model impact limiters is enveloped by the RBCUBED analysis of the full-scale UMS® impact limiters for a 30-foot side drop accident.

Post side drop test measurements of the upper model impact limiter in the trunnion cutout region indicated that the model impact limiter had experienced nonuniform crushing, which resulted in more crush of the redwood under the trunnion cutout than in the redwood outside the trunnion region. Directly under the trunnion cutout, a 0.31-inch thickness of the impact limiter remained. This resulted in a redwood crush strength larger than that in the remainder of the limiter, but did not constitute an impact of the model cask trunnion with the impact plane. The redwood crushing in the trunnion cutout region was further investigated by sectioning the scale model upper limiter in half, with the saw plane passing through the middle of the trunnion cutout. It was observed that the position of the model trunnion allowed the redwood to be pressed out from under the trunnion. To increase the impact limiter design margin for the side drop, design changes to the impact limiter surrounding the trunnion cutouts were incorporated (refer to Summary of the Side Drop Test in Section 2.10.3.8.2).

2.10.3.8.2 Accelerometer Data

The unfiltered accelerometer traces were electronically stored to permit filtering after the tests. Four accelerometer traces were obtained and a portion of one typical side drop acceleration trace is shown in Figure 2.10.3.5. An initial observation of the trace is that significant "noise" vibrations associated with the accelerations do exist and that filtering of the accelerometer data is appropriate. The filtered result is superimposed on the unfiltered data.

At the beginning of the impact, the scale model package is decelerating and the corresponding accelerations are negative. All acceleration traces show the same initial monotonic increase of the acceleration, in agreement with the high speed photographs which indicates that the model impacted in a near horizontal orientation. The accelerometer traces, even after the filtering of the high frequency content, indicates that a significant positive peak acceleration exists followed by another significant negative peak acceleration. The average of the two sets of accelerometers' (at each end of the model) maximum peaks are listed below along with the results from the RBCUBED impact limiter analysis:

Quarter-Scale Model Side Impact	[redacted]	UMS Quarter-Scale Model Accelerations / 4 (g) Negative Peak	RBCUBED Calculated Full-Scale Negative Acceleration (Table 2.6.7.5-4) (g)
Upper impact limiter	[redacted]	51.1	52.1
Bottom impact limiter	[redacted]	37.9	48.6

To understand the behavior of the UMS® scale model package during the side drop impact and the associated acceleration data, the quarter-scale model of the NAC-STC (Docket No. 71-9235) was compared to the UMS® quarter-scale model. Significant features of the two models are:

Quarter-Scale Model Comparison		
Item	NAC-UMS®	NAC-STC
Axial length of overlap of the model body and the impact limiter	2.75 inches	3.0 inches
Radial thickness of the upper impact limiter in the backed area for the side drop	4.7 inches	4.6 inches
Impact limiter energy absorbing material for a side impact	Redwood with grain parallel to crush direction	Redwood with grain parallel to crush direction
Outer diameter of limiter	31 inches	31 inches
Method to represent the contents weight in the scale model	Four weight disks with an average of 235 pounds for each weight disk	26 weight disks with an average weight of 49 pounds for each weight disk
Scale model diameter in the overlap region of model body and upper impact limiter	21.3 inches	21.7 inches
Model Weight	4,033 pounds	3,906 pounds
Apparent duration of the impact for the side drop (obtained from the acceleration traces)	18 milliseconds	9.3 milliseconds

Quarter-Scale Model Comparison		
Item	NAC-UMS®	NAC-STC
Occurrence of positive acceleration peak in the side drop impact	Yes (199 g)	No
Did the impact limiter remain attached to the model body during and after the side drop test	Yes	Yes
Occurrence of positive acceleration peak in the 75° oblique drop	Not performed	Yes (64 g)
Crush stroke for the bottom limiter for the side drop	2.86 inches	2.16 inches
Crush stroke for the upper limiter for the side drop	2.94 inches	2.04 inches

While minor differences do exist between the impact limiter designs for the NAC-UMS® and the NAC-STC, the most significant difference between the two scale models is the method of representing the weight of the contents. In both side drop tests, the ratios of the upper impact limiter crush to the bottom impact limiter crush are within 10% of each other, indicating that a relatively even distribution of energy absorption was accomplished for both package designs. This indicates that the impact limiters were crushed in the same manner for both packages. The existence of the positive peak in the NAC-STC test only occurs in the 75° oblique drop, which arises due to the conversion of the linear momentum to angular momentum, resulting in the momentary positive acceleration of the top end of the scale model. The top end direction of motion (for the NAC-STC for the 75° oblique) remained in the downward direction during this period of positive acceleration. For a positive acceleration to arise for the NAC-UMS® scale model in the side drop test, a significant inertia force must be generated in the direction opposite that of the impact. The presence of a positive acceleration for the NAC-UMS® scale model side drop test does not imply that the direction of the velocity or the displacement changed during the impact, but rather, it indicates that a delay occurred in completing the energy absorption, as evidenced by the longer time to complete the impact (18 milliseconds for the NAC-UMS® versus the 9.3 milliseconds forhe NAC-STC). Since the impact limiters were bolted to the scale model

bodies for both tests, it should be noted that the only remaining component which could potentially vibrate during the impact are the weight disks. In the NAC-STC scale model, any four weight disks comprise an insignificant contribution, whereas in the NAC-UMS® scale model, the four weight disks are greater than 60% of the weight of the model body which supports them. It is further noted that the NAC-STC scale model contained lead, which contributed to damping out vibrations generated by the weight disks, whereas in the NAC-UMS® scale model, the steel model body (steel pipe) only permits the weight disks to rebound and produce a positive accelerometer reading.

Based on the close similarities with the NAC-STC scale model and with that model's response to the 30-foot side drop impact, it is concluded that the response of the UMS® scale model as measured in this 30-foot drop test bounds the impact forces that occur on the cask, absent the extraneous large positive acceleration recorded during the test.

Summary of the Side Drop Test

The maximum measured acceleration in the UMS® scale model 30-foot side drop test was 52 g, which is enveloped by the UMS® Design Specification value of 60 g used in the SAR analyses. The maximum crush depth for the UMS® impact limiters, that was attained by ratioing from the measured crush depth for the scale model 30-foot drop test, 11.8 inches, is bounded by the crush depths calculated by the RBCUBED impact limiter program; i.e., 13.0 inches.

To increase the design margin of the UMS® transport cask upper impact limiter in the vicinity of the trunnion cutouts, two design changes have been implemented:

1. The trunnion cutout is radiused to matched the surface of the trunnion. This increases the volume of the redwood to be crushed adjacent to the trunnion and minimizes the open space available for displacement (rather than crushing) of the redwood.
2. An additional stainless steel plate is incorporated in the upper impact limiter structure underneath the block of redwood located outward of the trunnion cutouts to ensure the retention and crushing of that redwood in the event of a side drop directly on a trunnion.

These design changes in the UMS® upper impact limiter are only significant for a side drop or an oblique drop, since the trunnion cutout region may act as a section of the backed area for these drops. For the top end drop or top corner drop, the trunnion cutout region of the upper impact limiter is not active in the crushing of the impact limiter.

The results of the 30-foot side drop test of the UMS® quarter-scale model confirm that the NAC-UMS® transport cask impact limiters are adequately designed to limit the acceleration of the cask in a 30-foot side drop impact to be within the cask design specification values. The test also confirmed that the impact limiter design provides sufficient crush depth to ensure that the cask body does not impact the surface during a 30-foot side drop impact.

2.10.3.9 Evaluation of a 30-Foot Oblique Drop

The drop test program for the NAC-UMS® quarter-scale model does not include a 75° oblique drop test since test results for the NAC-STC® quarter-scale model drop tests, and drop evaluations performed by Sandia, show that no significant slapdown effect occurs in the cask. Consequently, the NAC-UMS quarter-scale model side drop impact test results (acceleration and crush distance) bound the oblique drop condition.

Evaluations performed by Sandia National Laboratory, reported in SAND90-2187 [58], show that for cask designs having a ratio of length to radius of gyration (L/r) less than 2, the oblique drop slapdown effect on surfaces without friction does not result in accelerations larger than those that occur in the side drop. This result is confirmed by a review of the NAC-STC quarter-scale model drop test data, which included a 75° oblique drop. These test results show the absence of a friction effect, and that the side drop impact accelerations bound the oblique drop accelerations.

The L/r ratios for the NAC-STC and NAC-UMS casks are 1.33 and 1.3, respectively as shown below. Since these ratios are nearly the same, it can be concluded that the results of the NAC-STC quarter scale model drop tests can be applied to the NAC-UMS cask design, and that no slap down effect occurs. Consequently, no separate oblique drop test is required.

	Length (L) (inches)	Radius of Gyration (r)(inches)	L/r
NAC-STC	257	193	1.33
NAC-UMS	272	209.5	1.3

2.10.3.10 Results/Evaluation for the 30-Foot Top Corner Drop Test

The 30-foot top corner drop was the third drop to be performed using the UMS® quarter-scale model. Prior to lifting the scale model package to the 30-foot drop height, the torques for the retaining rods and the two nuts were confirmed to ensure that the torque specifications were met.

Only the upper impact limiter was attached to the cask model. The bottom end of the scale model used the same test weight that was used for the top end drop. This test weight is an inexpensive substitute for a bottom impact limiter and ensures that the tested package has the proper weight and CG location for the UMS® transport cask.

Two high speed cameras were used to record the top corner drop impact. One of the high speed cameras recorded a close-up view of the impact limiter crush in the region of the impact plane. The other camera recorded an overall view of the drop test and showed that the cask orientation was very close to the target angle of 23° from vertical.

2.10.3.10.1 Impact Limiter Deformation and Attachment Data

After the top corner drop test, the scale model package was lifted off the ground to remove the impact limiter. Similar difficulties in removing the deformed impact limiter were encountered, as with the top end drop, due to the plastic buckling of the retaining rods inside the screw tubes. Upon removing the upper impact limiter, it was observed that the three retaining rods nearest the point of impact were broken. Removal of the upper impact limiter after the test may have broken these retaining rods (as in the case of the top end drop), due to the difficulty of the process. The remaining 13 of the 16 retaining rods were intact and were still threaded into the end of the model. These results indicate that the upper impact limiter remained attached to the cask model during and after the top corner drop test.

Measurements of the model impact limiter dimensions after the top corner drop test were obtained to determine the crush stroke. The measured crush stroke is tabulated as follows, along

with the RBCUBED calculated crush stroke. The quarter-scale model crush stroke is multiplied by 4 (the scaling factor) to obtain the full-scale design crush stroke. The crush stroke reported in this section is the maximum crush stroke for the upper impact limiter away from the trunnion cutout region.

	Quarter-scale model impact limiter crush stroke (in)	4 x Quarter-scale model impact limiter crush (in)	RBCUBED calculated crush stroke (Table 2.6.7.5-4) (in)
Upper impact limiter	3.2	12.8	27.7

The resulting crush stroke determined from the quarter-scale model top corner drop test is enveloped by the RBCUBED calculated design-basis crush strokes for the full-scale UMS® transport cask for a 30-foot top corner drop with impact limiters.

2.10.3.10.2 Accelerometer Data

The unfiltered accelerometer traces were obtained and a portion of a typical top corner drop acceleration trace is shown in Figure 2.10.3-7. An initial observation is that significant "noise" vibrations associated with the accelerations do exist and that filtering of the accelerometer data is appropriate. The filtered result is superimposed on the unfiltered data in Figure 2.10.3-8.

The results from the RBCUBED Impact Limiter Analysis Program, and the maximum accelerations determined from the three accelerometer traces, are:

	Quarter-Scale Model Accelerations (g)		Quarter-Scale Model Accelerations / 4 (g)		RBCUBED Calculated Full-Scale Acceleration (Table 2.6.7.5-4)
	Negative Peak	Positive Peak	Negative Peak	Positive Peak	
Upper impact limiter	86	121	22	30	47.8

The acceleration determined from the quarter-scale model top corner drop test is enveloped by the RBCUBED calculated design basis accelerations.

Summary of the Top Corner Drop Test

The crush stroke and impact accelerations determined from the 30-foot top corner drop test of the UMS® quarter-scale model are enveloped by the RBCUBED calculated design-basis analysis data used in the SAR. The UMS® impact limiters are confirmed to provide adequate design margin to limit the acceleration and the crush stroke of the transport cask for the 30-foot top corner drop. Thus, the UMS® cask body will not contact the impact plane during the 30-foot top corner drop.

2.10.3.11 Scale Model Drawings

The detailed dimensions, welding and materials are shown on the drawings of the model body and impact limiters. These drawings are included in this section for reference.

Drawing Number	Sheet	Revision	Title
790-300	1	3	Drop Test Assembly 1/4 Scale Model
790-301	1 through 3	6	1/4 Scale Cask Model, NAC-UMS®
790-401	1 through 3	2	Crush Fixture, End Drop, UMS® Testing
790-602	1	0	Lower Impact Limiter, 1/4 Scale Model NAC-UMS®
790-603	1	0	Upper Impact Limiter, 1/4 Scale Model NAC-UMS®

Figure 2.10.3-1 Typical Unfiltered Acceleration Time History for the UMS® Quarter-Scale Model Top End Drop

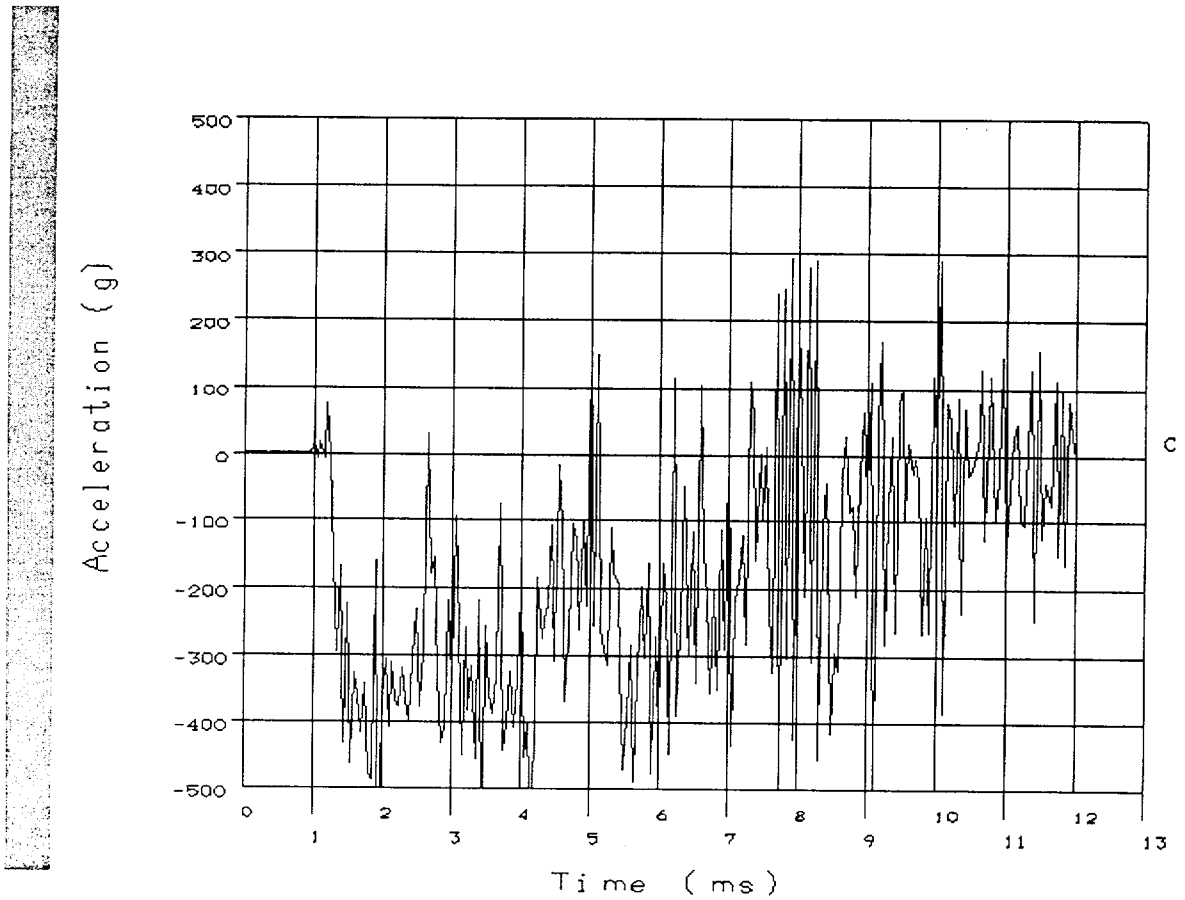

Figure 2.10.3-2 Typical Filtered Acceleration Time History for the UMS® Quarter-Scale Model Top End Drop, Overlayed with the Unfiltered Data

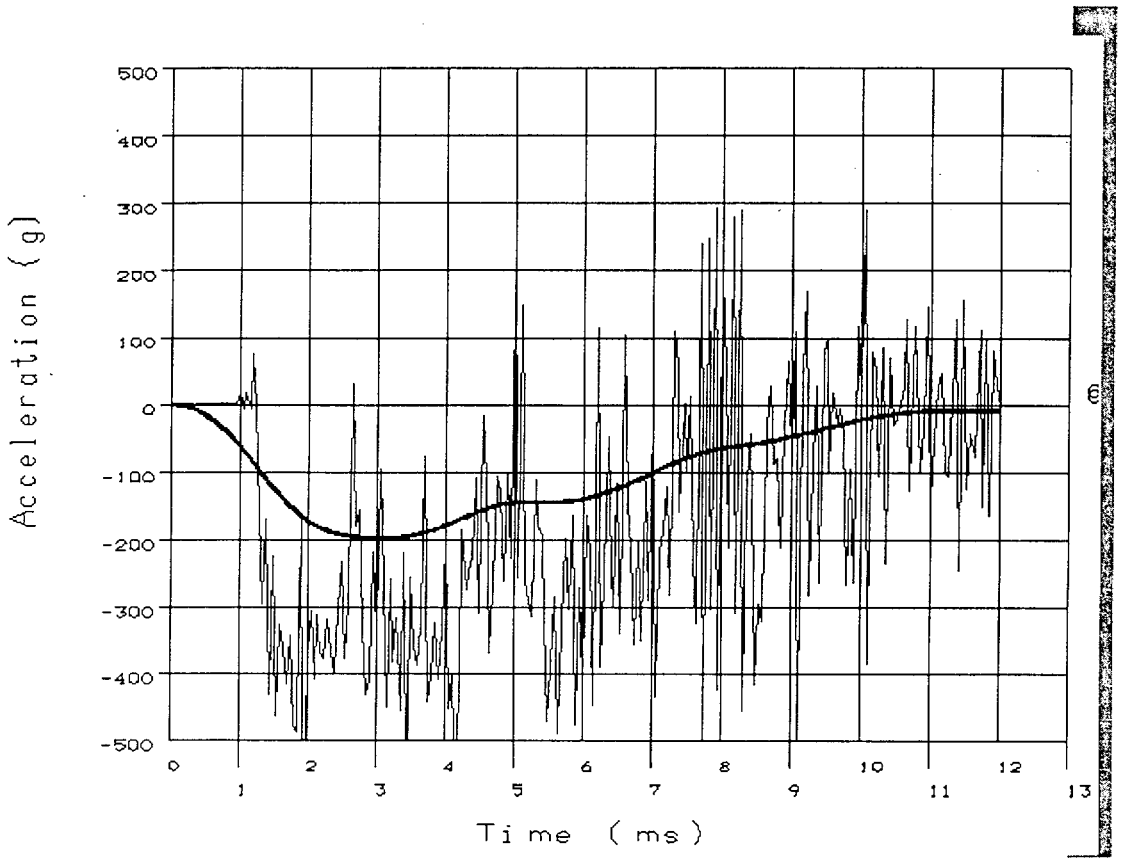

Figure 2.10.3-3 Force-Deflection Curve for Static Test 1 for a 45° Section of the UMS® Quarter-Scale Model Upper Impact Limiter

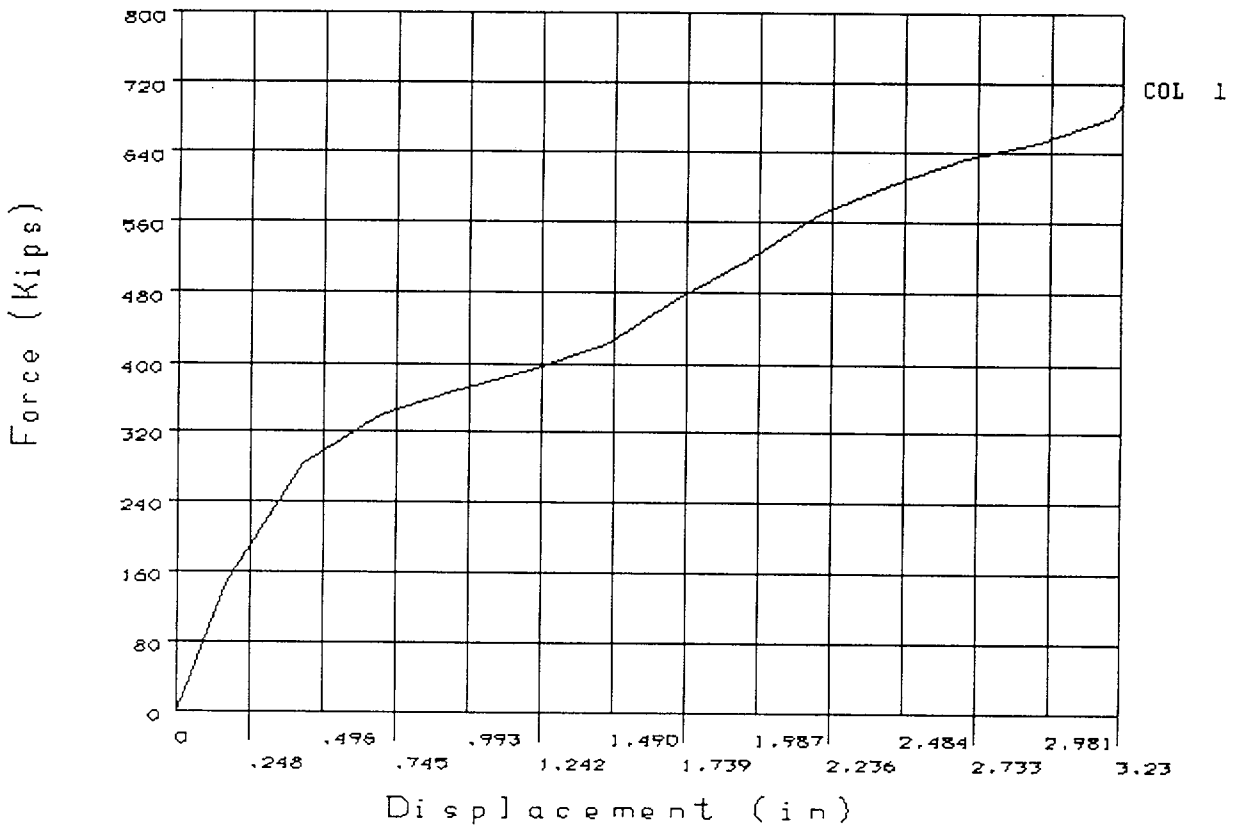

Note:

Forces correspond to a full quarter-scale model of the UMS® upper impact limiter. The forces have been factored by 1.058 to account for the dynamic crush strength of redwood.

Figure 2.10.3-4 Force-Deflection Curve for Static Test 2 for a 45° Section of the UMS® Quarter-Scale Model Upper Impact Limiter

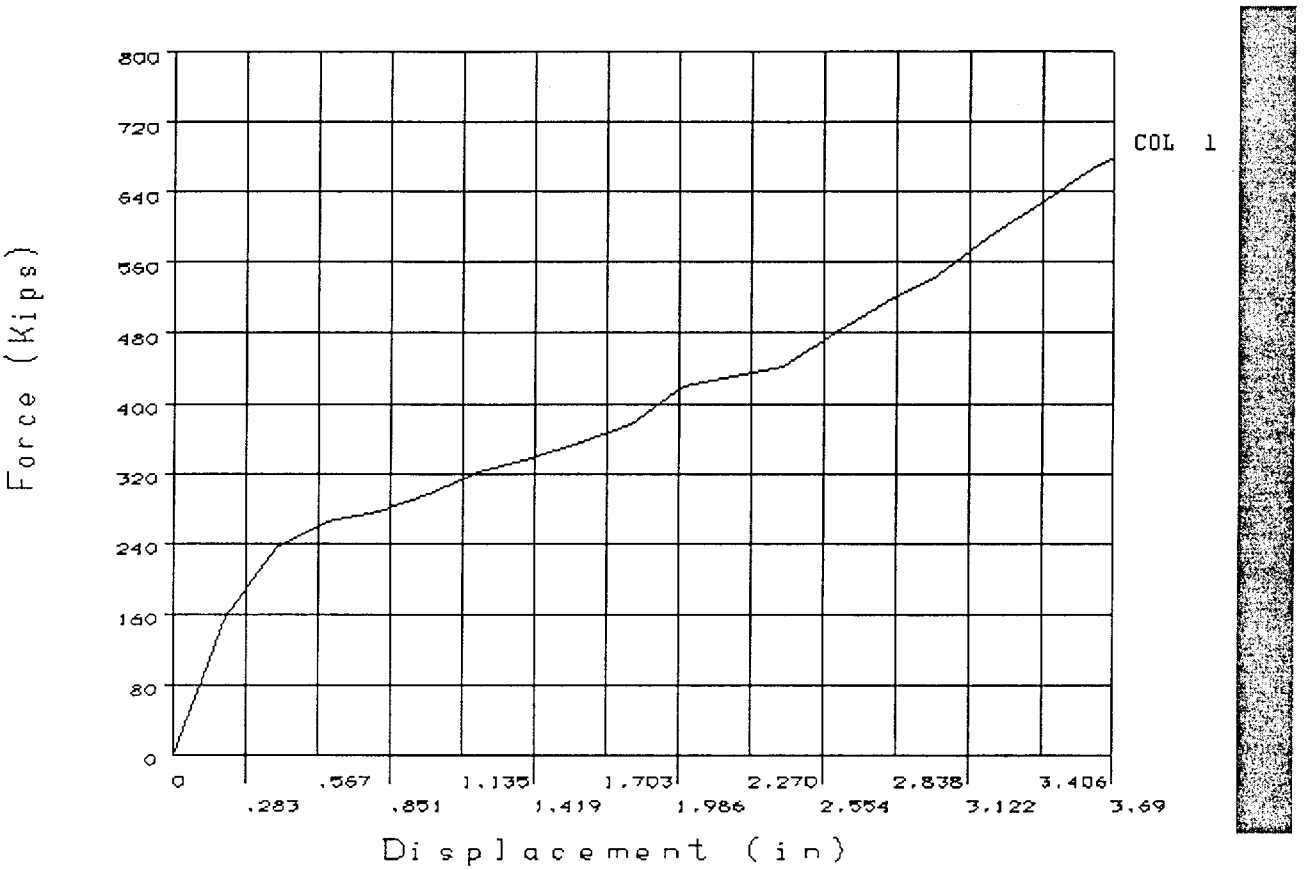

Note:

Forces correspond to a full quarter-scale model of the UMS® upper impact limiter. The forces have been factored by 1.058 to account for the dynamic crush strength of redwood.

Figure 2.10.3-5 Typical Unfiltered Acceleration Time History for the UMS® Quarter-Scale Model Side Drop

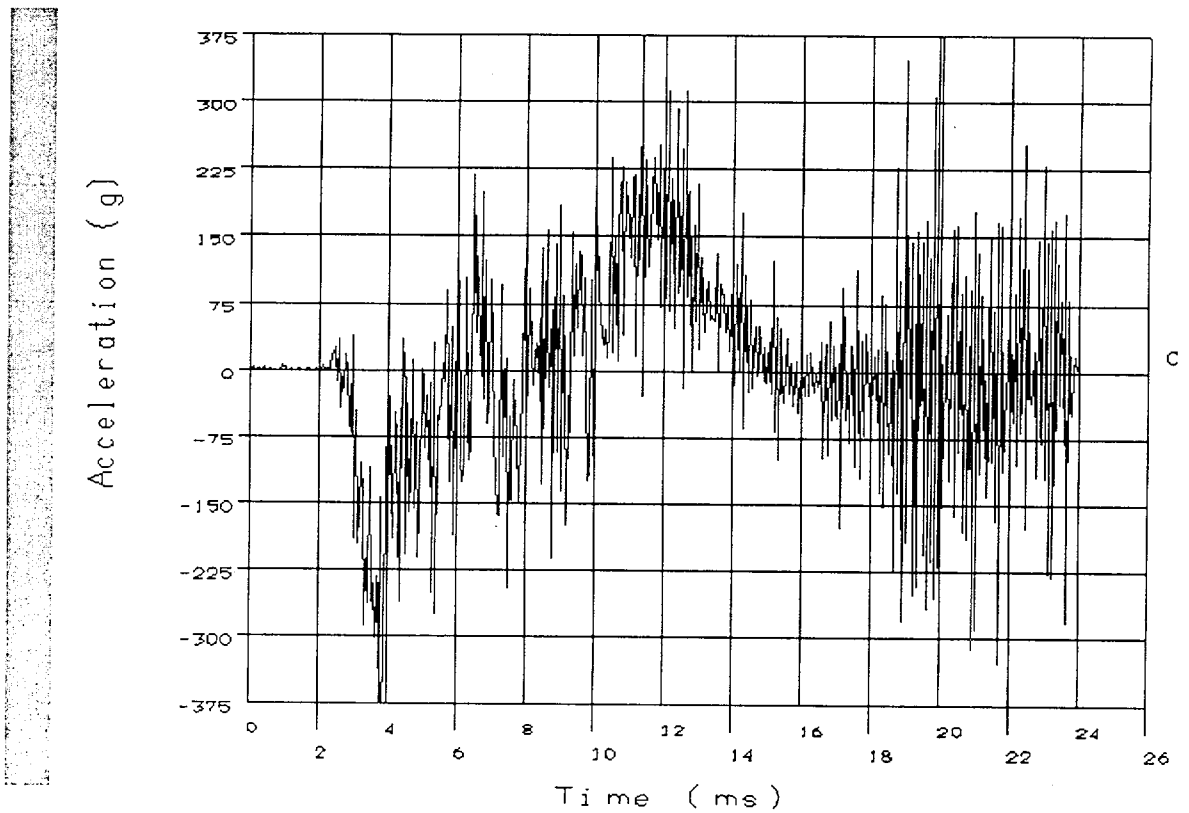

Figure 2.10.3-6 Typical Filtered Acceleration Time History for the UMS® Quarter-Scale Model Side Drop, Overlayed with the Unfiltered Data

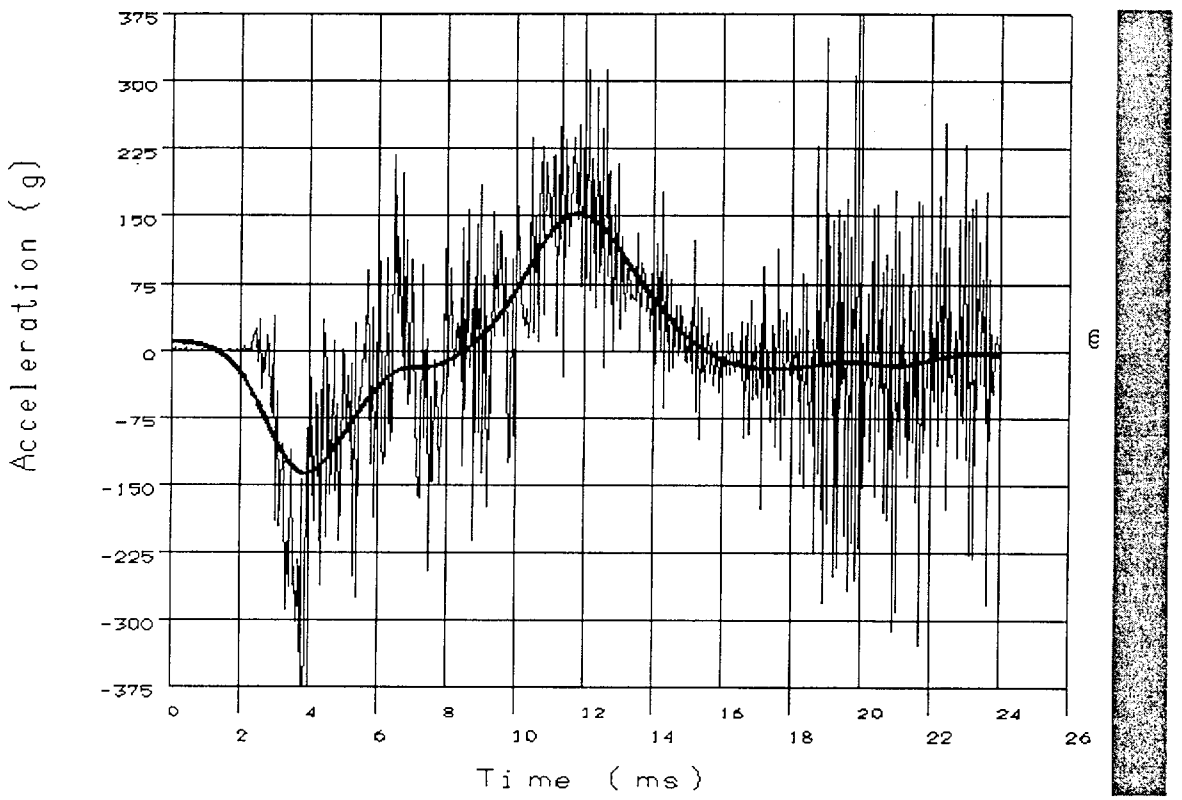

Figure 2.10.3-7 Typical Unfiltered Acceleration Time History for the UMS® Quarter-Scale Model Top Corner Drop

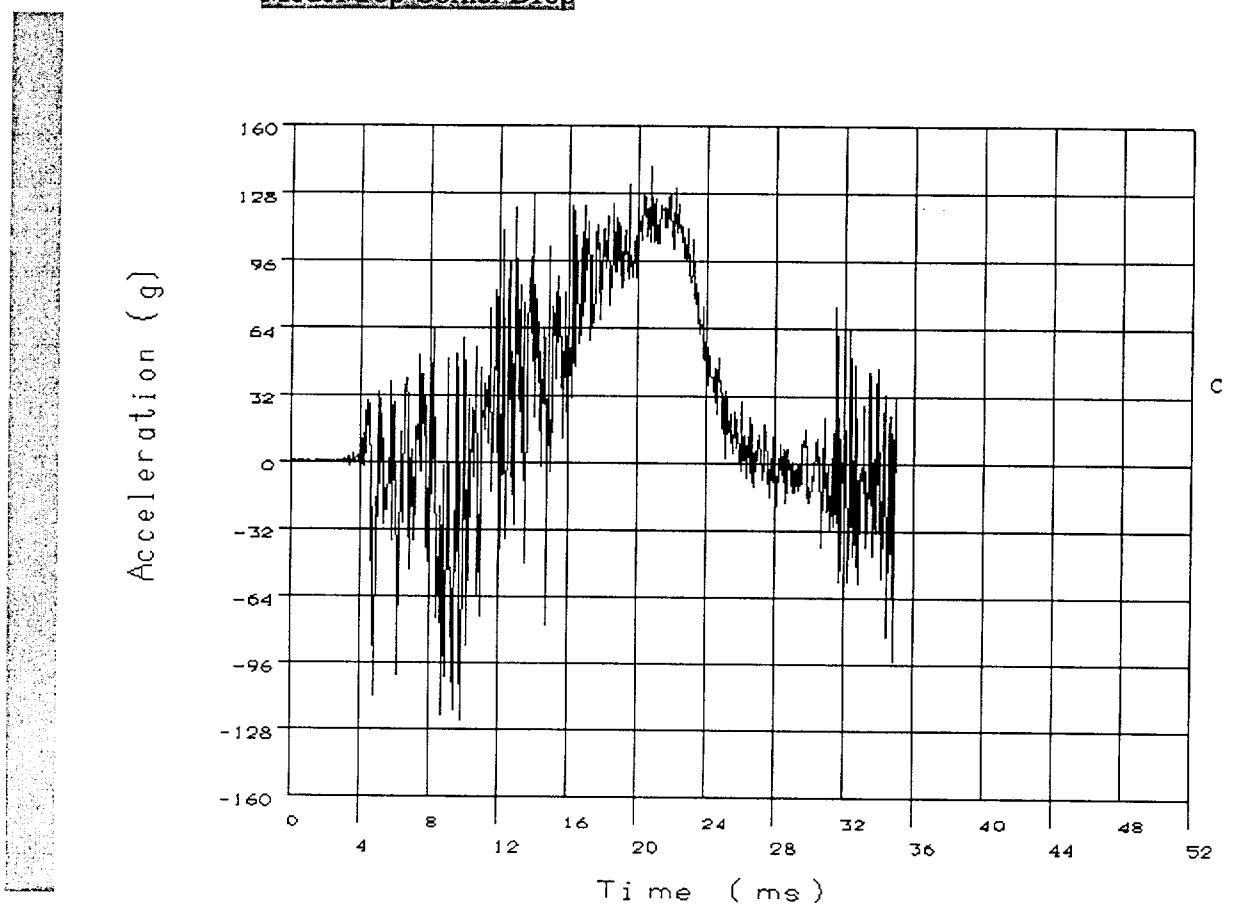

Figure 2.10.3-8 Typical Filtered Acceleration Time History for the UMS® Quarter-Scale Model Top Corner Drop, Overlayed with the Unfiltered Data

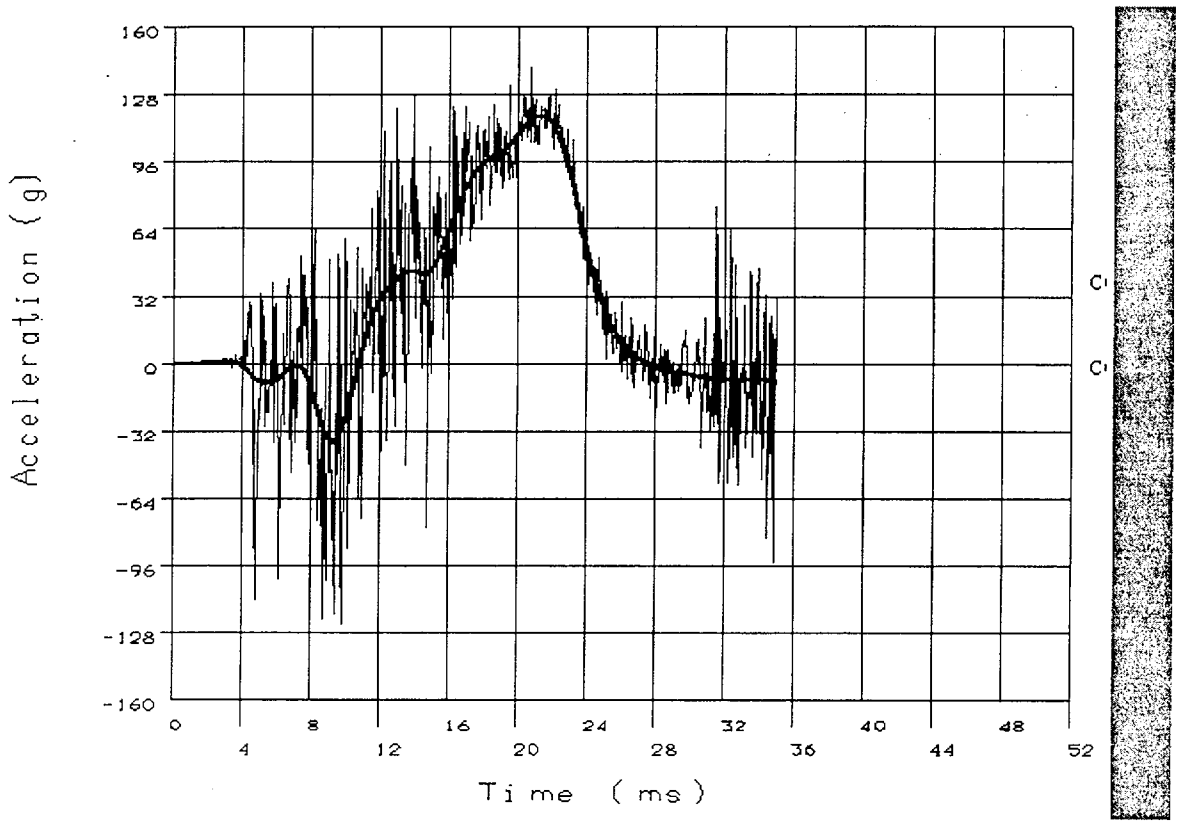

THIS PAGE INTENTIONALLY LEFT BLANK

2.10.4 Dynamic Load Factor (DLF) Evaluation for PWR and BWR Support Disks

Design basis accelerations of 20g and 60g are used in the PWR and BWR support disk evaluations for normal conditions (Sections 2.6.13 and 2.6.15) and accident conditions (Sections 2.7.8 and 2.7.10), respectively. This section is to demonstrate that, with the consideration of the Dynamic Load Factors (DLF), the maximum acceleration occurring at the support disks is bounded by the design basis accelerations. The 1-foot end drop and 1-foot side drop conditions are evaluated in Sections 2.10.4.1 and 2.10.4.2, respectively. Both the PWR and BWR support disks are considered.

2.10.4.1 1-Foot End Drop Analysis

Two ANSYS finite element models, constructed using SHELL63 elements, are used for the end drop analysis as shown in Figures 2.10.4.1-1 and 2.10.4.1-2 for PWR and BWR support disks, respectively. The model represents a single support disk restrained at the tie-rod locations in the Z-direction (perpendicular to the plane of the disk).

The maximum acceleration (g_{max}) at the cask surface determined by the impact limiter analysis is 17.1g for the 1-foot end drop (Table 2.6.7.5-1). The corresponding acceleration time histories are shown in Figure 2.10.4.1-3.

The steps used to determine the DLF, and the response acceleration of the support disk for the 1-foot drop condition, are:

1. The acceleration time history for the 1-foot end drop condition obtained from impact limiter analysis (Figure 2.10.4.1-3) is transformed into a frequency response spectrum as shown in Figure 2.10.4.1-4, using the response spectrum generator in ANSYS. The zero-period acceleration (>1000 Hz) is noted as 17.33g.

2. A modal analysis is performed for the PWR and BWR support disks using the ANSYS models shown in Figures 2.10.4.1-1 and 2.10.4.1-2. The modal frequencies and the corresponding modal participation factors (MPF) are determined by the analysis. Note that the MPFs for modes above 1000 Hz are negligible and hence not included.

3. Based on the frequency response spectrum obtained in Step 2, the response acceleration (g_{SRSS}) is calculated using the square-root-of-the-sum-of-the-squares (SRSS) method in conjunction with the absolute sum of the modal response for closely spaced modes (see NRC Regulatory Guide 1.92 [59]). As shown in Tables 2.10.4.1-1 and 2.10.4.1-2, the response acceleration is calculated to be 13.45g and 13.53g for PWR and BWR support disks, respectively. Only the out-of-plane vibrational modes are considered.

The DLF is determined by dividing the response acceleration (g_{SRSS}) by the maximum acceleration (g_{max}) from the impact limiter analysis results (i.e., DLF = (g_{SRSS}) / (g_{max})). Consequently, the DLF for the PWR support disks is calculated to be 0.79 (13.45/17.1). The DLF for the BWR support disks is calculated to be 0.79 (13.53/17.1).

As shown in Tables 2.10.4.1-1 and 2.10.4.1-2, the maximum response acceleration for both the PWR and BWR support disks for 1-foot end drop condition is less than 20g and, hence, are bounded by the design basis accelerations of 20g for normal conditions of transport. Similar results are expected for the accident conditions and, therefore, no further evaluation is performed.

Figure 2.10.4.1-1 ANSYS Finite Element Model of PWR Support Disk for End Drop Analysis

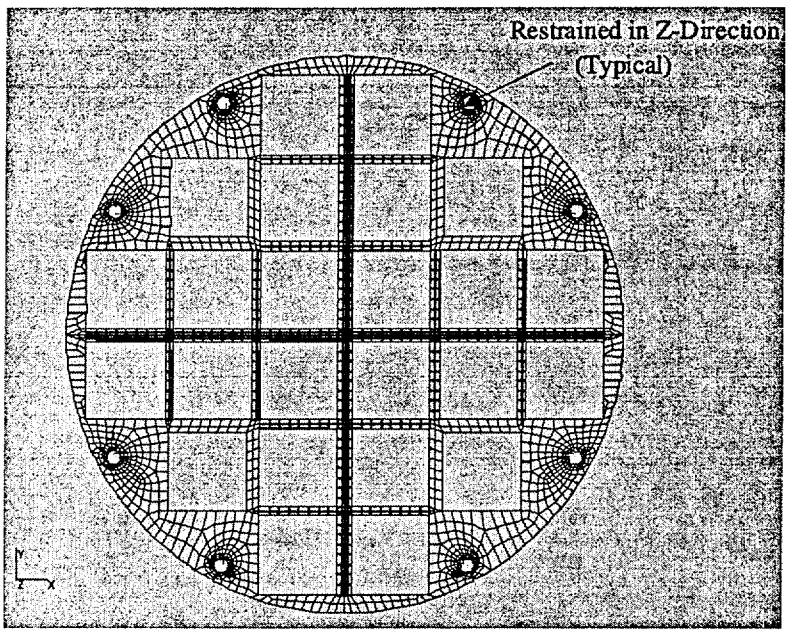

Figure 2.10.4.1-2 ANSYS Finite Element Model of BWR Support Disk for End Drop Analysis

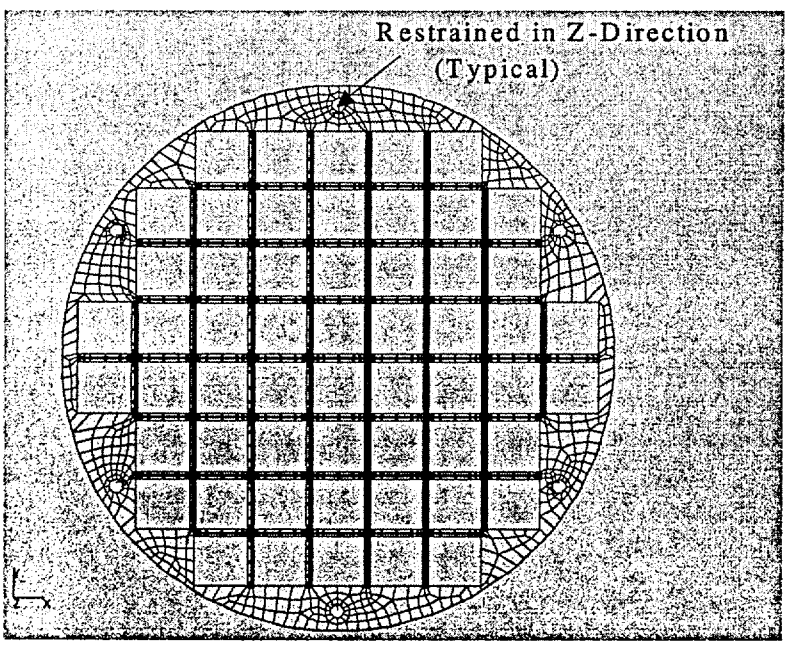

Figure 2.10.4.1-3 1-Foot End-Drop Acceleration Time-History

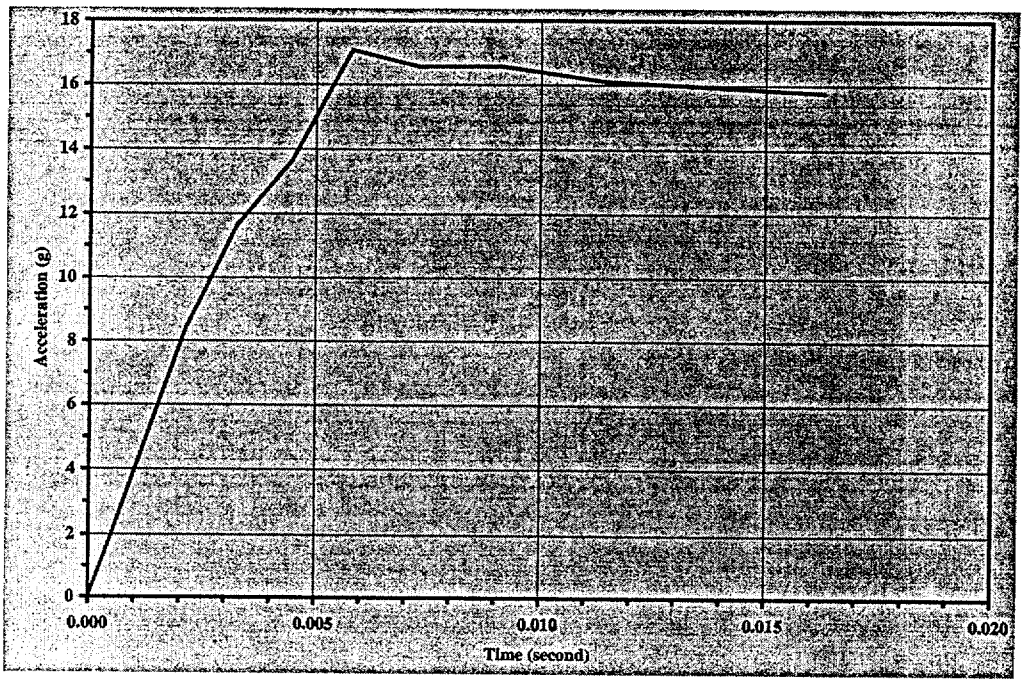

Figure 2.10.4.1-4 1-Foot End-Drop Frequency Response Spectrum

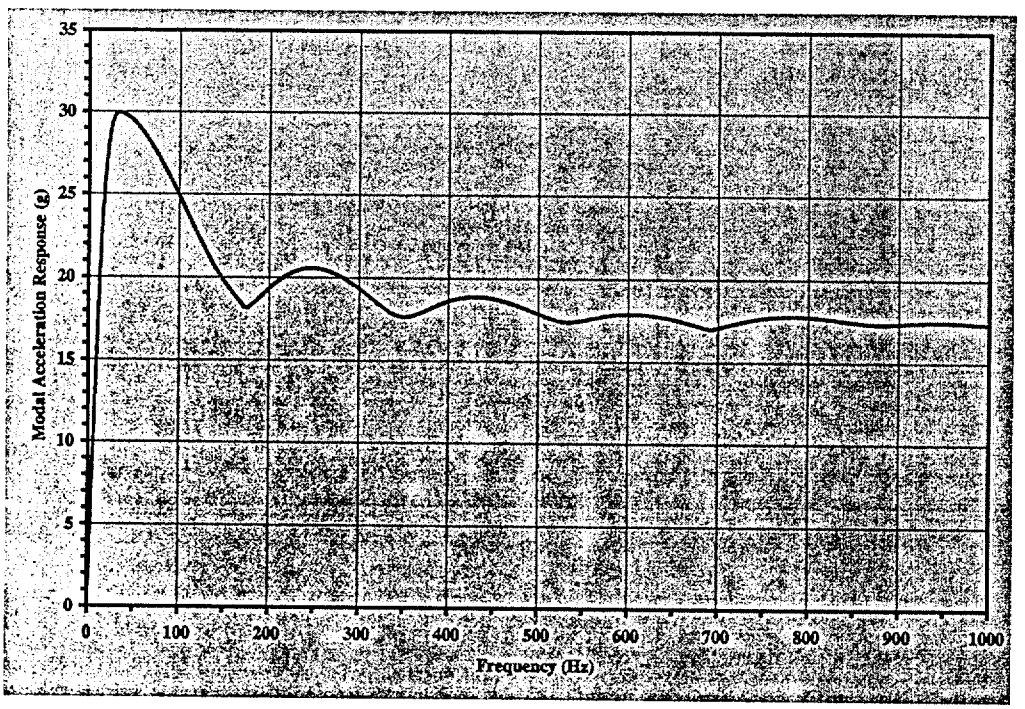

Table 2.10.4.1-1 Response Acceleration for PWR Support Disk for 1-Foot End Drop

PWR Modal Analysis for Out-of-Plane Vibration Modes (End-Drop)						
Mass of Single Disk = 0.485 slugs						
Mode Number	**Modal Frequency(Hz)**	**Closed Spaced**	**Modal Participation Factor (MPF)**	**Effective Mass (slugs)**	**% Mass MPF**	**Response Spectrum Acceleration (g)**
1	18.55	No	0.394842	0.155900	32.14	26.06
2	55.10	No	0.000000	0.000000	0.00	29.10
3	55.11	Yes	0.000000	0.000000	0.00	29.10
4	71.50	No	0.162000	0.026149	5.39	27.81
5	81.67	No	0.000000	0.000000	0.00	26.84
6	81.71	Yes	0.000000	0.000000	0.00	26.84
7	86.30	Yes	0.000284	0.000000	0.00	26.37
8	101.46	No	-0.000001	0.000000	0.00	24.75
9	112.35	No	-0.085600	0.007333	1.51	23.52
10	116.71	Yes	-0.000111	0.000000	0.00	23.03
Sum =				0.189382	39.04	
Missing Mass =				0.295618	60.96	17.08
SRSS Acceleration (g_{SRSS}) =						13.45

Table 2.10.4.1-2 Response Acceleration for BWR Support Disk for 1-Foot End Drop

BWR Modal Analysis for Out-of-Plane Vibration Modes (End-Drop)						
Mass of Single Disk = 0.528 slugs						
Mode Number	Modal Frequency(Hz)	Closed Spaced	Modal Participation Factor (MPF)	Effective Mass (slugs)	% Mass MPF	Response Spectrum Acceleration (g)
1	25.63	No	0.354122	0.125403	23.77	29.19
2	46.92	No	-0.000014	0.000000	0.00	29.56
3	63.40	No	0.013833	0.000191	0.04	28.50
4	63.57	Yes	-0.001899	0.000000	0.00	28.48
5	68.74	Yes	0.000009	0.000000	0.00	28.05
6	70.23	Yes	-0.000033	0.000000	0.00	27.92
7	88.86	No	0.000002	0.000000	0.00	26.11
8	101.35	No	-0.000056	0.000000	0.00	24.76
9	102.18	Yes	0.000736	0.000000	0.00	24.67
10	121.75	No	0.495608	0.245628	46.55	22.46
Sum =				0.380511	70.36	
Missing Mass =				0.147489	29.64	17.08
SRSS Acceleration (g_{SRSS}) =						13.53

2.10.4.2 Side Drop Analysis

The ANSYS PWR and BWR disk models used in the side drop analysis are shown in Figures 2.10.4.2-1 and 2.10.4.2-2, respectively. The models are the same as those for the end drop analyses except that different boundary conditions are applied, as shown. For each model, the support at location "A" allows movement in the "x" direction, but constrains movement in the "y" and "z" directions. Similarly, the support at location "B" allows movement in the "y" direction, but constrains movement in the "x" and "z" directions.

Figure 2.10.4.2-3 shows the LS-DYNA finite element model for the side drop analysis. This model represents a half-symmetry section (1.5 inch in longitudinal direction) of the cask body (outer shell, lead shell, inner shell), canister and a support disk.

Symmetry boundary conditions are applied at the plane of symmetry. Inertia load is applied in the negative "y" direction. The cask body is very heavy compared with the mass of the support disk and fuel. Hence, a model of cask body with an axial length equivalent to 3 times the disk thickness is sufficient to represent the physical interaction between the cask shells and the support disk. An effective density is used for the support disk to account for the self-weight of the disk and the weight of the fuel assembly.

The mass of the support disk is negligible compared with the mass of the cask shells. Therefore, there is no disk-to-cask interaction. The influence of the disk natural frequencies on the self-excitation of cask body is negligible. Since the main interaction is from cask-to-disk, the support disk is simply modeled as a rigid material. The BWR support disk configuration is used for the disk in the model. The density of the disk is adjusted to account for the actual weight for PWR and BWR configurations. The structural behavior of the cask shells is elastic-plastic. The model has four contact interfaces:

1. between the support disk and canister.
2. between the canister and inner shell.
3. between the inner shell and lead shell.
4. between the lead shell and outer shell.

The maximum acceleration (g_{max}) at the cask surface determined by the impact limiter analysis is 16.4g for the 1-foot side drop (Tables 2.6.7.5-1). The corresponding acceleration time histories are shown in Figure 2.10.4.2-4.

The steps used to determine the DLF, and the response acceleration of the support disk, are:

1. The acceleration time history for side drop condition obtained from the impact limiter analysis is used as a dynamic load input to the LS-DYNA model. The response acceleration time history corresponding to the support disk is determined by this analysis.

2. The response acceleration time history is filtered at 1000 Hz (because MPFs above this frequency are negligible) using the LS-DYNA post-processor to remove the high frequency components of the response. See Figures 2.10.4.2-5 and 2.10.4.2-6 for the unfiltered and filtered acceleration time histories for PWR and BWR, respectively.

3. The filtered acceleration time history obtained above is transformed into a frequency response spectrum using the response spectrum generator in ANSYS. The zero-period accelerations (>1000 Hz) are noted as 10.38g for PWR (Figure 2.10.4.2-7) and as 11.66g for BWR (Figures 2.10.4.2-8), respectively.

4. A modal analysis is performed for the PWR and BWR support disks using the ANSYS models (Figures 2.10.4.2-1 and 2.10.4.2-2). The modal frequencies and the corresponding modal participation factors (MPF) are determined by the analysis. Note that the MPFs for modes above 1000 Hz are negligible and hence not included.

5. Based on the frequency response spectrum obtained in step-4, the response acceleration (g_{SRSS}) is calculated using the square-root-of-the-sum-of-the-squares (SRSS) method in conjunction with the absolute sum of the modal response for closely spaced modes (see NRC Regulatory Guide 1.92). As shown in Tables 2.10.4.2-1 and 2.10.4.2-2, the acceleration response (g_{SRSS}) is calculated to be 14.99g and 15.72g for PWR and BWR support disks, respectively. Only the in-plane vibrational modes are considered.

The DLF is determined by dividing the response acceleration (g_{SRSS}) by the maximum acceleration (g_{max}) from the impact limiter analysis results (i.e. DLF = (g_{SRSS}) / (g_{max})). The DLF for the PWR and BWR support disks is calculated to be 0.91 (14.99/16.4) and 0.96 (15.72/16.4), respectively.

As shown in Tables 2.10.4.2-1 and 2.10.4.2-2, the maximum response acceleration for both the PWR and BWR support disks for 1-foot side drop condition are less than 20g and, hence, are bounded by the design basis accelerations of 20g for normal conditions of transport. Similar results are expected for the accident conditions and, therefore, no further evaluation is performed.

Figure 2.10.4.2-1 ANSYS Finite Element Model of PWR Support Disk for Side Drop Analysis

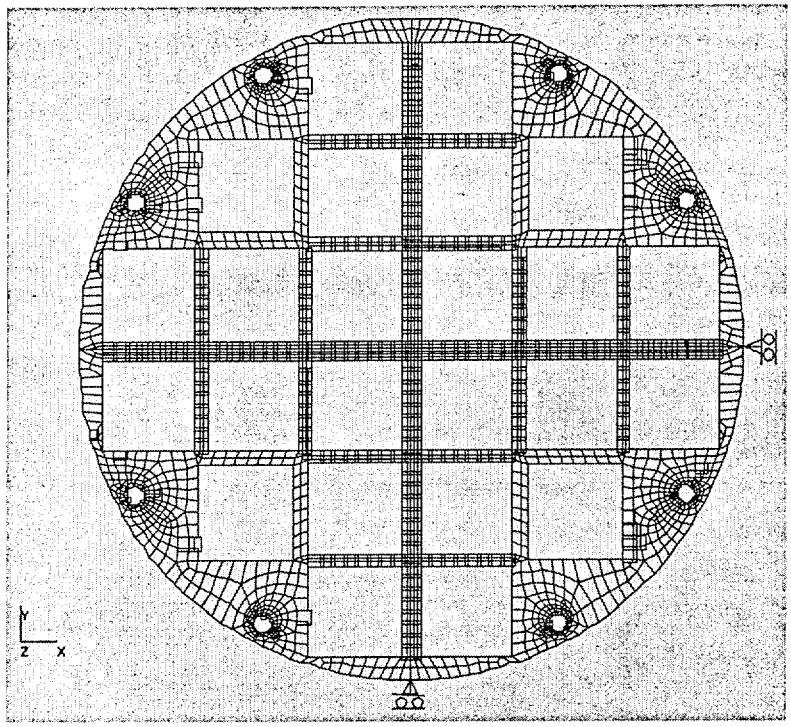

Figure 2.10.4.2-2 ANSYS Finite Element Model of BWR Support Disk for Side Drop Analysis

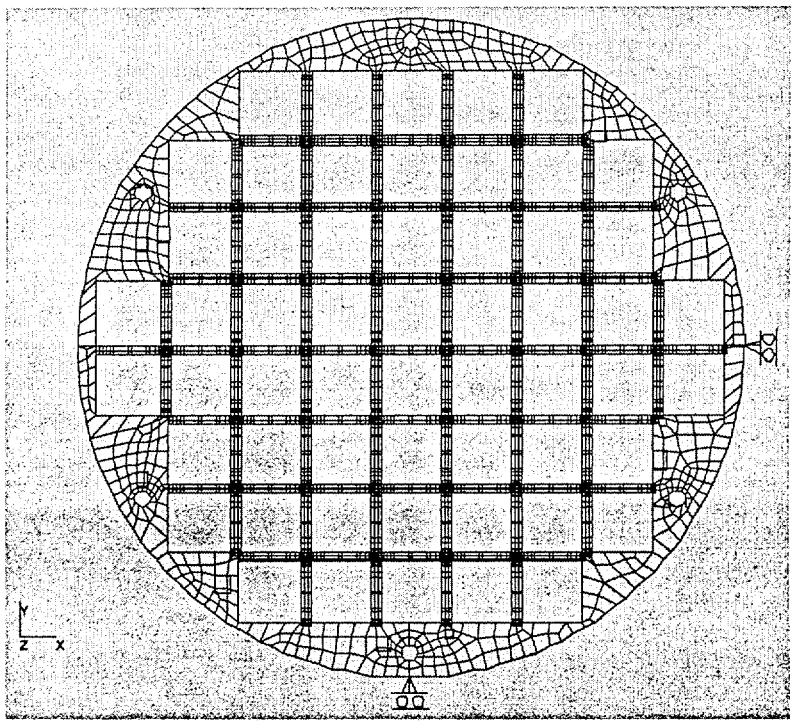

Figure 2.10.4.2-3 LS-DYNA Finite Element Model for Side-Drop Analysis

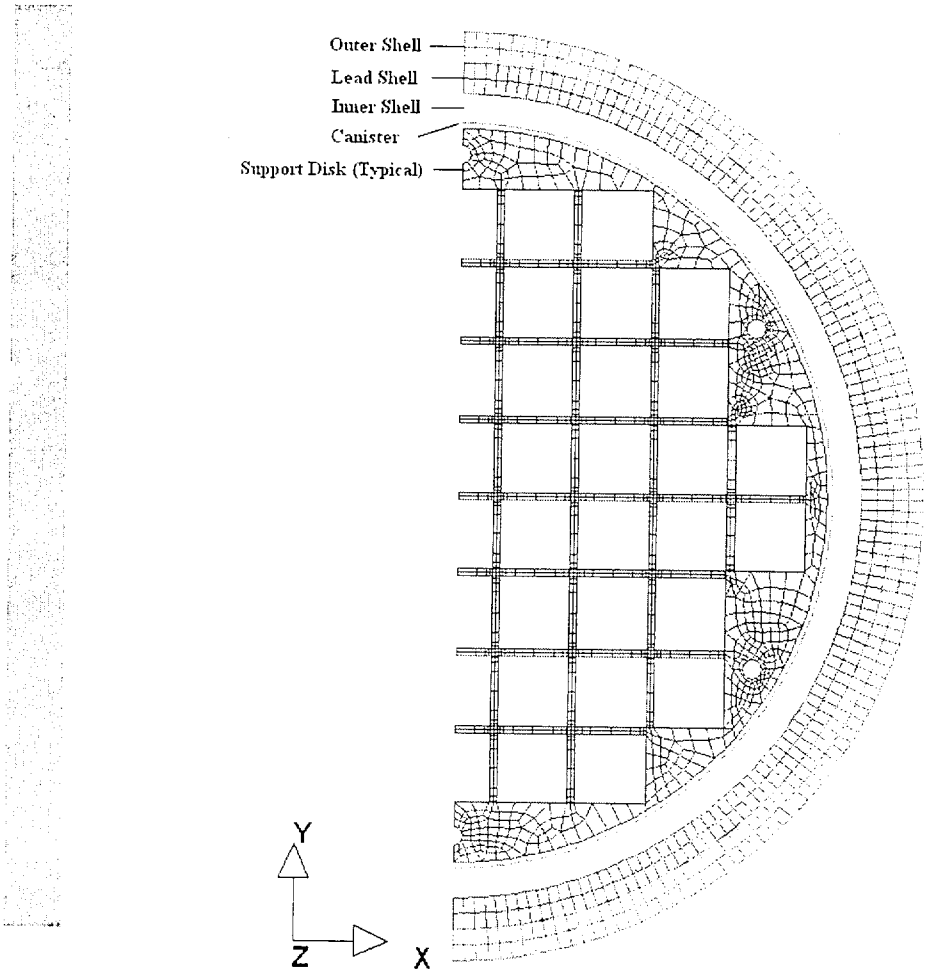

Figure 2.10.4.2-4 1-Foot Side-Drop Acceleration Time History

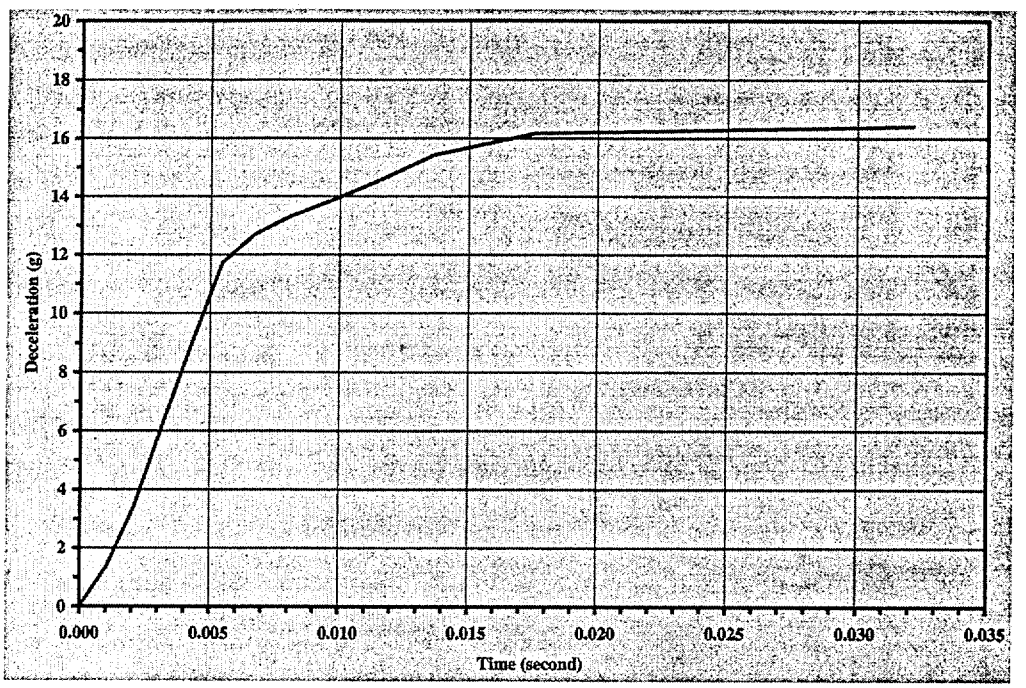

Figure 2.10.4.2-5 PWR Support Disk Acceleration Time History for 1-Foot Side-Drop

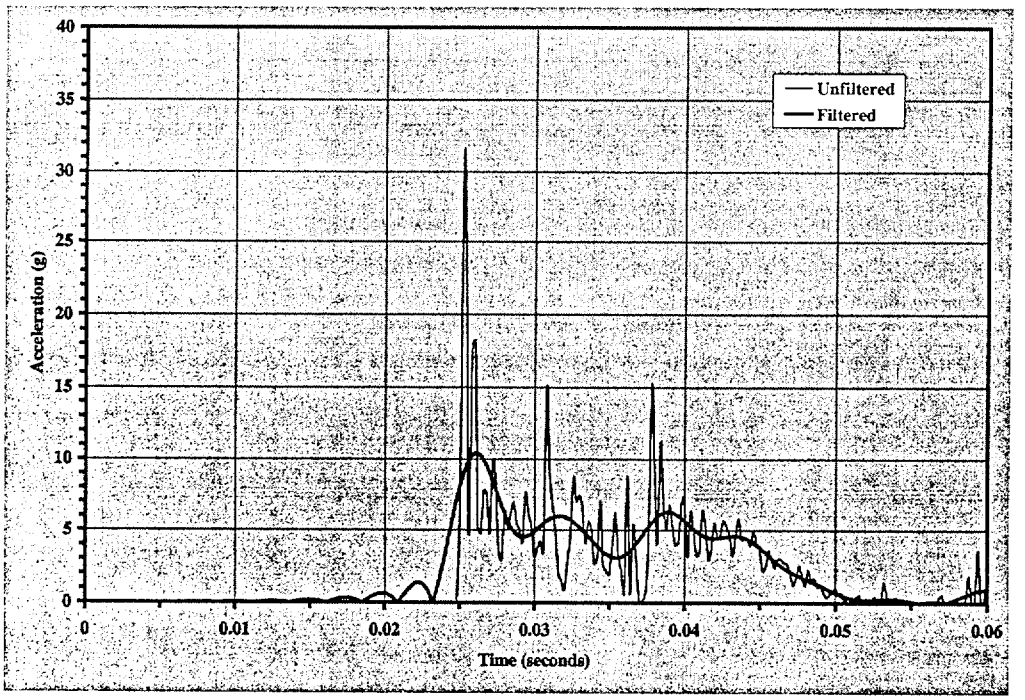

Figure 2.10.4.2-6 BWR Support Disk Acceleration Time History for 1-Foot Side-Drop

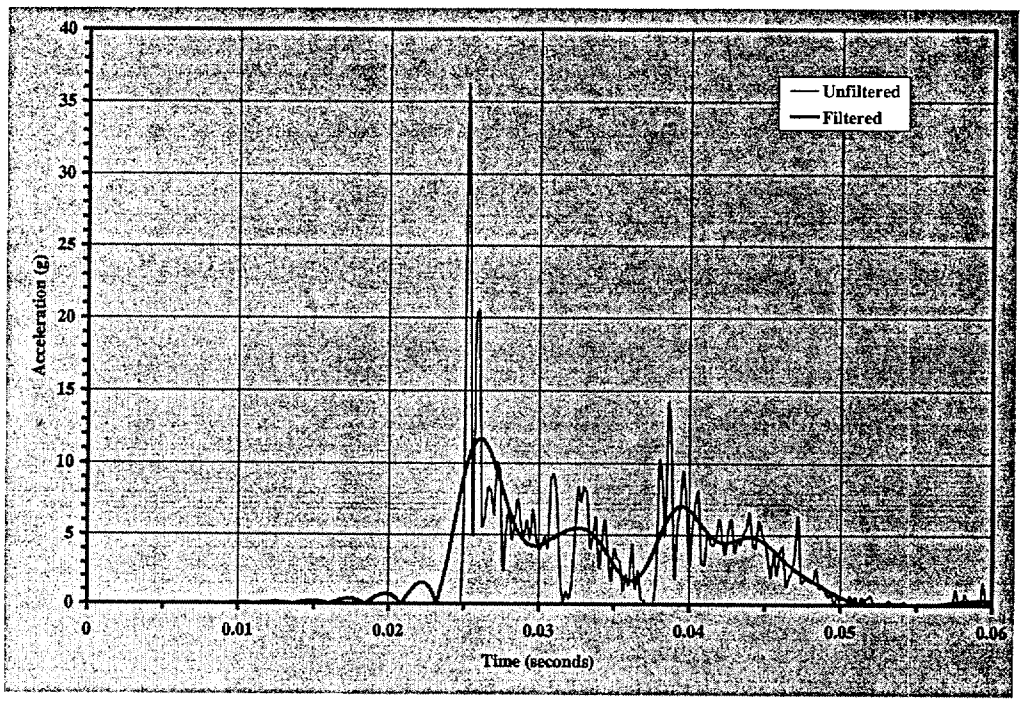

Figure 2.10.4.2-7 PWR Support Disk Frequency Response Spectrum for 1-Foot Side-Drop

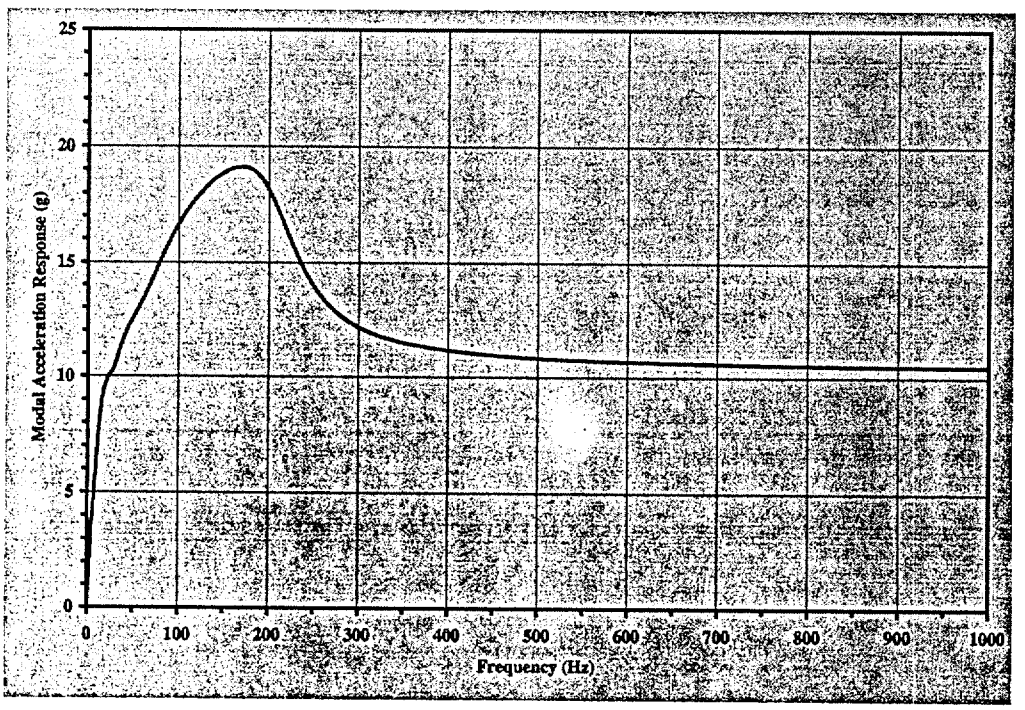

Figure 2.10.4.2-8 BWR Support Disk Frequency Response Spectrum for 1-Foot Side-Drop

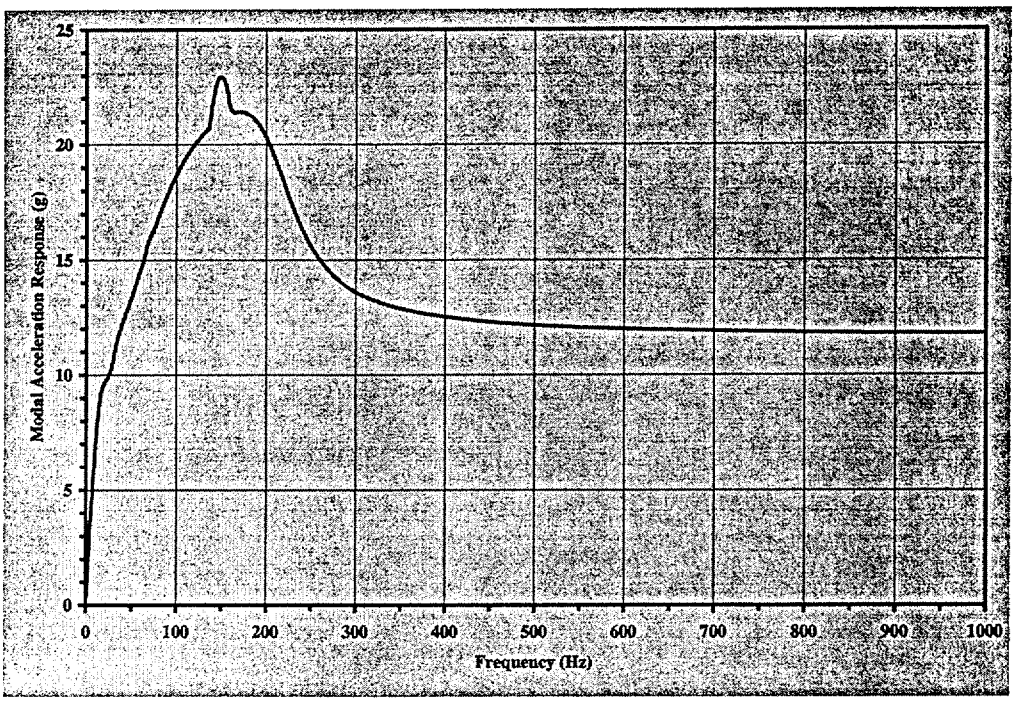

Table 2.10.4.2-1 Response Acceleration for PWR Support Disk for 1-Foot Side Drop

PWR Modal Analysis for In-Plane Vibration Modes (Side-Drop)						
Total Mass = 3.4846 slugs						
Mode Number	Modal Frequency (Hz)	Closed Spaced	Modal Participation Factor (MPF)	Effective Mass (slugs)	% Mass MPF	Response Spectrum Acceleration (g)
1	109.37	No	0.168620	0.028433	0.82	17.23
2	109.75	Yes	1.730000	2.988404	85.76	17.26
3	134.51	No	0.007300	0.000053	0.00	18.40
4	261.40	No	-0.001670	0.000003	0.00	13.35
5	370.08	No	0.305000	0.093141	2.67	11.34
6	371.06	Yes	0.501000	0.250640	7.19	11.34
7	466.53	No	-0.034000	0.001158	0.03	10.91
8	480.57	Yes	0.150000	0.022632	0.65	10.87
9	482.05	Yes	0.252000	0.063605	1.83	10.87
10	772.52	No	-0.001390	0.000002	0.00	10.56
Sum =				3.448071	98.95	
Missing Mass =				0.036529	1.05	16.42
SRSS Acceleration (g_{SRSS}) =						14.99

Table 2.10.4.2-2 Response Acceleration for BWR Support Disk for 1-Foot Side Drop

BWR Modal Analysis for In-Plane Vibration Modes (Side-Drop)						
Total Mass = 3.064 slugs						
Mode Number	Modal Frequency (Hz)	Closed Spaced	Modal Participation Factor (MPF)	Effective Mass (slugs)	% Mass MPF	Response Spectrum Acceleration (g)
1	11.93	No	0.004940	0.000024	0.00	7.74
2	45.88	No	0.007510	0.000056	0.00	12.86
3	79.27	No	1.080000	1.175923	38.38	16.78
4	80.22	Yes	1.300000	1.680653	54.85	16.88
5	139.46	No	0.002330	0.000005	0.00	21.60
6	194.33	No	0.006340	0.000040	0.00	20.69
7	202.88	Yes	0.028700	0.000825	0.03	20.05
8	210.86	Yes	0.323000	0.104419	3.41	19.28
9	282.31	No	0.102000	0.010488	0.34	14.08
10	289.17	Yes	0.001990	0.000004	0.00	13.87
Sum =				2.972437	97.01	
Missing Mass =				0.091561	2.99	16.42
SRSS Acceleration (g_{SRSS}) =						15.72

THIS PAGE INTENTIONALLY LEFT BLANK

FIGURE WITHHELD UNDER 10 CFR 2.390

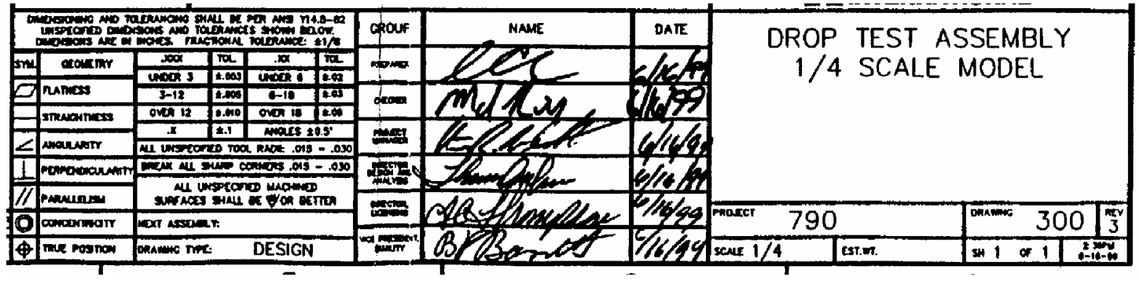

FIGURE WITHHELD UNDER 10 CFR 2.390

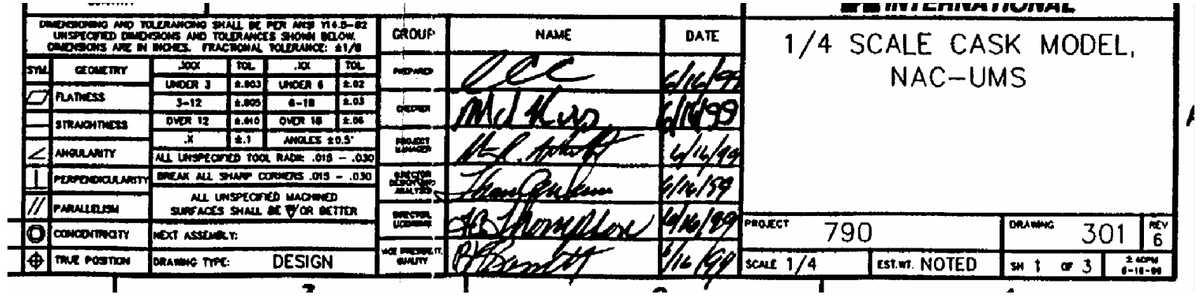

FIGURE WITHHELD UNDER 10 CFR 2.390

NAC INTERNATIONAL

1/4 SCALE CASK MODEL,
NAC-UMS

PROJECT 790		DRAWING 301	REV 6
SCALE 1/4	EST.WT. NOTED	SH 2 OF 3	2:43PM 6-16-06

FIGURE WITHHELD UNDER 10 CFR 2.390

FIGURE WITHHELD UNDER 10 CFR 2.390

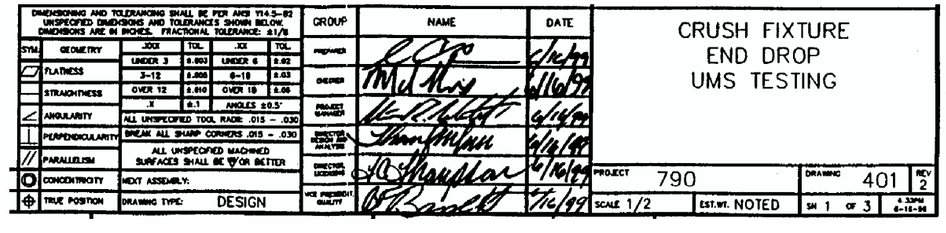

DIMENSIONING AND TOLERANCING SHALL BE PER ANSI Y14.5-82
UNSPECIFIED DIMENSIONS AND TOLERANCES SHOWN BELOW.
DIMENSIONS ARE IN INCHES. FRACTIONAL TOLERANCE: ±1/8

SYM.	GEOMETRY	.XXX	TOL.	.XX	TOL.
	FLATNESS	UNDER 3	±.003	UNDER 6	±.02
	STRAIGHTNESS	3-12	±.005	6-18	±.03
		OVER 12	±.010	OVER 18	±.06
∠	ANGULARITY	.X	±.1	ANGLES ±0.5°	
⊥	PERPENDICULARITY	ALL UNSPECIFIED TOOL RADII: .015 – .030			
//	PARALLELISM	BREAK ALL SHARP CORNERS .015 – .030			
○	CONCENTRICITY	ALL UNSPECIFIED MACHINED SURFACES SHALL BE ▽ OR BETTER			
⌖	TRUE POSITION	NEXT ASSEMBLY:			
		DRAWING TYPE: DESIGN			

GROUP	NAME	DATE
PREPARED		6/14/99
CHECKED		6/16/99
PROJECT MANAGER		6/16/99
DIRECTOR NUCLEAR SAFETY ANALYSIS		6/16/99
DIRECTOR, LICENSING		6/16/99
VICE PRESIDENT QUALITY		7/6/99

CRUSH FIXTURE
END DROP
UMS TESTING

PROJECT	790	DRAWING	401	REV 2
SCALE 1/2	EST.WT. NOTED	SH 1 OF 3	6.32PM 6-16-99	

FIGURE WITHHELD UNDER 10 CFR 2.390

NAC INTERNATIONAL

CRUSH FIXTURE
END DROP
UMS TESTING

PROJECT 790		DRAWING 401	REV 2
SCALE 1/2	EST.WT. NOTED	SH 2 OF 3	6-30PM 8-16-99

FIGURE WITHHELD UNDER 10 CFR 2.390

FIGURE WITHHELD UNDER 10 CFR 2.390

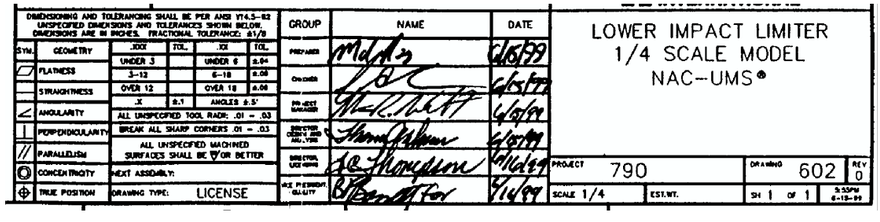

FIGURE WITHHELD UNDER 10 CFR 2.390

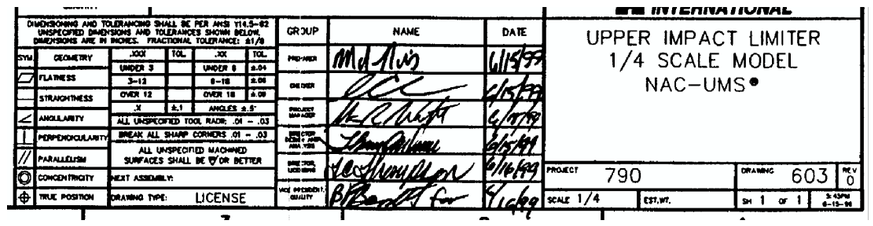

2.11 Site Specific Contents Structural Evaluations

This section describes fuel assembly characteristics and configurations, or waste configurations, which are unique to specific reactor sites. These site specific contents configurations result from conditions that occurred during reactor operations, participation in research and development programs, testing programs intended to improve reactor operations, from decommissioning activities, and from the placement of control components or other items within the fuel assembly. Site specific fuel assembly configurations are either shown to be bounded by the analysis of the standard design basis fuel assembly configuration of the same type (PWR or BWR), or are shown to be acceptable contents by specific evaluation of the configuration.

Site specific Greater Than Class C (GTCC) waste configurations are shown to be acceptable by specific evaluation.

2.11.1 Site Specific Spent Fuel

This section describes the structural evaluation for site specific spent fuel configurations. As noted above, site specific spent fuels are those fuel assembly configurations which result from the modification of standard fuel. The principal modifications are of three general types:

- The removal of fuel rods without replacement;
- The replacement of removed fuel rods or burnable poison rods with rods of another material, such as stainless steel, or with fuel rods of a different enrichment; and
- The insertion of control elements, or instrument or plug thimbles, in guide tube positions.

Also included as site specific fuel are fuel assemblies that are different by design from the standard fuel used at a reactor site. These fuel assemblies are not modified, but differ from the cask design basis fuel assemblies that are described in Tables 1.2-4 and 1.2-5, and which are bounded by the structural evaluation presented in Sections 2.6 and 2.7.

THIS PAGE INTENTIONALLY LEFT BLANK

2.11.1.1 Maine Yankee Site Specific Spent Fuel

The standard spent fuel assembly for the Maine Yankee site is the Combustion Engineering (CE) 14x14 fuel assembly. Fuel of the same design has also been supplied by Westinghouse and by Exxon. The standard 14x14 fuel assemblies are included in the population of the design basis PWR fuel assemblies for the UMS® Transport System (See Table 1.2.5). The structural evaluation for the UMS® transport system loaded with the standard Maine Yankee fuels is bounded by the structural evaluations in Sections 2.6 and 2.7 for the normal conditions of transport and hypothetical accident conditions, respectively. The Maine Yankee site specific fuel is described in Section 1.3.1.

The weight of a standard 14x14 fuel assembly with the control element assembly inserted is 1,360 lbs. This weight is bounded by the weight of the design basis PWR fuel assembly (37,608/24 = 1,567 lbs) used in the PWR support disk analysis presented in Section 2.6.13. The fuel configurations with removed fuel rods, with fuel rods replaced by solid stainless steel or Zircaloy rods, or with poison rods replaced by hollow Zircaloy rods, all weigh less than the standard 14x14 fuel assembly. The configuration with instrument thimbles installed in the center guide tube position weighs less than the standard assembly with the control element assembly installed. Consequently, this configuration is also bounded by the weight of the design basis fuel assembly. Since the weight of any of these fuel assembly configurations is bounded by the design basis fuel assembly weight, no additional analysis of these configurations is required.

A structural evaluation is required for the support disk for the configuration holding consolidated fuel. There are two consolidated fuel lattices, each constructed of 17x17 Zircaloy fuel grids and stainless steel end fittings which are connected by 4 stainless steel support rods. One of the consolidated fuel lattices has 283 fuel rods with 2 empty positions. The other has 172 fuel rods with the remaining positions either empty or holding stainless steel rods. The calculated weight for the heaviest of the two consolidated fuel lattices is 2,100 lbs.

A parametric study is performed to show that the PWR support disk holding a Maine Yankee consolidated fuel lattice is bounded by the UMS® PWR support disk stress evaluation presented in Section 2.6.13. Note that only one consolidated fuel lattice will be loaded in any single Transportable Storage Canister and that the loading position of the consolidated fuel assembly is restricted to a basket corner position (see Section 1.3.1.1).

The two-dimensional ANSYS model used in the support disk evaluation (see Figure 2.6.13-2) in Section 2.6.13 is employed for the parametric study. The boundary condition of the model is modified by restraining the outer surface of the canister shell. The load from a PWR fuel assembly is modeled as a pressure load at the inner surface of each support disk slot opening. The design basis fuel pressure loading is 12.26 psi (see Section 2.6.13.2). Based on the same design parameters (slot size = 9.272 in., disk thickness = 0.5 inch, and the number of disks = 30), the pressure load corresponding to a standard 14x14 fuel assembly and the consolidated fuel are 10.3 psi and 17.0 psi, respectively.

This study considers both the 1-foot (20g) and the 30-foot (60g) side drop conditions for four different drop orientations: 0°, 18.22°, 26.28°, and 45°, as shown in Figure 2.11.1.1-1. The Base Case considers that all 24 slots are loaded with the design basis PWR fuel assembly (pressure=12.26 psi, multiplied by the appropriate g-load factor). Case 1 considers that one consolidated fuel assembly is loaded in position 1 (see Figure 2.11.1.1-1 for location) with all other slots loaded with the standard CE 14x14 fuel assemblies. Similarly, Cases 2 through 4 have the consolidated fuel assembly loaded in positions 2 through 4. Inertial loads are also applied to the support disk.

Table 2.11.1.1-1 provides a parametric comparison between the Base Case and the 4 cases evaluated, based on the maximum sectional stresses in the support disk. As shown in the table, the maximum stress in the UMS® basket support disk loaded with Maine Yankee fuel, including one consolidated fuel lattice is bounded by the design basis PWR fuel evaluation of the support disks.

Additionally, a support disk analysis is performed for the Maine Yankee fuel configuration (23 standard fuel assemblies and one consolidated fuel assembly), using the two-dimensional PWR support disk model for the governing case (45° basket orientation and thermal condition B) for the side drop condition (Section 2.6.13.6).

The loading condition corresponds to Case 1 of the parametric study previously discussed. The analysis results of the P_m and $P_m + P_b$ stresses are summarized in Tables 2.11.1.1-2 and 2.11.1.1-3, respectively. The minimum Margins of Safety for the P_m and $P_m + P_b$ stresses are + 0.82 and + 0.24, respectively.

The minimum margin of safety for the corresponding analysis for the support disk for the UMS® System design basis PWR configuration is +0.79 and +0.19 for P_m and $P_m + P_b$ stresses, respectively (See Tables 2.6.13.6-16 and 2.6.13.6-17). This comparison further substantiates the conclusion of the parametric study based on the normalized stress ratios using a two-dimensional model (Table 2.11.1.1-1).

Figure 2.11.1.1-1 PWR Basket Drop Orientations and Case Study Loading Positions for Maine Yankee Consolidated Fuel

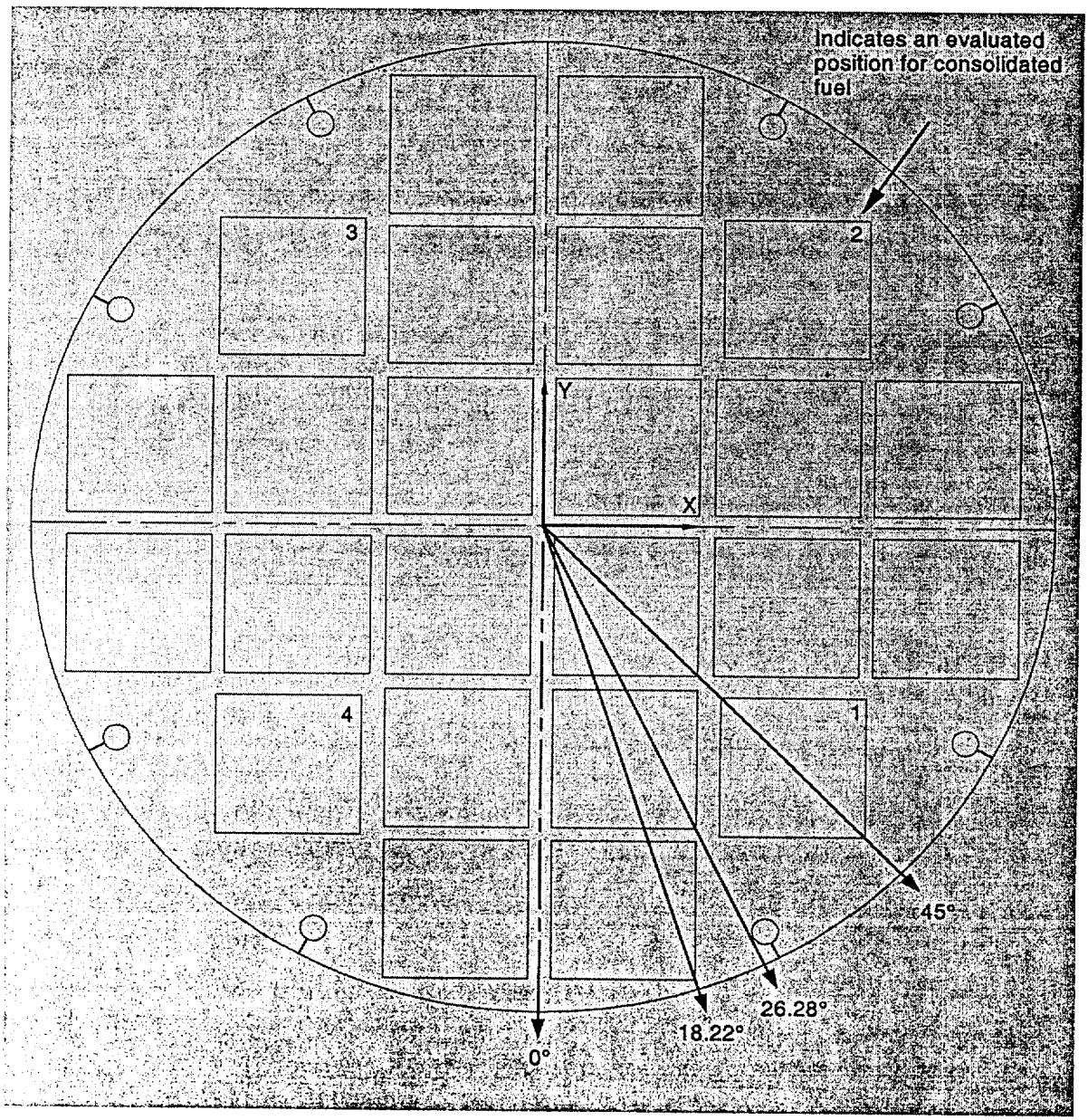

Table 2.11.1.1-1 Normalized Stress Ratios - UMS® PWR Basket Support Disk Sectional Stresses Due to Maine Yankee Consolidated Fuel to the Design Basis PWR Fuel Basket Maximum Stresses (Base Case)

Case	Support Disk Sectional Stress Intensity (ksi) – Membrane							
	Normal Conditions, 20g				Accident Conditions, 60g			
	0°	18.22°	26.28°	45°	0°	18.22°	26.28°	45°
Base Case[1]	1.00	1.00	1.00	1.00	1.00	1.00	1.00	1.00
Case 1	0.96	0.91	0.96	0.96	0.91	0.94	0.94	0.94
Case 2	0.95	0.92	0.96	0.96	0.91	0.94	0.94	0.95
Case 3	0.96	0.93	0.97	0.96	0.91	0.95	0.95	0.95
Case 4	0.95	0.93	0.97	0.96	0.91	0.95	0.95	0.96
Case	Support Disk Sectional Stress Intensity (ksi) – Membrane + Bending							
	Normal Conditions, 20g				Accident Conditions, 60g			
	0°	18.22°	26.28°	45°	0°	18.22°	26.28°	45°
Base Case[1]	1.00	1.00	1.00	1.00	1.00	1.00	1.00	1.00
Case 1	0.96	0.92	0.96	0.95	0.96	0.94	0.94	0.94
Case 2	0.96	0.92	0.96	0.96	0.95	0.95	0.95	0.95
Case 3	0.96	0.93	0.96	0.95	0.96	0.95	0.95	0.95
Case 4	0.96	0.93	0.97	0.97	0.96	0.98	0.98	0.97

1. Tables 2.6.13.6-16 and 2.6.13.6-17.

Table 2.11.1.1-2 P_m Stresses for Support Disk—1-Foot Side Drop, 45° Orientation, Thermal Case B , Structural Case 1

Section	Sx (ksi)	Sy (ksi)	Sxy (ksi)	Stress Intensity (ksi)	Allowable Stress (ksi)	Margin of Safety
120	9.7	-9.8	7.6	24.8	45	0.82
114	-9.9	9.7	7.6	24.8	45	0.82
35	13.9	-1.5	6.4	20	45	1.25
23	-1.4	14.1	6.3	20	45	1.25
21	-7.6	-15.9	6.6	19.5	45	1.31
37	15.8	-7.8	6.6	19.5	45	1.31
112	7.1	-5.9	6.1	17.8	45	1.52
111	-5.8	7.1	6.1	17.7	45	1.54
63	1.6	-9.8	5.5	15.9	45	1.83
96	-9.5	1.6	5.6	15.7	45	1.86
9	-0.5	-11.2	5.6	15.5	45	1.91
49	11	-0.5	5.6	15.4	45	1.92
28	-9	2.8	4.3	14.7	45	2.07
40	2.8	-8.9	4.4	14.6	45	2.07
7	3	11.6	5.5	14.3	45	2.15
104	-7	0.2	6.1	14.2	45	2.17
51	11.3	3	5.5	14.1	45	2.19
66	0.2	-7.1	6	14.1	45	2.2
72	10.6	-9.6	3.8	14	45	2.23
98	-9.7	-10.7	3.7	13.9	45	2.23
95	-3.2	-11.6	4.1	13.3	45	2.4
42	-6.3	-10.2	4.6	13.2	45	2.4
26	10.3	-6.2	4.5	13.2	45	2.4
110	13.2	-0.1	-0.5	13.2	45	2.41
64	11.3	-3.3	4.2	13.1	45	2.43
119	-0.1	-13.1	-0.5	13.1	45	2.43
94	12.1	-0.1	-0.3	12.2	45	2.7
71	-0.1	-12	-0.3	12	45	2.74
79	1	8.9	3.7	10.8	45	3.17
80	8.6	1	3.7	10.7	45	3.2
124	3.6	-6.5	1.3	10.4	45	3.34
108	-4.1	5	2.2	10.1	45	3.44
22	-2.5	-0.8	-4.9	10	45	3.5
36	-0.8	-2.6	-4.9	9.9	45	3.53
74	-0.2	9	2.1	9.8	45	3.6
99	9	-0.2	2.1	9.8	45	3.61
115	0.5	-4.6	3.9	9.3	45	3.82
122	-4.5	0.5	3.9	9.3	45	3.85
116	-0.1	-9.1	0	9.1	45	3.96
92	2.2	-6.8	0.2	9	45	4.02

Table 2.11.1.1-3 $P_m + P_b$ Stresses for Support Disk—1-Foot Side Drop, 45° Orientation, Thermal Case B, Structural Case 1

Section	Sx (ksi)	Sy (ksi)	Sxy (ksi)	Stress Intensity (ksi)	Allowable Stress (ksi)	Margin of Safety
37	-38.5	-45.1	12	54.2	67.5	0.24
21	-44.9	-38.5	12	54.1	67.5	0.25
23	33.4	36.6	10.2	45.3	67.5	0.49
35	36.5	33.4	10.1	45.2	67.5	0.49
34	-40.7	-41.2	3.2	44.2	67.5	0.53
20	-41	-40.8	3.2	44.1	67.5	0.53
4	37.9	41.6	3	43.3	67.5	0.56
1	41.6	37.9	3	43.3	67.5	0.56
112	-18.1	-42	3.7	42.5	67.5	0.59
111	-41.6	-18	3.6	42.2	67.5	0.6
51	30.9	34.8	9	42.1	67.5	0.6
7	34.6	31.1	9.1	42	67.5	0.61
2	-37.8	-37.2	2.6	40.1	67.5	0.68
3	-37.2	-37.8	2.6	40.1	67.5	0.68
49	-30.8	-31	8.6	39.6	67.5	0.71
9	-30.9	-30.9	8.7	39.5	67.5	0.71
64	-31	-30.4	8.2	38.9	67.5	0.73
95	-30.1	-31.2	8.2	38.8	67.5	0.74
63	-30.2	-30.7	8.3	38.8	67.5	0.74
96	-30.4	-30.5	8.3	38.8	67.5	0.74
120	0.2	-34.9	5.5	36.7	67.5	0.84
114	-34.8	0.2	5.4	36.6	67.5	0.84
42	-18.9	-33	7.6	36.3	67.5	0.86
26	-32.9	-18.7	7.5	36.1	67.5	0.87
6	32.1	33.1	1.6	34.3	67.5	0.97
48	32.9	32.3	1.6	34.2	67.5	0.98
36	-4	-32	-4.1	32.6	67.5	1.07
22	-31.7	-3.7	-4.2	32.4	67.5	1.09
80	25	25	6.5	31.5	67.5	1.14
79	24.7	25.2	6.5	31.5	67.5	1.14
72	-18	-25.2	8.8	31.1	67.5	1.17
98	-25	-17.9	8.7	30.8	67.5	1.19
40	-9.7	-29.6	4.8	30.7	67.5	1.2
28	-29.3	-9.5	4.7	30.4	67.5	1.22
108	7.8	28.1	6.3	29.9	67.5	1.26
75	13.4	19.9	-12.3	29.4	67.5	1.3
39	-18.8	-28	1.6	28.3	67.5	1.39
25	-27.9	-18.6	1.6	28.1	67.5	1.4
123	-14.5	-18.3	-11.1	27.6	67.5	1.44
115	-12.4	-27.6	-0.3	27.6	67.5	1.44

THIS PAGE INTENTIONALLY LEFT BLANK

2.11.2 Site Specific Greater Than Class C Waste

Greater Than Class C (GTCC) waste is defined in 10 CFR 61.55(a)(3) and (4) by the concentration of long-lived radionuclides, i.e., ^{14}C, ^{59}Ni, and ^{94}Nb, and/or short-lived radionuclides, i.e., ^{3}H, ^{60}Co, and ^{63}Ni. The disposal of GTCC waste is controlled by 10 CFR 61.

GTCC waste typically consists of radiation activated and surface contaminated steel. Stainless steel core baffle structure, which is located adjacent to the reactor vessel in a high neutron flux field, is the major component of GTCC waste. The core baffle structure is typically cut under water into pieces of a size that are loaded into a waste basket. In some cases, the waste may be separately containerized to fit the fuel loading positions in the PWR spent fuel basket.

2.11.2.1 Maine Yankee Greater Than Class C Waste

The Maine Yankee Greater Than Class C (GTCC) waste results from the removal of the reactor core barrel. The barrel was cut into sections under water in the spent fuel pool and is directly loaded into the GTCC waste basket. The waste basket is sized to fit the UMS® Class 1 Transportable Storage Canister. The GTCC waste basket and canister are shown in Drawings 790-611 and 790-612, respectively, in Section 1.3.4.

The description of the Maine Yankee GTCC waste and the GTCC waste basket and canister design is also presented in Section 1.3.1. The GTCC waste basket is designed to transport up to 20,000 pounds of GTCC waste with the maximum weight of GTCC waste in each compartment limited to 10,000 pounds. The basket cavity is divided into two compartments with a separator plate. The GTCC waste basket is loaded into a GTCC waste canister, which is essentially identical to the PWR Class 1 Transportable Storage Canister (canister) except for the placement of lifting lugs and the placement of a keyway within the GTCC waste canister. The weight of the loaded GTCC waste canister is less than the weight of the Class 1 canister. The Center of Gravity (C.G.) for the transport cask containing the loaded GTCC waste canister is essentially identical to the C.G. for the transport cask containing PWR Class 1 fuels as shown in Tables 2.2-1 and 2.2-3. Therefore, no additional evaluation for the GTCC waste canister is required for the Universal Transport Cask. For the same reasons, the structural evaluation for the GTCC waste

canister is bounded by the evaluation for the Class 1 canister, with the exception of the bearing stress in the canister shell. Bearing stress is evaluated in the side drop condition since the waste basket has fewer support disks than the Class 1 fuel basket.

2.11.2.1.1 Maine Yankee GTCC Basket Structural Evaluation

The GTCC basket is evaluated for side and end impact conditions for both normal conditions of transport (1-foot drops, 20g) and hypothetical accident conditions (30-foot drops, 60g). The oblique drops are considered to be bounded by the side and end drop evaluations. The allowable stresses are taken from ASME Code, Section III, subsection NF, using the stress limits for Class 1 Plate and Shell Type component supports. The basket component temperatures are determined by the thermal analysis for the GTCC basket presented in Section 3.6.1.2.

2.11.2.1.1.1 Maine Yankee GTCC Basket Side Drop Evaluation

Basket Weldment

The basket weldment consists of a 3-inch thick cylinder having fourteen (14) disk sections welded to it. During a side drop event, the basket weldment is subjected to an inertia load and the load from the contained GTCC waste. The effect of the 3-inch thick separator plate on the basket weldment is also considered.

A three-dimensional half-symmetry finite element model is developed using the ANSYS program. The model represents a periodical section of the basket weldment, which consists of the 3-inch thick shield cylinder, one disk section and two (2) half-thickness disk sections and the canister shell, as shown in Figure 2.11.2.1-1. ANSYS SOLID45 elements and CONTAC52 elements are used to construct the model. Contact elements are used to represent the interface between the disks and the canister shell and the interface between the canister shell and the cask inner shell. A stiffness of 1.0E6 lb/in. is used for the contact elements. Symmetry boundary conditions are applied to the planes of symmetry. A constant temperature of 75°F is used in the model for determination of material properties.

Loads applied to the model include the inertia load and the load from the GTCC wastes. To ensure that the worst case conditions are considered, five cases (Cases 1 through 5) with different

load locations are evaluated. The definition of the load locations is shown in Figure 2.11.2.1-2. For Cases 1 through 3, the load from the GTCC waste in each basket compartment is conservatively assumed to be concentrated in two localized regions. Each region has an area less than 5 inch^2. Due to symmetry, the force applied in the localized region in the model (by specifying element pressure) is 2,500 lb. (10,000/2/2) with an appropriate g-load factor. While Cases 1 and 3 are used to account for the maximum possible bending moment (Mx) in the basket model (see Figure 2.11.2.1-2 for coordinate system), Case 4 is used to account for bending moment (Mz) in the model. The force applied in Case 4 is also 2,500 pound with the appropriate g-load factor. Case 4 represents the condition where the load from the GTCC waste is assumed concentrated in four localized regions. Each region has an area less than 2.5 inch^2. Case 5 is used to account for additional load due to the 3-inch thick Separator Plate or the 3-inch thick bottom plate of the basket. In addition to the 2,500 lb. load (with g-load factor) applied to the center of the span between two support disks, a load of 800 lb (1,600/2) lb. with g-load factor is applied to a localized region (2.5 inch in the z-direction and 5° in the circumferential direction).

Analysis is performed for all five (5) cases described above for normal (20g) and accident (60g) conditions. Sectional stresses are obtained for fifteen (15) section locations, as shown Figure 2.11.2.1-3. One additional section (Section No. 16, not shown in Figure 2.11.2.1-3) is defined for Case 4. The section has the same location as the applied load for Case 4 (40-degree from the plane of symmetry, and the section is defined through the thickness of the shield cylinder, similar to Section No. 2). Note that Sections 1 through 9 and Section 16 are used for the evaluation of the basket weldment. Sections 10 through 15 are used to evaluate bearing stresses in the canister shell.

Primary membrane stress (P_m) and primary membrane plus bending stress ($P_m + P_b$) at Sections No. 1 through No. 9 for each case are listed in Tables 2.11.2.1-1 and 2.11.2.1-2 for normal conditions and accident conditions, respectively. Additionally, stresses are also obtained at Section No. 16 for Case 4. However, the stresses at Section No. 16 are well below the stresses at other Sections for Case 4. For the normal conditions, maximum primary membrane stress (P_m) of 9.6 ksi occurs at Section No. 5 for Case 5 and maximum primary membrane plus bending stress ($P_m + P_b$) of 12.4 ksi occurs at Section No. 2 for Case 1.

For the accident condition, the maximum primary membrane stress (P_m) of 28.2 ksi occurs at section No. 5 for case No. 5 and maximum primary membrane plus bending stress ($P_m + P_b$) of 33.7 ksi occurs at section No. 2 for case No. 1. The comparison of the maximum calculated stresses with allowable stresses and the calculation of the margin of safety are contained in Table 2.11.2.1-3. The allowable stresses are established in accordance with ASME Code, Section III, Subsection NF-3200. The calculated maximum temperature for the basket weldment is 287°F in the thermal analysis as shown in Section 3.6.1.2. A temperature of 300°F is conservatively used in determining the allowable stresses. As shown in Table 2.11.2.1-3, the minimum margin of safety is +1.08 and +0.64 for normal conditions and accident conditions, respectively.

Weld Between the Shield Cylinder and a Disk Section

The weld between the shield cylinder and a disk section is a 3/8-inch fillet weld, on both sides of the disk. A unit length of the weld is considered as shown:

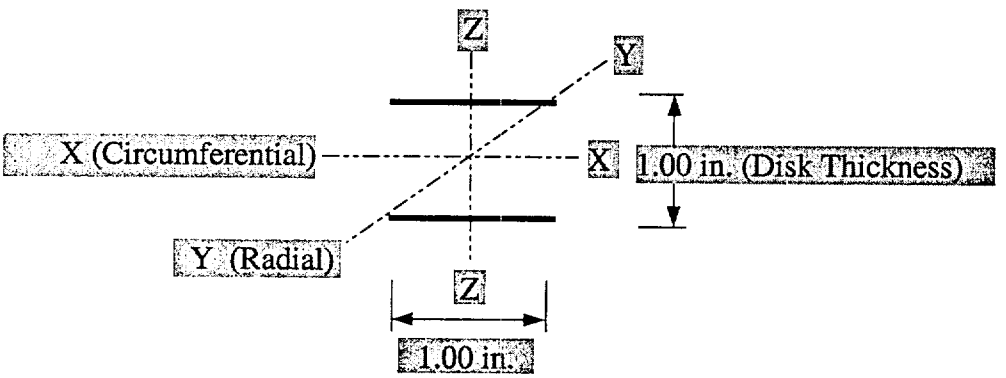

The forces and moments on the weld are determined based on sectional stress results from the finite element analysis of the basket weldment.

Allowable stress for weld evaluation is based on Table NF-3324.5(a)-1 for normal (Level A) conditions. The limiting allowable stress is $0.4S_y$ for the shear stress on the base metal, since the weld metal strength is much higher than that of the base metal (Type 304 Stainless Steel). The shear stress allowable of $0.42\ S_u$ is utilized for accident (Level D) conditions per ASME Code, Section III, Appendix F.

Sectional stresses at Sections No. 7, 8 and 9 are used for the weld evaluation. Forces on the weld (F_x, F_y and F_z) are determined based on the membrane stresses (S_{xy}, S_y, and S_{yz}) and the area of the disk cross-section ($A_d = 1 \times 1 = 1$ inch^2).

$$F_x = (S_{xy})_m \times A_d$$

$$F_y = (S_y)_m \times A_d$$

$$F_z = (S_{yz})_m \times A_d$$

Moment (M_x) on the weld is calculated based on the bending stresses (S_y) and the section modulus of the disk cross-section ($S_d = 1 \times 1^2/6 = 1/6$ in.^{3}).

$$M_x = (S_y)_b \times S_d$$

$$M_y \approx 0$$

$$M_z \approx 0$$

The stress components (kip/inch) acting on the weld are:

$$f_x = \frac{F_x}{A_w}$$

$$f_y = \frac{F_y}{A_w} + \frac{M_x}{S_w}$$

$$f_z = \frac{F_z}{A_w}$$

where:

A_w is the Area of the weld (inch)
S_w is Section Modulus of the weld (inch^2)

(Note that the weld is considered to consist of two "lines")
The resultant (f_r) of the weld stresses is

$$f_r = \sqrt{f_x^2 + f_y^2 + f_z^2}$$

For the 3/8-inch weld, the allowable stresses are:

$$f_{allowable} = 0.4 \times S_y \times \frac{3}{8} = 0.4 \times 22.5 \times \frac{3}{8} = 3.375 \text{ kip/inch (Normal Condition)}$$

$$f_{allowable} = 0.42 \times S_u \times \frac{3}{8} = 0.4 \times 66.0 \times \frac{3}{8} = 10.395 \text{ kip/inch (Accident Condition)}$$

The governing cases for the weld evaluation are Cases 2 and 5 (at Section No. 8). A summary of the weld evaluation results for the governing cases is provided in Table 2.11.2.1-4. The minimum margin of safety for the weld evaluation is +0.09 and +0.12 for normal and accident conditions, respectively.

Canister Shell Bearing Stress Evaluation

Bearing stresses in the canister shell produced by the disk section of the GTCC waste basket weldment for the side drop conditions are obtained from the finite element analysis results for the Basket Weldment. Based on ASME Code, Section III, Division 1, Appendix F, bearing stress evaluation is not required for accident (Level D) conditions. Therefore, the evaluation is performed for normal conditions only. The bearing stresses in the canister shell are obtained from Sections 10 through 15 of the finite element model (See Figure 2.11.2.1-3 for locations) for all Cases. As shown, the maximum bearing stress occurs in Section 15 for Case 5.

	Bearing Stresses (ksi)					
	Section 10	Section 11	Section 12	Section 13	Section 14	Section 15
Case 1	7.0	2.7	2.5	2.4	1.9	5.9
Case 2	5.9	2.3	2.6	2.6	2.1	6.4
Case 3	5.5	2.1	2.4	2.5	2.5	7.6
Case 4	5.3	2.1	2.1	2.1	1.9	5.9
Case 5	6.2	2.4	2.8	2.9	2.8	8.4

The allowable bearing stress is the material yield strength (S_y) in accordance with ASME Code, Section III, Division 1, Subsection NB. For Type 304 stainless steel at 300°F, the allowable stress is 22.5 ksi. As shown, the maximum bearing stress is 8.4 ksi.

The minimum margin of safety for canister shell bearing stress is:

$$M.S. = \frac{22.5}{8.4} - 1 = 1.68$$

Shield Cover Evaluation

The shield cover provides shielding for the GTCC waste at the top end of the GTCC waste basket. During a side drop, the inner surface of the shield cover will bear against the outer surface of the 3-inch shield cylinder. The maximum gap between the GTCC waste basket shield cover and the shield cover is 0.90 inch. The ring of the shield cover is 1.5-inches long and therefore the minimum bearing length is 0.6 inch. Therefore, the shield cover cannot disengage from the shield cylinder during a side drop so as to expose the GTCC waste. The 0.375-inch bevel weld between the shield cover ring and plate is evaluated in accordance with ASME Code, Section III, Subsection NF.

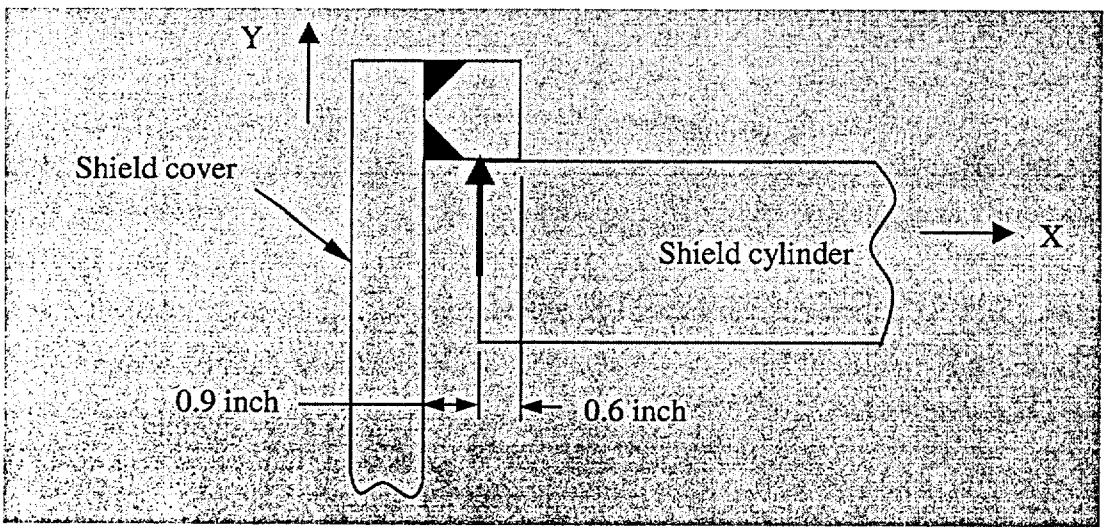

The circumferential contact width, b, between shield cover and the shield cylinder is calculated using formulas in Roark's:

$$b = 2.15\sqrt{\frac{PK_d}{E}} = 2.15\sqrt{\frac{1303\times 20\times 3058}{27E06}} = 3.70 \text{ inch for 20g}$$

As shown below, an effective length of 6.7 inches is used for the weld evaluation:

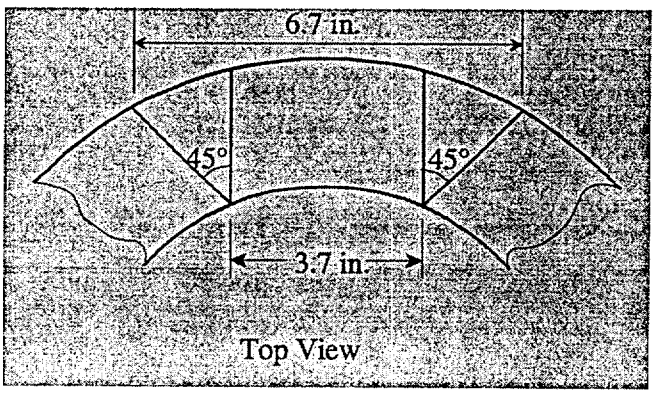

$$\text{Weld shear stress (1g): } f_y = \frac{P}{A_w} = \frac{1303}{2\times 6.70} = 98 \text{ lb/in.}$$

$$\text{Weld bending stress (1g): } f_x = \frac{M}{S_w} = \frac{1303\times 0.9}{6.70\times 1.5} = 117 \text{ lb/in.}$$

$$\text{Weld Stress (1g): } f_r = \sqrt{98^2 + 117^2} = 153 \text{ lb/in.}$$

$$\text{For normal conditions: M.S.} = \frac{0.40\times S_y\times 0.38}{S_w} - 1 = \frac{0.4\times 22500\times 0.38}{20\times 153} - 1 = 0.12$$

$$\text{For accident conditions: M.S.} = \frac{0.42\times S_u\times 0.38}{S_w} - 1 = \frac{0.42\times 66000\times 0.38}{60\times 153} - 1 = 0.15$$

Support Weldment

The support weldment consists of the "support wall" and "separator plate." The support wall is a cylinder of 0.25-inch thickness and 48.3-inches outside diameter. The separator plate has a thickness of 3 inches. The support weldment is placed inside the shield cylinder of the basket weldment to maintain the integrity of the upper and lower compartments.

In a side drop, the support weldment bears against the shield cylinder. Using Table 33, Case 2c in "Roark's Formulas for Stress and Strain" (Roark) [28], the bearing stress (S_b) between the separator plate and the inner surface of the 3-inches thick shield cylinder is:

Support weldment weight = 2,372 lbs.
Separator plate thickness = 2.00 inches (portion bearing on shield cylinder)
Support weldment OD = 48.3 inches
Shield cylinder I.D = 48.8 inches
Temperature at the bearing surface = 300°F
Normal conditions of transport impact acceleration = 20g

$$p = \frac{2372 \times 20}{2} = 23{,}720 \text{ lb/in.} \qquad K_d = \frac{48.8 \times 48.3}{48.8 - 48.3} = 4{,}714$$

$$S_b = 0.591\sqrt{\frac{23720 \times 27E6}{4714}} = 6{,}889 \text{ psi} = 6.89 \text{ ksi}$$

$$M.S. = \frac{S_y}{S_b} - 1 = \frac{22.50}{6.89} - 1 = 2.27$$

During a side drop, the GTCC waste weight is transferred directly through the 0.25-inch thick support wall (cylinder) to the 3-inch thick shield cylinder. The cylinder portion of the support wall, which is subjected to self-weight only, is evaluated using a finite element model, as shown in Figure 2.11.2.1-4. The model represents a 1-inch section of the cylinder portion of the support wall. ANSYS BEAM3 elements are used to construct the model. The model is restrained for all degrees of freedom at both ends. The maximum stress (S) in the support wall for normal and accident conditions is 9.12 ksi and 27.37 ksi, respectively. The temperature of the support wall is taken as 300°F.

The margins of safety for the support wall are:

$$\text{For normal conditions : } M.S. = \frac{1.5 \times S_m}{S} - 1 = \frac{1.5 \times 20.00}{9.2} - 1 = 2.29$$

$$\text{For accident conditions : } M.S. = \frac{S_u}{S} - 1 = \frac{66.00}{27.37} - 1 = 1.41$$

2.11.2.1.1.2 Maine Yankee GTCC Waste Basket End Drop Evaluation

This section presents the evaluation of the waste basket components for the normal conditions of transport (20g), and accident conditions (60g) end drop.

Basket Weldment

This section evaluates the 3-inch thick shield cylinder for an end drop condition. The total weight of the entire GTCC basket (32,400 lb) and maximum GTCC waste payload (20,000 lb) is conservatively applied to the top of the shield cylinder. The compressive stress in the shield cylinder for normal and accident condition is

$$S_{normal} = \frac{P}{A} \times 20 = \frac{32,400 + 20,000}{488.2} \times 20 = 2.15 \text{ ksi}$$

$$S_{accident} = \frac{P}{A} \times 60 = \frac{32,400 + 20,000}{488.2} \times 60 = 6.44 \text{ ksi}$$

Where:

$$A = \frac{\pi}{4}\left(54.8^2 - 48.8^2\right) = 488.2 \text{ in}^2, \text{ the cross-sectional area of the cylinder}$$

The margin of safety for normal and accident conditions is:

For the normal condition (20g):

$$M.S. = \frac{S_m}{S_{normal}} - 1 = \frac{20.0}{2.15} - 1 = 8.32$$

For the accident condition (60g):

$$M.S. = \frac{0.7 \times S_u}{S_{accident}} - 1 = \frac{0.7 \times 66.0}{6.44} - 1 = 6.17$$

The critical buckling stress (S_{CR}) in the shield cylinder is determined using the formulas in Table 35, Case 15 of "Roark's Formulas for Stress & Strain" [28]. Note that the lower bound value (40% of the theoretical values) is conservatively used:

$$S_{CR} = 0.4 \times \frac{1}{\sqrt{3}} \frac{E}{\sqrt{1-\upsilon^2}} \frac{t}{r} = 0.4 \times \frac{1}{\sqrt{3}} \frac{27.0 \times 10^3}{\sqrt{1-0.31^2}} \frac{3.0}{25.9}$$

$$= 759.67 \text{ ksi}$$

Where:

υ = 0.31, the Poisson's ratio at 300°F
E = 27.0×10^3 ksi, the modulus of elasticity at 300°F
t = 3.0 inch, thickness of the shield cylinder
r = 25.9 inch, the mean radius of the shield cylinder

In accordance with ASME Code, Section III, Subsection NF, the allowable buckling stress for normal and accident conditions is $0.5 \times S_{CR}$ and $0.67 \times S_{CR}$, respectively. The margin of safety is:

For the normal condition (20g):

$$M.S. = \frac{0.5 \times S_{CR}}{S_{normal}} - 1 = \frac{0.5 \times 759.67}{2.15} - 1 = +\text{large}$$

For the accident condition (60g):

$$M.S. = \frac{0.67 \times S_{CR}}{S_{accident}} - 1 = \frac{0.67 \times 759.67}{6.44} - 1 = +large$$

Support Disk

The support disk is subjected to a bending moment due to self-weight during end drop conditions. A unit width of the disk is considered for the evaluation of the disk and the weld between the disk and the shield cylinder. The disk is 1-inch thick with inner diameter and outer diameter of 54.8-inches and 65.3-inches, respectively.

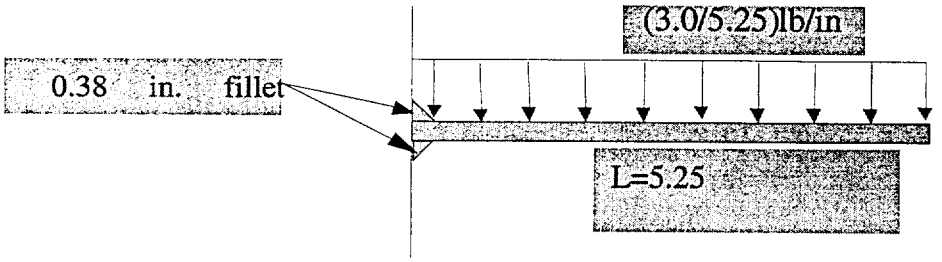

The weight of one disk is $W = \frac{4035}{14} = 288$ lbs for 1 g

The weight per unit width is $w = \frac{288}{\pi \times \frac{54.8+65.3}{2}} \approx 3.0$ lb (conservatively)

The maximum bending moment (1 g) for the disk is:

$$M = \frac{wl^2}{2} = \frac{\left(3.0/5.25\right) \times 5.25^2}{2} = 7.9 \text{ inch - lb}$$

The bending stress and margin of safety for normal and accident conditions are calculated below. Allowable stress is determined at 300°F.

Normal Condition (20g):

$$S = \frac{6M}{bt^2} = \frac{6 \times 7.9 \times 20}{1.00 \times 1.00^2} = 948 \text{ psi} = 0.948 \text{ ksi}$$

$$M.S. = \frac{1.5 \times S_m}{S} - 1 = \frac{1.5 \times 20.0}{0.948} - 1 = +\text{large}$$

Accident Condition (60g):

$$S = \frac{6 \times 7.9 \times 60}{1.00 \times 1.00^2} = 2{,}844 \text{ psi} = 2.84 \text{ ksi}$$

$$M.S. = \frac{S_u}{S} - 1 = \frac{66.00}{2.84} - 1 = +\text{large}$$

The fillet welds are evaluated for normal and accident conditions as shown below:

Weld properties for 2-line weld:
$A_w = 2$ inch
$S_w = 1.0 \times 1.0 = 1$ inch^2

For 1g the shear stress across weld is: $f_y = \frac{p}{A_w} = \frac{3.0}{2} = 1.5$ lb/in

For 1g the stress due to bending across weld is: $f_x = \frac{M}{S_w} = \frac{7.9}{1} = 7.9$ lb/in

The 1g weld stress is: $f_r = \sqrt{1.5^2 + 7.9^2} = 8.02$ lb/in

A 300°F temperature is used to determine the allowable stress for the weld evaluation. For the 3/8-inch weld, the margin of safety of the weld for normal and accident conditions is:

For the normal condition (20g), the margin of safety is:

$$M.S. = \frac{0.4 \times S_y \times \frac{3}{8}}{S} - 1 = \frac{0.4 \times 22500 \times \frac{3}{8}}{20 \times 8.02} - 1 = +large$$

For the accident condition (60g) the margin of safety is:

$$M.S. = \frac{0.42 \times S_u \times \frac{3}{8}}{S} - 1 = \frac{0.42 \times 66000 \times \frac{3}{8}}{60 \times 8.02} - 1 = +large$$

Support Weldment

The support weldment consists of the separator plate and support wall. As shown in Figure 2.11.2.1-5, a finite element model is generated using the ANSYS program to evaluate the separator plate for end drops. SHELL63 elements with a thickness of 3.0-inch and a modulus of elasticity of 25.8E6 psi (Type 304 stainless steel at 500°F) are used in the model. Loads from the GTCC waste (10,000 lb) are distributed over the inner 25% of the plate area for conservatism. In addition, the inertia load due to the self-weight of the separator plate is considered in the analysis. Because the separator plate (3-inch thick) is much stiffer than the support wall (1/4-inch thick), which is welded to the separator plate, the separator plate model is assumed to be simply supported at the edges. The analysis is performed for normal (20g) and accident (60g) bottom end drop conditions. The calculated maximum stress intensity in the model is 19.90 ksi and 59.70 ksi for normal and accident conditions, respectively. The allowable stresses are conservatively determined at 500°F.

For the normal condition, the margin of safety is:

$$M.S. = \frac{1.5 \times S_m}{S} - 1 = \frac{1.5 \times 17.50}{19.90} - 1 = 0.32$$

For the accident condition, the margin of safety is:

$$M.S. = \frac{3.6 \times S_m}{S} - 1 = \frac{63.00}{59.70} - 1 = 0.06$$

During a top end drop condition, the support wall (cylinder) is subjected to compression loads from the separator plate and the GTCC waste of the lower compartment. The support wall (cylinder) has the following dimensions:

Length = 76.5 in.
Outside radius = 24.15 in.
Thickness = 0.25 in.

Since the separator plate (3-inch thick) is much more rigid than the support wall (1/4-inch thick), the end rotation of the support wall is taken from the edge rotation of the finite element model for the separator plate (Figure 2.11.2.1-5). The rotation of the edge of the separator plate (θ) is 0.004 rad and 0.012 rad for normal and accident conditions, respectively. The bending moment is determined by using the formula for a cantilever beam with applied rotation at the free end (a unit width of the support wall is considered).

Normal Conditions: $\theta = 0.004$ rad

$$M = \frac{E\theta}{L} = \frac{27 \times 10^6 \times \frac{1 \times 0.25^3}{12} \times 0.004}{76.8} = 1.83 \text{ in} - \text{lb} \qquad \text{(Weaver) [55]}$$

$$S_b = \frac{6M}{bt^2} = \frac{6 \times 1.83}{1 \times .25^2} = 176 \text{ psi}$$

Accident Conditions: $\theta = 0.012$ rad

$$M = \frac{E\theta}{L} = \frac{27 \times 10^6 \times \frac{1 \times 0.25^3}{12} \times 0.012}{76.8} = 5.49 \text{ in} - \text{lb} \qquad \text{(Weaver)}$$

$$S_b = \frac{6M}{bt^2} = \frac{6 \times 5.49}{1 \times .25^2} = 527 \text{ psi} = 0.527 \text{ ksi}$$

The axial load conservatively applied to the cylinder for 1g is:

$$W = 10000 + 1529 + 843 = 12,372 \text{ lbs}$$

Where:

Waste = 10,000 lb
Separator plate = 1,529 lb
Support wall = 843 lb

The formula for compression stress is:

$$S = \frac{P}{A} \qquad A = \pi \times (24.15^2 - 23.9^2) = 37.7 \text{ in}^2 \text{ (cross - sectional area of cylinder)}$$

For normal conditions (20g):

$$S_{normal} = \frac{20 \times 12.40}{37.7} = 6.58 \text{ ksi}$$

$$M.S. = \frac{S_m}{S_{normal}} - 1 = \frac{20.0}{6.58} - 1 = 1.04$$

For accident conditions (60g):

$$S_{accident} = \frac{60 \times 12.40}{37.7} = 19.70 \text{ psi}$$

$$M.S. = \frac{0.7 \times S_u}{S_{accident}} - 1 = \frac{0.7 \times 66.00}{19.70} - 1 = 1.35$$

Note that the margin of safety is calculated for P_m stresses only, since the bending stresses are negligible as shown above.

The critical buckling stress (S_{CR}) in the shield cylinder is determined using the formulas in Table 35, Case 15 of "Roark's Formulas for Stress & Strain" [28]. Note that the lower bound value (40% of the theoretical value) is conservatively used.

$$S_{CR} = 0.4 \times \frac{1}{\sqrt{3}} \frac{E}{\sqrt{1-\upsilon^2}} \frac{t}{r} = 0.4 \times \frac{1}{\sqrt{3}} \frac{27.0 \times 10^3}{\sqrt{1-0.31^2}} \frac{0.25}{24.025}$$

$$= 68.25 \text{ ksi}$$

Where:

υ = 0.31, the Poisson's ratio at 300°F
E = 27.0×10^3 ksi, modulus of elasticity at 300°F
r = 0.25 inch, thickness of the support wall
t = 24.025 inch, the mean radius of the support wall

In accordance with ASME Code Section III, Subsection NF, the allowable buckling stress for normal and accident conditions is $0.5 \times S_{CR}$ and $0.67 \times S_{CR}$, respectively. The margin of safety is:

Normal Conditions (20g):

$$M.S. = \frac{0.5 \times S_{CR}}{S_{normal}} - 1 = \frac{0.5 \times 68.25}{6.58} - 1 = 4.2$$

Accident Conditions (60g):

$$M.S. = \frac{0.67 \times S_{CR}}{S_{accident}} - 1 = \frac{0.67 \times 68.25}{19.70} - 1 = 1.32$$

Shield Cover

The shield cover is evaluated for bearing stress for top end drop conditions. During a top end drop there are two separate components bearing on the plate: the first is the GTCC basket and the second is the support weldment. For this evaluation, the support weldment weight includes

the weight of the separator plate and the GTCC waste in the lower compartment. Also note that the bearing evaluation is required for the normal condition (20g) only. Bearing stress, S_b, due to the weight of the GTCC waste basket is:

$$W = 32{,}302 - 1303 - 1529 - 843 = 28{,}627 \text{ lbs}$$

$$A = \frac{\pi}{4} \times \left(54.8^2 - 48.8^2\right) = 488.2 \text{ in}^2 \text{ (cross - sectional area of GTCC waste basket)}$$

$$S_b = \frac{20 \times 28{,}627}{488.2} = 1{,}173 \text{ psi} = 1.17 \text{ ksi}$$

Bearing stress, S_b, due to the weight of the support cylinder, separator plate, and 10,000 lb GTCC waste, is:

$$W = 1{,}529 + 843 + 10{,}000 = 12{,}372 \text{ lb}$$

$$A = \frac{\pi}{4} \times \left(48.3^2 - 47.8^2\right) = 37.7 \text{ in}^2 \text{ (cross - sectional area of support weldment)}$$

$$S_b = \frac{20 \times 12372}{37.7} = 6563 \text{ psi} = 6.56 \text{ ksi}$$

The minimum margin of safety is:

$$M.S. = \frac{S_y}{S} - 1 = \frac{22.50}{6.56} - 1 = +2.42$$

In the bottom end drop, the shield cover acts as a simply supported circular plate under its own weight. Using a shield cover weight of 1,303 lbs, and Table 24 Case 10a from "Roark's Formulas for Stress and Strain," the maximum stress on the cover is:

Thickness = 1.50 in.

Radius (r_a) = 29.4 in

Area = $\pi(29.4)^2 = 2715.5$ in^2

1g load = 1,303/2,715.5 = 0.48 psi

E = 27.0 E6 psi

Poisson's ratio = 0.31

r_o = 0.00 in

The maximum stress occurs at the center of the plate. The moment at this location is:

$$M = q \cdot r^2 \cdot L_{17}$$

Where:

$$L_{17} = \frac{1}{4}\left[1-\left(\frac{1-\upsilon}{4}\right)\left[1-\left(\frac{r_o}{r_a}\right)^4\right]-\left(\frac{r_o}{r_a}\right)^2\left[1+(1+\upsilon)\ln\left(\frac{r_a}{r_0}\right)\right]\right] = 0.207$$

$$M = 0.48 \times 29.4^2 \times 0.207 = 86 \text{ inch - lbs}$$

The maximum stress (S) at the center of the plate is calculated by:

$$S = g \times \frac{6M}{t^2}$$

For the normal condition (20g):

$$S = 20 \times \frac{6 \times 86}{1.5^2} = 4{,}587 \text{ psi} = 4.59 \text{ ksi}$$

$$M.S. = \frac{1.5 \times S_m}{S} - 1 = \frac{1.5 \times 20.00}{4.59} - 1 = +5.54$$

For the accident condition (60g):

$$S = \frac{60}{20} \times 4{,}587 = 13{,}761 \text{ psi}$$

$$M.S. = \frac{S_u}{S} - 1 = \frac{66{,}000}{13{,}761} - 1 = +3.80$$

Support Ring

The support ring is welded to the inside surface of the shield cylinder to support the Support Weldment when the GTCC waste basket is vertical. The load applied to the support ring is the sum of the weight of the separator plate (1,529 lb), support wall (843 lb), the GTCC waste in the upper compartment (10,000 lb). The cross section of the ring is 1.0 in. x 1.0 in.

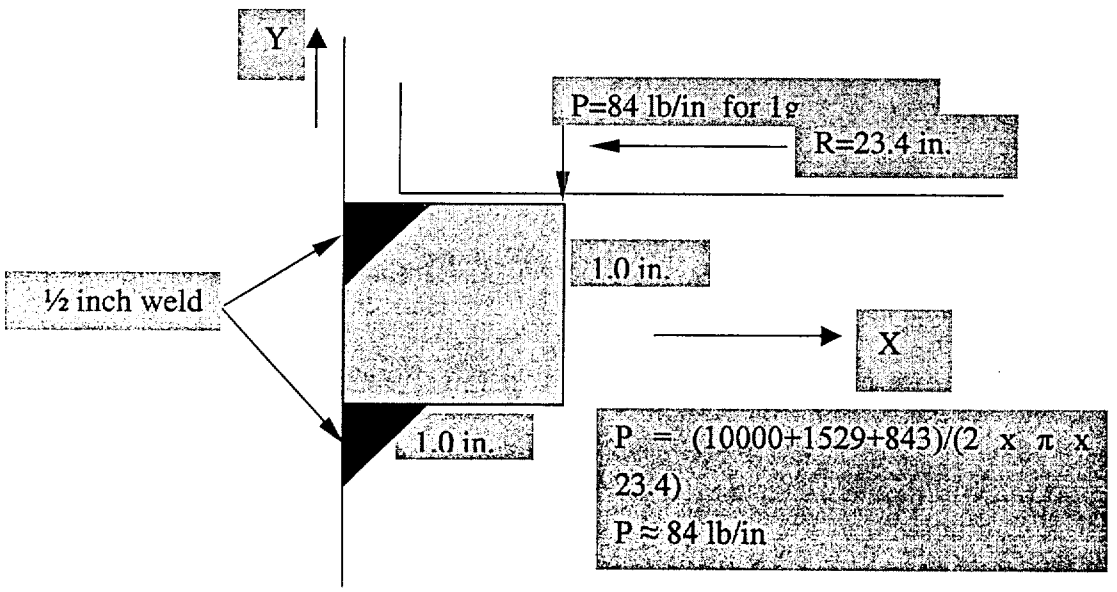

A unit length of the weld is considered for the weld evaluation. The inner radius of the ring is 23.4 inch. Considering the weld as two lines;

$$A_w = 2 \text{ inch}$$
$$S_w = 1 \times 1 = 1 \text{ in}^2$$

For 1g the shear stress across the weld is : $f_y = \frac{P}{A_w} = \frac{84}{2} = 42$ lb/in

For 1g the stress due to the moment across the weld is: $f_x = \frac{83 \times 1.0}{1.0} = 84$ lb/in

The total weld stress is: $f_r = \sqrt{42^2 + 84^2} = 94$ lb/in for 1g

For the ½ inch weld, the margin of safety is calculated as:

For the normal condition (20g):

$$M.S. = \frac{0.4 \times S_y \times 0.5}{g \times S} - 1 = \frac{0.4 \times 22{,}500 \times 0.5}{20 \times 94} - 1 = 1.39$$

For the accident condition (60g):

$$M.S. = \frac{0.42 \times S_u \times 0.5}{g \times S} - 1 = \frac{0.42 \times 66{,}000 \times 0.5}{60 \times 94} - 1 = 1.46$$

Figure 2.11.2.1-1 Maine Yankee GTCC Basket Finite Element Model

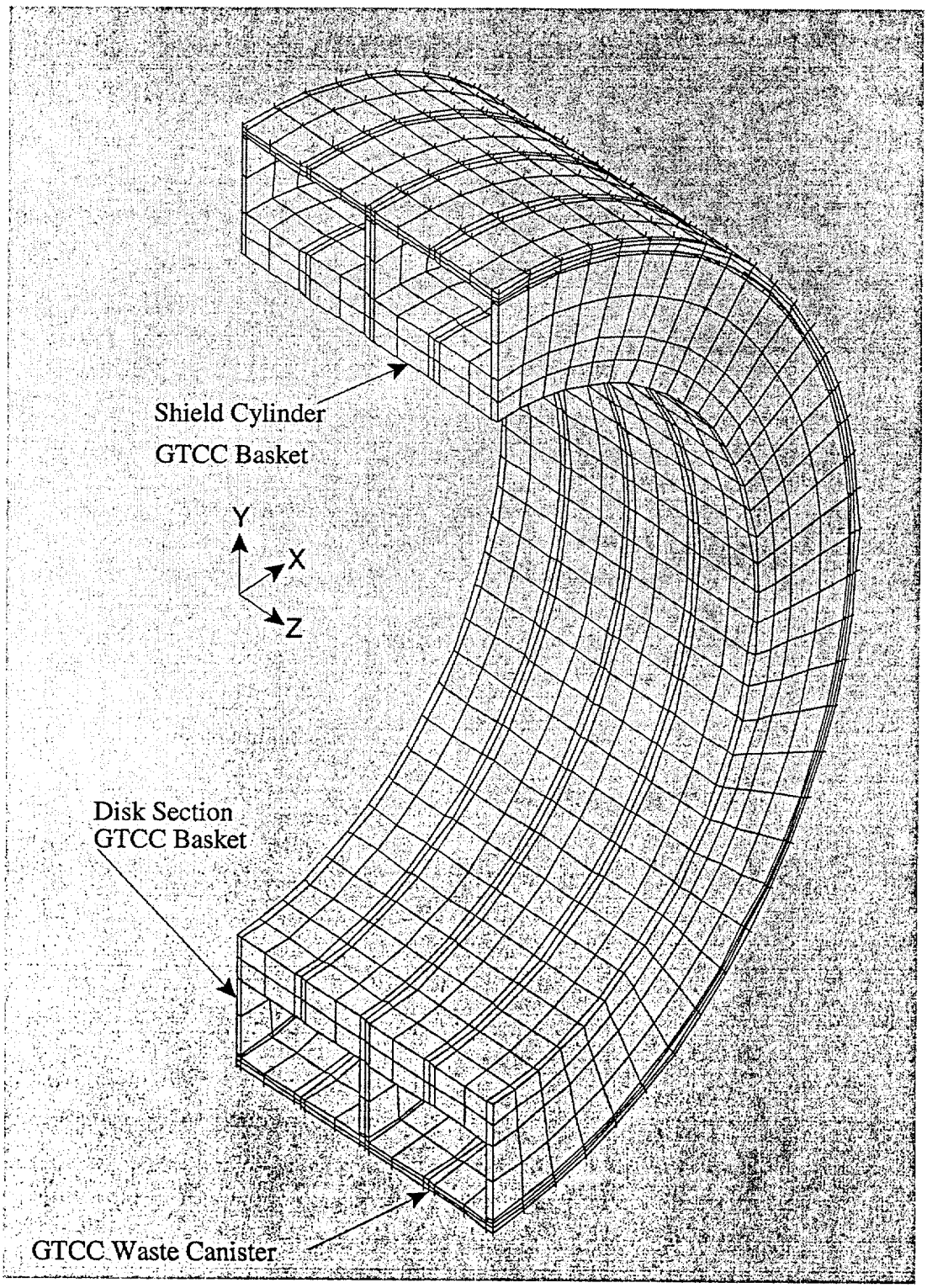

Figure 2.11.2.1-2 Maine Yankee GTCC Basket Finite Element Model Pressure Loading Locations

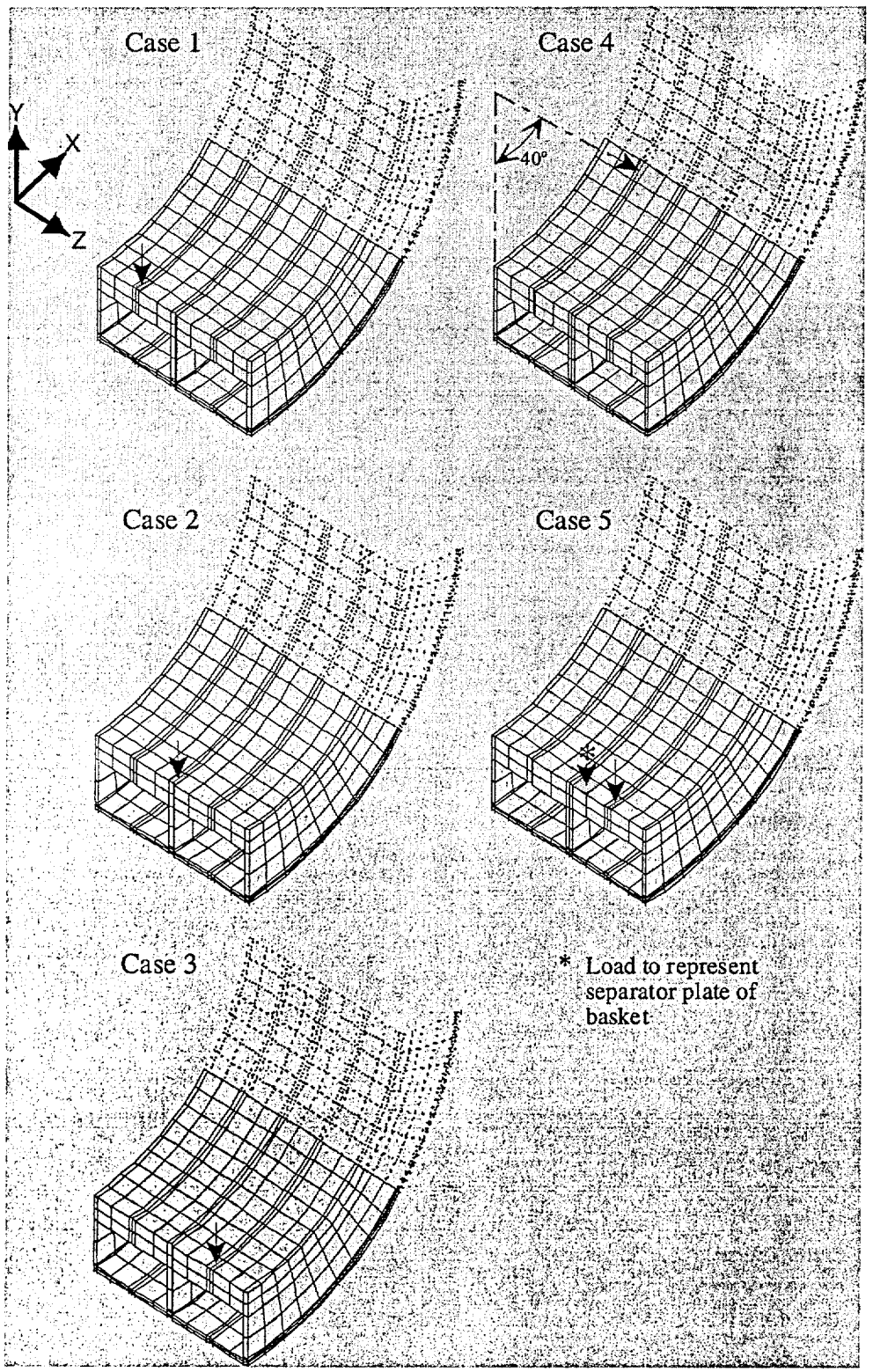

Figure 2.11.2.1-3 Maine Yankee GTCC Basket Finite Element Model Section Locations for Stress Evaluation

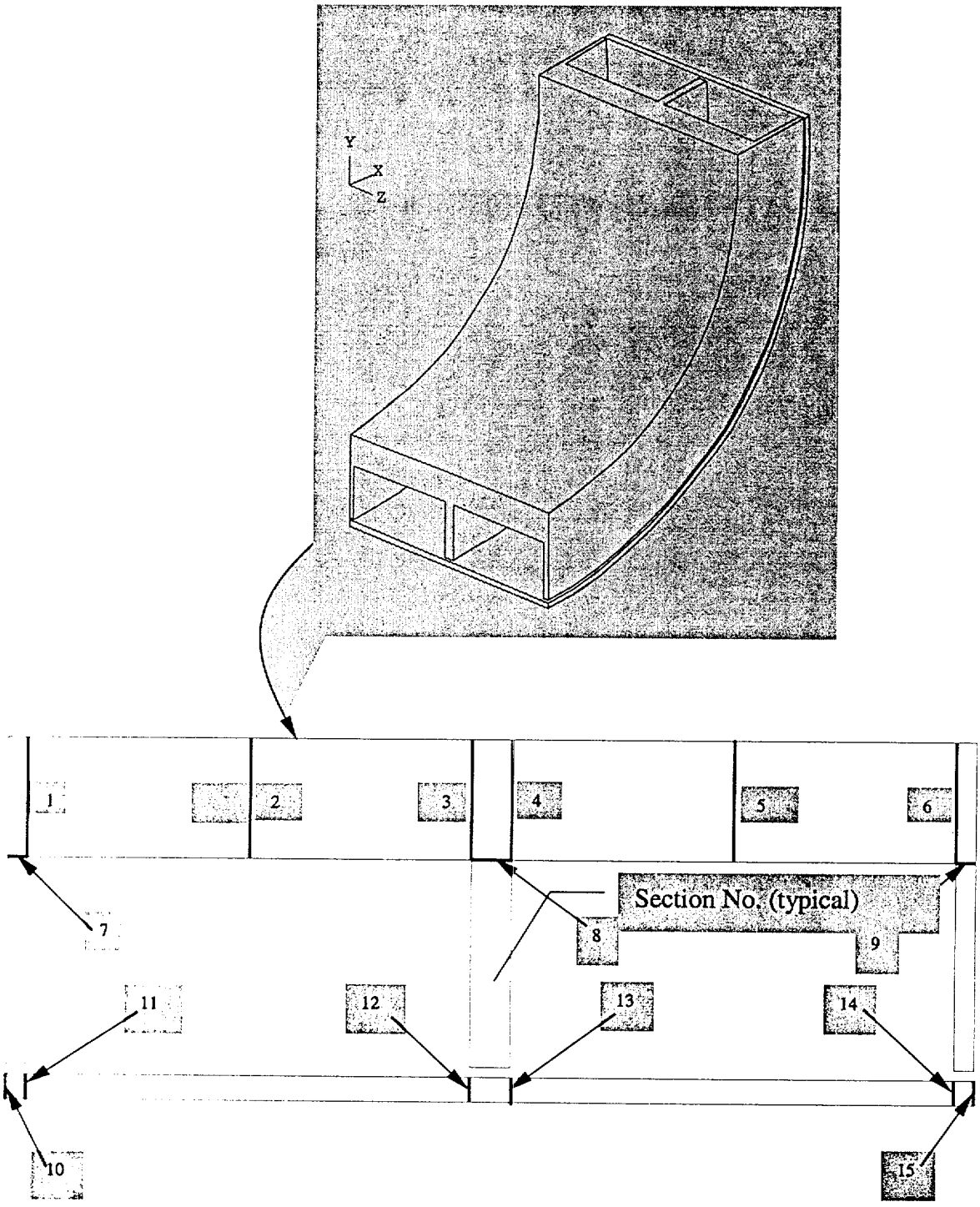

Figure 2.11.2.1-4 Finite Element Model for Maine Yankee GTCC Basket Support Wall

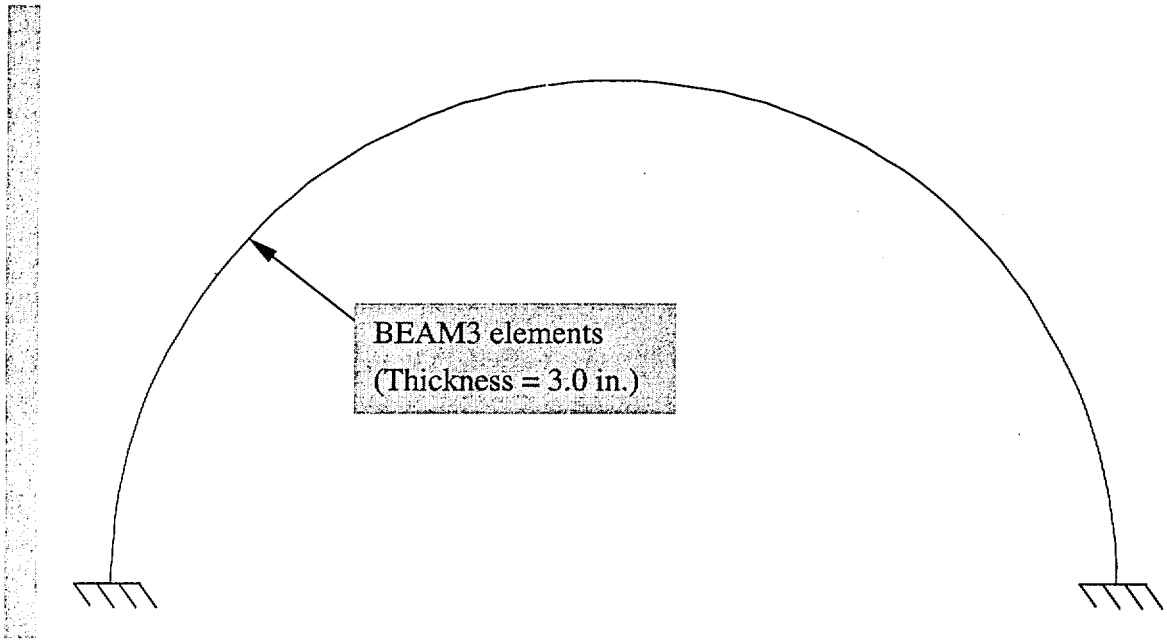

Figure 2.11.2.1-5 Finite Element Model for Maine Yankee GTCC Basket Separator Plate

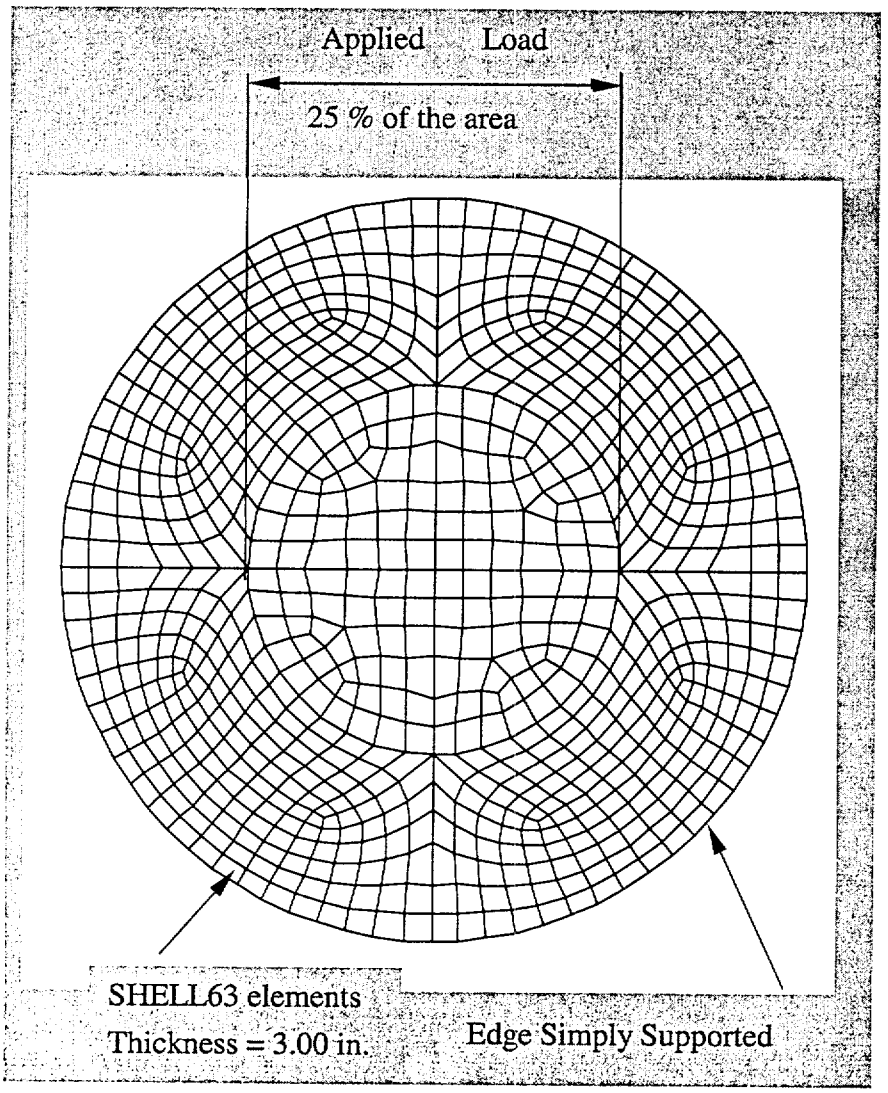

Table 2.11.2.1-1 Maine Yankee GTCC Basket Weldment Sectional Stresses for Normal Condition Side Drop (ksi)

		Section No.1	Section No. 2	Section No. 3	Section No. 4	Section No. 5	Section No. 6	Section No. 7	Section No. 8	Section No. 9
Case 1	P_m	3.7	9.4	3.1	2.2	0.2	1.7	4.1	2.0	2.4
	P_m+P_b	5.4	12.0	4.9	4.8	4.6	4.9	4.5	3.3	2.7
Case 2	P_m	1.9	1.0	7.6	7.6	1.0	2.1	2.0	8.5	1.9
	P_m+P_b	5.0	3.7	10.0	10.0	3.7	4.8	2.4	8.6	2.1
Case 3	P_m	1.5	0.2	2.2	3.1	9.4	3.9	2.5	2.0	4.0
	P_m+P_b	5.1	4.6	4.8	4.9	12.0	5.1	2.8	3.3	4.6
Case 4	P_m	3.6	1.7	3.1	3.1	1.1	2.8	3.4	3.7	4.0
	P_m+P_b	11.0	10.3	10.0	9.9	8.6	8.6	3.6	3.8	4.3
Case 5	P_m	1.6	0.3	2.7	5.2	9.6	4.4	2.6	3.9	4.4
	P_m+P_b	5.2	4.6	4.6	6.5	11.5	6.1	2.9	5.7	5.0

Table 2.11.2.1-2 Maine Yankee GTCC Basket Weldment Sectional Stresses for Accident Condition Side Drop (ksi)

		Section No.1	Section No. 2	Section No. 3	Section No. 4	Section No.5	Section No.6	Section No.7	Section No.8	Section No.9
Case 1	P_m	9.6	27.9	7.9	4.4	0.7	2.9	9.6	3.4	7.0
	P_m+P_b	15.3	33.7	12.2	11.9	11.8	11.9	10.2	7.3	8.2
Case 2	P_m	3.8	2.7	21.2	15.3	2.7	4.4	4.9	23.3	4.8
	P_m+P_b	12.0	8.9	28.5	28.5	8.9	11.5	5.3	23.3	5.8
Case 3	P_m	2.4	0.7	4.4	7.9	28.0	10.3	6.8	3.4	9.2
	P_m+P_b	12.4	11.9	11.6	12.2	33.7	14.6	7.0	7.4	10.9
Case 4	P_m	8.3	4.8	6.8	6.7	2.8	5.7	11.2	11.2	11.6
	P_m+P_b	29.4	28.0	26.5	26.0	20.3	22.5	11.8	11.2	13.6
Case 5	P_m	2.3	1.0	5.8	14.2	28.2	11.3	6.9	9.0	10.5
	P_m+P_b	11.9	11.3	11.5	16.9	33.1	17.1	7.5	14.2	12.3

Table 2.11.2.1-3 Summary of Maine Yankee GTCC Basket Weldment Side Drop Stress Evaluation

		Maximum Stress Intensity (ksi)	Allowable Stress (ksi)	Margin of Safety $\left(\frac{\sigma_{allowable}}{\sigma_{Max.}} - 1\right)$
Normal Condition	P_m	9.6	20.0 (S_m @ 300°F)	1.08
	$P_m + P_b$	12.0	30.0 (1.5 S_m @ 300°F)	1.50
Accident Condition	P_m	28.2	46.2 (0.7 Su @ 300°F)	0.64
	$P_m + P_b$	33.7	66.0 (Su @ 300°F)	0.96

Table 2.11.2.1-4 Evaluation of the Weld Between the Shield Cylinder and Support Disk

	Normal Condition of Transport		Accident Condition	
	Case 2 Section 8*	Case 5 Section 8	Case 2 Section 8	Case 5 Section 8
F_x (kip)	0.494	0.188	2.500	0.405
F_y (kip)	6.181	5.677	18.400	13.120
F_z (kip)	0.000	0.512	0.000	1.527
M_x (kip)	0.000	0.118	0.000	2.136
M_y (kip)	0.000	0.000	0.000	0.000
M_z (inch-kip)	0.000	0.000	0.000	0.000
f_x (kip/inch)	0.247	0.094	1.250	0.203
f_y (kip/inch)	3.091	2.957	9.200	8.696
f_z (kip/inch)	0.000	0.256	0.000	0.764
f_r (10^3 kip/inch)	3.10	2.970	9.285	8.732
$f_{allowable}$ (ksi)	3.375	3.375	10.395	10.395
Margin of Safety $\left(\frac{f_{allowable}}{f_r} - 1\right)$	0.09	0.14	0.12	0.19

* Note that the stresses on Section 8 for Case 2 (Normal Condition) are averaged over an area from the plane of symmetry to 5 degree along the circumferential direction.

2.12 References

1. Title 10 of the Code of Federal Regulations, Part 71 (10 CFR 71), "Packaging and Transportation of Radioactive Materials," April 1996.

2. IAEA Safety Series No. 6, "Regulations for the Safe Transport of Radioactive Materials," International Atomic Energy Agency, Vienna, Austria, 1985 Edition, as amended 1990.

3. NUREG-0612, "Control of Heavy Loads at Nuclear Power Plants," U.S. Nuclear Regulatory Commission, July 1980.

4. ANSI N14.6-1993, "Radioactive Materials - Special Lifting Devices for Shipping Containers Weighing 10,000 Pounds (4,500 kg) or More," American National Standards Institute, 1983.

5. Title 10 of the Code of Federal Regulations, Part 72 (10 CFR 72), "Licensing Requirements for the Independent Storage of Spent Nuclear Fuel and High Level Radioactive Waste," April 1996.

6. ASME Boiler and Pressure Vessel Code, Division I, Section III, Subsection NB, "Class 1 Components," 1995 Edition with 1995 Addenda.

7. NUREG/CR-3019, "Recommended Welding Criteria for Use in the Fabrication of Shipping Containers for Radioactive Materials," March 1984.

8. NUREG/CR-3854, "Fabrication Criteria for Shipping Containers," March 1985.

9. NUREG/CR-6007, "Stress Analysis of Closure Bolts for Shipping Casks," Mok, G.C, Fischer, L.E., Hsu, S.T., January 1993.

10. US NRC Regulatory Guide 7.6, "Design Criteria for the Structural Analysis of Shipping Cask Containment Vessels," Revision 1, March 1978.

11. US NRC Regulatory Guide 7.8, "Load Combinations for the Structural Analysis of Shipping Casks for Radioactive Material," Revision 1, March 1989.

12. ASME Boiler and Pressure Vessel Code Cases, Nuclear Components, Case N-284-1, "Metal Containment Shell Buckling Design Methods," Approved March 1995.

13. US NRC Regulatory Guide 7.11, "Fracture Toughness Criteria of Base Material for Ferritic Steel Shipping Cask Containment Vessels with a Maximum Wall Thickness of 4 Inches (0.1 m)," June 1991.

14. US NRC Regulatory Guide 7.12, "Fracture Toughness Criteria of Base Material for Ferritic Steel Shipping Cask Containment Vessels with a Wall Thickness Greater than 4 Inches (0.1 m) But Not Exceeding 12 Inches (0.3m)," June 1991.

15. ASME Boiler and Pressure Vessel Code, Section III, Division I, Subsection NG, "Core Support Structures," 1995 Edition with 1995 Addenda.

16. NUREG/CR-6322, "Buckling Analysis of Spent Fuel Baskets," May 1995.

17. ASME Boiler and Pressure Vessel Code, Division 1, Section III, Part A, "Appendices," 1995 Edition with 1995 Addenda.

18. NUREG/CR-1815, "Recommendations for Protecting Against Failure by Brittle Fracture in Ferritic Steel Shipping Containers Up to Four Inches Thick," Holman, W.R., and Langland, R.T., June 1981.

19. ASME Boiler and Pressure Vessel Code, Subsection NG, Subarticle NG-3225, "Level D Service Limits," 1995 Edition with 1995 Addenda.

20. ASME Boiler and Pressure Vessel Code, Division 1, Section III, Subsection NE, "Class MC Components," 1995 Edition with 1995 Addenda.

21. ASME Boiler and Pressure Vessel Code, Section II, Part D, "Material Properties," 1995 Edition with 1995 Addenda.

22. MIL-HDBK-5F, "Metallic Materials and Elements for Aerospace Vehicle Structures," U.S. Department of Defense, November 1990.

23. Tietz, T.E., "Determination of the Mechanical Properties of High Purity Lead and a 0.05% Copper-Lead Alloy," Stanford Research Institute, Menlo Park, CA, WADC Technical Report 57-695, ASTIA Document Number 151165, April 1958.

24. NUREG/CR-0481, SAND77-1872, Rack, H.J., Knorovsky, G.A., "An Assessment of Stress-Strain Data Suitable for Finite-Element Elastic-Plastic Analysis of Shipping Containers," September 1978.

25. Baumeister, T., and Marks, L.S., Standard Handbook for Mechanical Engineers, 7th Edition, New York, McGraw-Hill Book Co., New York, N.Y., 1967.

26. NS-4-FR Fire Resistant Neutron and/or Gamma Shielding Material - Product Technical Data, Genden Engineering Services & Construction Company, Tokyo, Japan.

27. US NRC Bulletin 96-04, "Chemical, Galvanic, or Other Reactions in Spent Fuel Storage and Transportation Casks," July 1996.

28. Roark, R. J., and Young, W.C., Formulas for Stress and Strain, 6th Edition, New York, McGraw Hill, Inc., 1989.

29. Blake, A., "How to Find Deflection and Moment of Rings and Arcuate Beams," Product Engineering, January 1963.

30. Spotts, M. F., Design of Machine Elements, 2nd Edition, Prentice Hall, 1953.

31. Field Manual of the Interchange Rules as Adopted by the Association of American Railroads, Rule 88, "Mechanical Requirements for Acceptance," Washington, D.C., 1986.

32. ANSYS Revision 5.2, Computer Program, ANSYS, Inc., Houston, PA.

33. RBCUBED Version 3.0, "A Program to Calculate Impact Limiter Dynamics," Proprietary Computer Program developed by NAC International, November 1996.

34. NUREG/CR-0322, SAND 77-1589, Von Riesemann, W.A., and Guess, T.R., "The Effects of Temperature on the Energy-Absorbing Characteristics of Redwood," August 1978.

35. Technical Report 32-944, Knoell, A.C., "Environmental and Physical Effects on the Response of Balsa Wood as an Energy Dissipator," Jet Propulsion Laboratory, June 1966.

36. Technical Report 32-1295, The Wood Handbook, Jet Propulsion Laboratory.

37. NAC Services Inc., Safety Analysis Report for the NAC Storable Transport Cask (Docket Number 71-9235), Revision 8, Norcross, Georgia, August 1994.

38. Military Specification MIL-S-7998 "A Sandwich Construction Core Material, Balsa Wood," March 1970 with Amendment 1, February 1978.

39. Resnick, R., and Halliday, D, Physics, 3rd Edition, Part 1, New York, John Wiley & Sons, 1977.

40. NUREG/CR-0481, SAND77-1872, Rack, H.J., and Knorovsky, G.A, "An Assessment of Stress-Strain Data Suitable for Finite Element Elastic-Plastic Analysis of Shipping Containers," September 1978.

41. US NRC Regulatory Guide 7.9, "Standard Format and Content of Part 21 Applications for Approval of Packaging for Radioactive Material," May 1986.

42. "Guidelines for the Use of Aluminum with Food and Chemicals, 5th Edition, the Aluminum Association, Washington, D.C., April 1984.

43. UCID - 21246, "Dynamic Impact Effects on Spent Fuel Assemblies," Chun, R., Witte, M., and Schwartz, M., Lawrence Livermore Laboratory, October 1987.

44. ORNL/TM-1312, "Structural Analysis of Shipping Casks, Volume 8, Experimental Study of the Stress-Strain Properties of Lead Under Specified Impact Conditions," Evans, J.H., Volume 8, Oak Ridge National Laboratory, Oak Ridge, TN, August 1970.

45. Parker Seals "O-Ring Handbook," ORD-5700, 1992.

46. Oberg, Erik, et al, Machinery's Handbook, 25th Edition, First Printing, Industrial Press, Inc., New York, New York, 1984.

47. Clough, Ray W. and Joseph Penzien, "Dynamics of Structures," 2nd Edition, 1993.

48. Rust, James H., "Nuclear Power Plant Engineering," 1979.

49. ISG-4, Revision 1, "Cask Closure Weld Inspections," May 1999.

50. Blevins, R.D., *Formulas for Natural Frequency and Mode Shape*, Krieger Publishing Co., Malabar, Florida, 1995.

51. ARMCO Product Data Bulletin No. S-22, "17-4PH, Precipitation Hardening Stainless Steel," ARMCO, Inc., 1988.

52. ASTM B733-97, "Standard Specification for Autocatalytic (Electroless) Nickel-Phosphorus Coatings on Metal," Annual Book of ASTM Standards, Vol. 02.05, American Society for Testing and Materials, Conshohocken, PA, 1996.

53. American Society for Metals, "Metals Handbook," 1985.

54. Duncan, R.N., "Corrosion Resistance of High-Phosphorus Electroless Nickel Coatings," Plating and Surface Finishing, July 1986, pages 52-56.

55. Weaver, William Jr. and James M. Gere, "Matrix Analysis of Framed Structures," Second Edition, D. Van Nostrand Company, New York, 1980.

56. Marks' Standard Handbook for Mechanical Engineers, 9th Edition, McGraw-Hill Book Company, New York, New York.

57. NUREG-1617, "Standard Review Plan for Transportation Packages for Spent Nuclear Fuel," U.S. Nuclear Regulatory Commission, Washington, DC.

58. Sandia Report SAND90-2187 TTC-1012 UC-80, "An Analysis of Parameters Affecting Slapdown of Transportation Packages," Sandia National Laboratories, Albuquerque, NM, 1991.

59. US NRC Regulatory Guide 1.92, "Combining Modal Responses and Spatial Components in Seismic Response Analysis," Revision 1, February 1976.

THIS PAGE INTENTIONALLY LEFT BLANK